ANALYSIS OF CIRCULAR WAVEGUIDES COUPLED BY AXIALLY UNIFORM SLOTS

A THESIS SUBMITTED TO
THE GRADUATE SCHOOL OF NATURAL AND APPLIED SCIENCES
OF
MIDDLE EAST TECHNICAL UNIVERSITY

BY

MENSUR ÖZTÜRK

IN PARTIAL FULFILMENT OF THE REQUIREMENTS
FOR
THE DEGREE OF MASTER OF SCIENCE
IN
ELECTRICAL AND ELECTRONICS ENGINEERING

SEPTEMBER 2006

Approval of the Graduate School of Natural and Applied Sciences

Prof. Dr. Canan ÖZGEN
Director

I certify that this thesis satisfies all the requirements as a thesis for the degree of Master of Science.

Prof. Dr. İsmet ERKMEN
Head of Department

This is to certify that we have read this thesis and that in our opinion it is fully adequate, in scope and quality, as a thesis for the degree of Master of Science.

Prof. Dr. Fatih CANATAN
Supervisor

Examining Committee Members

Prof.Dr. Altunkan HIZAL (METU, EE) ______________________________

Prof.Dr. Fatih CANATAN (METU, EE) ______________________________

Prof.Dr. Nilgün GÜNALP (METU, EE) ______________________________

Assoc.Prof.Dr. Sencer KOÇ (METU, EE) ______________________________

Assist.Prof.Dr. Önder Haluk TEKBAŞ (KHO) ______________________________

I hereby declare that all information in this document has been obtained and presented in accordance with academic rules and ethical conduct. I also declare that, as required by these rules and conduct, I have fully cited and referenced all material and results that are not original to this work.

Name, Last name : Mensur ÖZTÜRK

Signature :

ABSTRACT

ANALYSIS OF CIRCULAR WAVEGUIDES COUPLED BY AXIALLY UNIFORM SLOTS

ÖZTÜRK, Mensur

M.S., Department of Electrical and Electronics Engineering

Supervisor : Prof. Dr. Fatih CANATAN

September 2006, 121 pages

The characteristics of slotted circular waveguides with different dimensions, including cutoff frequencies of TE and TM modes, impedance and modal field distributions will be analyzed using the generalized spectral domain approach. The Method of Moment will be applied, basis functions that include the edge conditions will be used and a computer program will be developed. Obtained results will be presented for different number, depth and thickness of coupling slots, and compared with available data to demonstrate the accuracy and the efficiency of the approach. Plots of the electric and magnetic field lines corresponding to the dominant as well as a number of higher order modes will be presented for quadruple ridge case.

Key words: Slotted circular waveguide, cutoff frequency, Method of Moments.

ÖZ

EKSENSEL OLARAK EŞ OYUKLARLA KUPLE EDİLMİS DAİRESEL DALGA KILAVUZLARININ ANALİZİ

ÖZTÜRK, Mensur
Yüksek Lisans, Elektrik ve Elektronik Mühendisliği Bölümü
Tez Yöneticisi : Prof. Dr. Fatih CANATAN

Eylül 2006, 121 Sayfa

Oyuklu dairesel dalga kılavuzlarının özellikleri, TE ve TM modlarının kesim frekansları, empedansları ve alan dağılımlarını içerecek şekilde genelleştirilmiş tayf alanı yaklaşımı kullanılarak analiz edilecektir. Moment metodu uygulanacak, kenar şartlarını içeren temel fonksiyonlar kullanılacak ve bir bilgisayar programı geliştirilecektir. Farklı sayıda, genişlikte ve derinlikteki kuplaj oyukları için elde edilen sonuçlar sunulacak ve yaklaşımın doğruluğunu ve etkinliğini gösterecek şekilde mevcut verilerle karşılaştırılacaktır. Dört oyuklu durum için, baskın modların ve bir miktar daha yüksek dereceli modların elektrik ve manyetik alan çizimleri sunulacaktır.

Anahtar Kelimeler: Oyuklu dairesel dalga kılavuzu, kesim frekansı, Momentler Yöntemi.

To My Family

ACKNOWLEDGMENTS

I express sincere gratitude to my advisor Prof. Dr. Fatih CANATAN for his continuous support and guidance throughout this thesis. I am grateful for his friendship and encouragement for successful completion of my study. He carefully guided me throughout the pursuit of my Master's degree. I would like to thank him for being my advisor.

I would like to express my sincere appreciation to Mehmet TAŞTAN, Aşir BAHÇEBAŞI and Ahmet ŞENOL for their valuable friendship, help and support.

I am also grateful to my superiors in Turkish General Staff for their tolerances for the completion of this thesis.

Last in the list but first in my heart, I am grateful to my wife, Yasemin, because she always supported emotionally and encouraged me when needed.

TABLE OF CONTENTS

LIST OF FIGURES

FIGURES

LIST OF TABLES

TABLES

CHAPTER 1

INTRODUCTION

1.1 Scope of the Study

Ridges in waveguides increase the operating frequency bandwidth through lowering the cutoff frequencies of certain modes. Because of this advantage of ridge waveguides, they are useful in wide band applications. They have been used as transmission lines in systems, where a wide frequency range must be covered and only the fundamental mode can be tolerated. Ridged waveguides are important components in modern microwave filters, septum polarizers and matching networks.

Ridged waveguides are also called as slotted waveguides in the literature. So many numerical techniques have been employed in the analysis of different types of ridged waveguide structures. In this study, the circular waveguides with axially uniform slots (ridges) are analyzed. The analysis is done by the same method presented in [1].

The scope of the study can be summarized as follows:

- Derivation of the details of the formulation presented in [1]
- Demonstration of the validity and the efficiency of the method
- Applications of the solution to the structures with different dimensions
- Development of a computer program using MATLAB with a graphical user interface (GUI)
- Determination of the operating modes and their behaviours while changing dimensions.

- Calculation of the power handling capacities of triple and quadruple ridged waveguides for the fundamental mode

1.2 Previous Studies and Motivation of the Study

The first analysis of the ridge in circular waveguides was done by Dally [2] for double ridge case. His work showed that the ridged waveguide has the advantages of reduced cutoff frequency and impedance, and increased bandwidth over the ordinary circular waveguide. He used finite element method in his analysis, but the results of his work are not of satisfactory precision due to the mesh size chosen. Another study done on the ridged circular waveguides is that of Canatan [3]. He analyzed both double and quadruple ridged circular waveguides using Ritz-Galerkin method. His results and computational approach used for the quadruple ridged waveguides were new. He showed that the quadruple ridged circular waveguides possess low cutoff and wide bandwidth properties similar to those found for double ridged circular waveguides [4] [5]. This work was restricted to the symmetrical TE modes.

The analysis done on the ridged waveguide showed that the introduction of ridges inside the guide could greatly increase the bandwidth of the dominant mode. Further improvements can be achieved by dielectric loading or adding more ridges in the guide.

The ridged waveguides have been used successfully as matching or transition elements. The cavity structure with the cross section shown in Figure-1.1 is introduced as a solution to overcome the mode competition problem for the gyrotron applications [6] [7]. It is stated in [6] that a gradually changing slotted waveguide has a perfect function of converting the TE_{0n} mode to $TE_{0,n+p}$ mode.

In [6] and [7], it has shown that how a mode competition can be reduced by the way of mode converter.

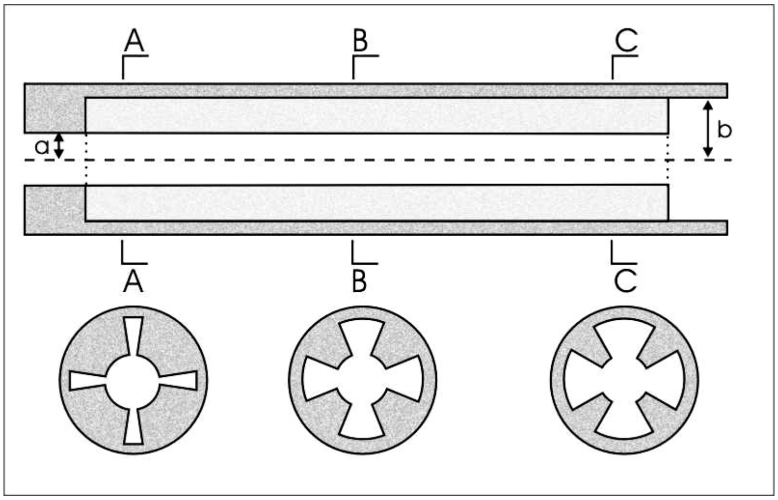

Figure 1.1 $TE_{0,n}$-$TE_{0,n+p}$ Mode Converter.

In [6], a conventional field matching method has been applied to analyze the composite waveguide in Figure 1.1. But this method is not suitable for this structure because the expansion functions do not fulfil the edge conditions at the slot edges. This leads to oversized matrices, slow convergence and inaccurate field distributions [8]. In addition to this, since TM wave is not taken into account from the beginning of the analysis, it is impossible to calculate TE-TM coupling.

The triple and quadruple ridged waveguides are analyzed in [9] by radial mode matching technique. The characteristics of square, circular and diagonal quadruple waveguides are analyzed in [10] systematically by using surface magnetic field integral equation and found that the fundamental modes are primarily dependent on the ridge gap and thickness, not on the type of waveguide cross section.

Various numerical techniques have been employed in the analysis of these structures. The cutoff wavelengths of the first two modes of a septum polarizer were determined by the finite element method (FEM). The mode matching technique (MMT) was used to investigate the eigenvalue problem of single and multiple symmetric ridge waveguides. The method of lines (MoL) was also applied to the eigenmode problem of a partially loaded ridge waveguide [11].

The Method of Moments (MoM) has been used extensively to solve electromagnetic problems. However, due to its dense matrix, especially for large structures, the MoM suffers from long matrix solution time and large storage requirement. In this thesis it is shown that use of edge conditioned basis functions result in a MoM matrix that is smaller and more rapidly convergent size.

1.3 Thesis Organisation and Contributions of the Study

The work can be outlined as follows: In chapter 2, the waveguide structure is analyzed and the basic formulations to find the cutoff wavenumbers of TE and TM modes and to determine the corresponding field distributions in the composite waveguides are introduced. In this chapter, the edge condition is discussed and the convenience of edge conditioned basis functions is proved. The infinite sums over the eigenmodes, which appears as a result of the application of the generalized spectral domain method to the analysis of waveguides, are given in Appendix A.

In chapter 3, the computer programs developed in MATLAB for the numerical evaluation of the problem are described and the simulation results carried on MATLAB are presented. The convergence behaviour of cutoff wavenumbers according to the different numbers of field and current expansion functions are investigated for triple ridge waveguide. The cutoff wavenumbers and field plots are provided for triple and quadruple ridged waveguides. The breakdown conditions and power handling capacities are investigated for the dominant mode as a contribution. Graphical user interface of computer programs is described in Appendix B. Finally, the conclusion part is provided in the last chapter.

CHAPTER 2

BASIC THEORY AND FORMULATION

2.1 Introduction

To analyze waveguides, dielectric and magnetic inhomogeneities are replaced by polarization and magnetization currents, respectively, while metal inserts and slots are replaced by electric and magnetic surface currents, respectively, so that the structure can be treated as empty and completely shielded. The method here is based on short circuiting the coupling slots, replacing the non vanishing slot tangential electric field at the short circuited boundary by two surface magnetic currents at the two sides of the short circuit and analyzing the structure decomposed into circular and sector waveguides separately.

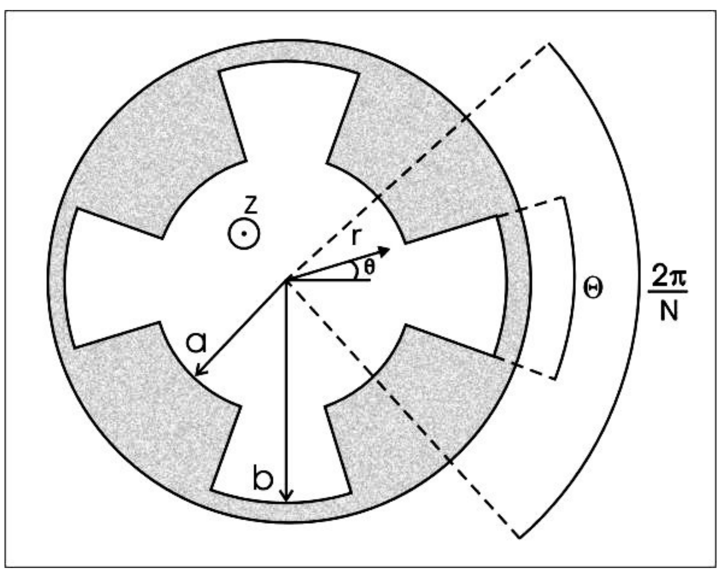

Figure 2.1 Transverse cross section of waveguide and dimensional parameters.

The electromagnetic fields in the individual waveguides, which are isolated from each other, are analyzed using the equivalent surface magnetic currents which guarantee the continuity of the tangential electric field across the slot.

The expectation of the study is to calculate the cutoff wavenumbers of the waveguide structure with the cross section given in Figure 2.1, and to develop a method, which is efficient, accurate and without any simplification assumptions.

In the following sections, the waveguide structure is described and the problem is stated first. The formulation begins with the determination of field expansion functions and the relation between the expansion coefficients. Then, the expressions are transformed to a matrix formulation. Finally, the integral equations and infinite sums are derived to make the matrix entries analytic fully.

2.2 Description of the Waveguide Structure

The structure of the slotted waveguide is characterized by the slot number 'N', the angle of the slot 'Θ' and the radii 'a' and 'b'.

The first point to be decided is the coordinate system in which the problem is to be treated. It is convenient to work in a coordinate system that is related to the symmetry of the system under consideration. Since the problem is to treat a metallic waveguide of circular cross section containing conically shaped uniform slot surfaces aligned with cylindrical coordinate planes, the obvious coordinates to choose are the cylindrical coordinates, with r, θ and z.

The structure is considered as a simple homogeneous waveguide consisting of a metal tube containing air. As in the elementary theory, the metal is taken to be a perfect conductor and air is taken as free space.

2.3 Decomposing the Structure

Decomposing the structure reduces the problem into smaller and better-conditioned sub problems that can be efficiently optimized. It is possible to separate the structure under consideration to sub problems with appropriate portions and calculate them independently.

The slotted circular waveguide given in Figure 2.1 can be decomposed into one hollow circular waveguide with radius ‘a’ and ‘N’ sector waveguides with minimum and maximum radii ‘a’ and ‘b’, and an angular width ‘Θ’.

It is known from uniqueness concepts, that the tangential components of only E or H fields are needed to determine the complete fields. It will be used that equivalent problems can be found in terms of only magnetic currents (tangential E). Placing a perfect conductor over the surface between hollow circular waveguide and N sector waveguides sets up the equivalent problem and the tangential electric field at the slot aperture can be replaced by two equivalent surface magnetic currents at both side of the short circuit.[13].

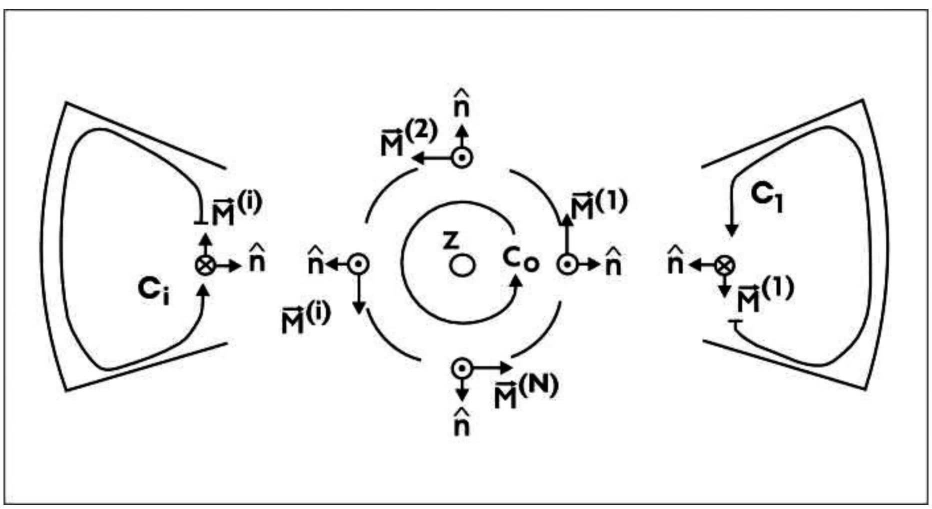

Figure 2.2 Decomposition of the structure into subregions

These two surface magnetic currents that can be considered as the sources of individual waveguides are equal in magnitude and opposite in direction, which guarantee the continuity of the tangential electric field across the slot.

At the interface between two waveguide sections, the relation between magnetic surface currents and electric field intensity is defined as:

$$\vec{M} = -\vec{E}\big|_c \times \hat{n} \tag{2.1}$$

where $\hat{n}$ is the unit vector normal to the surface of the slot C_i. The surface magnetic current M is determined to satisfy the continuity of the tangential electric field across the slot surface S.

The following relations are obtained by separating the surface magnetic current into its transverse and longitudinal components:

$$\begin{aligned} \vec{M}_t &= -(E_z\big|_c\, \hat{a}_z) \times \hat{n} \\ M_z \hat{a}_z &= -\vec{E}_t\big|_c \times \hat{n} \end{aligned} \tag{2.2}$$

where $\hat{a}_z$ is the unit vector in the longitudinal direction.

2.4 Field Definitions and Coupling Expressions

The aim of this section is to specify the coupling conditions of field amplitudes that are used to expand the field components by using the orthogonality relation between the eigenwaves.

Maxwell's equations are a summary of the laws of electromagnetism and can be taken as the starting point for the solution of any problem in electromagnetic theory. It is desirable to use the approach from Maxwell's equations since a complete set of solutions can be obtained in this way [12].

A technique often used in solving problems is to decompose the problem and its solution into two separate ones: TE (transverse electric) and TM (transverse magnetic). It can be shown that an arbitrary field in a homogeneous source free region can be expressed as the sum of a TE field and a TM field [14].

In a source free region, a solution can be expressed in terms of the Lorentz scalar potentials that satisfy the following homogeneous Helmholtz equations, subject to the boundary and radiation conditions:

$$\nabla_t^2 \Psi_n + (k_{nTE})^2 \Psi_n = 0 \tag{2.3.1}$$

$$\nabla_t^2 \Phi_n + (k_{nTM})^2 \Phi_n = 0 \tag{2.3.2}$$

where ∇_t is the transverse component of del operator and Ψ_n and Φ_n are the complete sets of longitudinal electric and magnetic fields which characterize TE and TM modes respectively and are real functions of transverse coordinates, which correspond to the cutoff wavenumbers k_{nTE} and k_{nTM}, respectively.

Because of preferential role played by the guiding direction z, it provides convenience to decompose Maxwell's equations into components that are longitudinal (along z direction) and components that are transverse (along the r and θ directions). The fields at any waveguide cross-section can be defined as follows:

$$\vec{E}_t = \left(\sum_{(n)} A_n (\nabla_t \Phi_n) + \sum_{(n)} B_n (\nabla_t \Psi_n \times \hat{a}_z)\right) \cdot e^{-j\beta z} \tag{2.4.1}$$

$$\vec{H}_t = (\sum_{(n)} C_n (\nabla_t \Psi_n) + \sum_{(n)} D_n (\hat{a}_z \times \nabla_t \Phi_n)) \cdot e^{-j\beta z} \tag{2.4.2}$$

$$E_z = (\sum_{(n)} k_{nTM} F_n \Phi_n) \cdot e^{-j\beta z} \tag{2.4.3}$$

$$H_z = (\sum_{(n)} k_{nTE} G_n \Psi_n) \cdot e^{-j\beta z} \tag{2.4.4}$$

where a z-dependence $e^{-j\beta z}$ assumed and A_n, B_n, C_n, D_n, F_n, G_n are series expansion coefficients. The set $\nabla_t \Phi_n$ is complete with respect to the curl free transverse electric fields, while the set $\nabla_t \Psi_n \times \hat{a}_z$ is complete with respect to the divergence free transverse electric fields. The two sets $\nabla_t \Psi_n$ and $\hat{a}_z \times \nabla_t \Phi_n$ have the same properties with respect to transverse magnetic fields.

The field expansions are not only complementary but also orthogonal and satisfy the following orthogonality relations [15]:

$$\begin{aligned} (\Phi_n, \Phi_m) &= \frac{1}{(k_{nTM})^2} \delta_{nm} \\ (\Psi_n, \Psi_m) &= \frac{1}{(k_{nTE})^2} \delta_{nm} \end{aligned} \tag{2.5}$$

$$\begin{aligned} (\nabla_t \Phi_n, \nabla_t \Phi_m) &= \delta_{nm} \\ (\nabla_t \Psi_n, \nabla_t \Psi_m) &= \delta_{nm} \\ (\nabla_t \Phi_n, \nabla_t \Psi_n \times \hat{a}_z) &= 0 \end{aligned} \tag{2.6}$$

Here;

$$(f, g) := \int_S f \cdot g^* dS \tag{2.7}$$

describes the inner product of two functions. S is the area of the waveguide cross-section and (*) means conjugation.

Replacing ∂z by -jβ and ∂t by jω because of the assumed z-dependence and time dependence and introducing these decompositions into the source free Maxwell' equations:

$$\begin{aligned} \nabla_t \times \vec{E}_t &= -j\omega\mu_0 H_z \hat{a}_z \\ \nabla_t \times \vec{H}_t &= j\omega\varepsilon_0 E_z \hat{a}_z \end{aligned} \tag{2.8}$$

$$\begin{aligned} \nabla_t E_z + j\beta \vec{E}_t &= j\omega\mu_0 (\vec{H}_t \times \hat{a}_z) \\ \nabla_t H_z + j\beta \vec{H}_t &= j\omega\varepsilon_0 (\hat{a}_z \times \vec{E}_t) \end{aligned} \tag{2.9}$$

Expanding the transverse and longitudinal components of the electromagnetic field with respect to TM and TE normal modes of the corresponding empty waveguide, substituting these expansions into Maxwell's equations and making use of the orthogonality relation, one obtains the interrelations between the different expansion coefficients as well as their relations to the defined surface magnetic currents M [16].

$$\begin{aligned} (\vec{H}_t, \nabla_t \Psi_n) &= \frac{j\omega\varepsilon_0}{j\beta} (\hat{a}_z \times \vec{E}_t, \nabla_t \Psi_n) - \frac{1}{j\beta} (\nabla_t H_z, \nabla_t \Psi_n) \\ &= \frac{k_0}{Z_0 \beta} (\vec{E}_{t,} \nabla_t \Psi_n \times \hat{a}_z) - \frac{1}{j\beta} \oint_c H_z (\nabla_t \Psi_n)^* \cdot \hat{n} dl + \frac{1}{j\beta} (H_z, \nabla_t^2 \Psi_n) \\ &= \frac{k_0}{Z_0 \beta} (\vec{E}_{t,} \nabla_t \Psi_n \times \hat{a}_z) - \frac{(k_{nTE})^2}{j\beta} (H_z, \Psi_n) \\ &= \frac{k_0}{Z_0 \beta} B_n e^{-j\beta z} - \frac{k_{nTE}}{j\beta} G_n e^{-j\beta z} \\ &= C_n e^{-j\beta z} \end{aligned} \tag{2.10}$$

where

$$Z_0 = \sqrt{\frac{\mu_0}{\varepsilon_0}} \tag{2.11}$$

is the free space wave impedance and

$$k_0 = \omega\sqrt{\mu_0\varepsilon_0} \tag{2.12}$$

is the free space wavenumber.

In the same way, the following equalities are obtained:

$$\begin{aligned}
(\vec{E}_t, \nabla_t\Phi_n) \quad &= \frac{j\omega\mu_0}{j\beta}(\vec{H}_t \times \hat{a}_z, \nabla_t\Phi_n) - \frac{1}{j\beta}(\nabla_t E_z, \nabla_t\Phi_n) \\
&= \frac{Z_0 k_0}{\beta}(\vec{H}_{t,} \hat{a}_z \times \nabla_t\Phi_n) - \frac{1}{j\beta}\oint_c E_z(\nabla_t\Phi_n)^* \cdot \hat{n}dl + \frac{1}{j\beta}(E_z, \nabla_t^2\Phi_n) \\
&= \frac{k_0 Z_0}{\beta}(\vec{H}_{t,} \hat{a}_z \times \nabla_t\Phi_n) + \frac{1}{j\beta}\oint_c \vec{M}_t \cdot (\hat{a}_z \times \nabla_t\Phi_n) \cdot dl - \frac{(k_{nTM})^2}{j\beta}(E_z, \Phi_n) \\
&= \frac{k_0 Z_0}{\beta} D_n e^{-j\beta z} + \frac{1}{j\beta}\oint_c \vec{M}_t \cdot (\hat{a}_z \times \nabla_t\Phi_n) \cdot dl - \frac{k_{nTM}}{j\beta} F_n e^{-j\beta z} \\
&= A_n e^{-j\beta z}
\end{aligned} \tag{2.13}$$

$$\begin{aligned}
(\vec{H}_t, \hat{a}_z \times \nabla_t\Phi_n) \quad &= \frac{j\omega\varepsilon_0}{j\beta}(\vec{E}_t, \nabla_t\Phi_n) - \frac{1}{j\beta}(\nabla_t H_z, \hat{a}_z \times \nabla_t\Phi_n) \\
&= \frac{k_0}{Z_0\beta}(\vec{E}_t, \nabla_t\Phi_n) - \frac{1}{j\beta}\oint_c H_z(\hat{a}_z \times \nabla_t\Phi_n)^* \cdot \hat{n}dl + \frac{1}{j\beta}(H_z, \nabla_t \cdot (\hat{a}_z \times \nabla_t\Phi_n)) \\
&= \frac{k_0}{Z_0\beta} A_n e^{-j\beta z} \\
&= D_n e^{-j\beta z}
\end{aligned} \tag{2.14}$$

$$
\begin{aligned}
(\vec{E}_t, \nabla_t \Psi_n \times \hat{a}_z) &= \frac{j\omega\mu_0}{j\beta}(\vec{H}_t, \nabla_t \Psi_n) - \frac{1}{j\beta}(\nabla_t E_z, \nabla_t \Phi_n \times \hat{a}_z) \\
&= \frac{Z_0 k_0}{\beta}(\vec{H}_t, \nabla_t \Psi_n) - \frac{1}{j\beta}\oint_c E_z (\nabla_t \Psi_n \times \hat{a}_z)^* \cdot \hat{n} dl \\
&= \frac{k_0 Z_0}{\beta} C_n e^{-j\beta z} + \frac{1}{j\beta}\oint_c \vec{M}_t \cdot (\nabla_t \Psi_n) \cdot dl \\
&= B_n e^{-j\beta z}
\end{aligned} \tag{2.15}
$$

$$
\begin{aligned}
(H_z, \Psi_n) &= -\frac{1}{j\omega\mu_0}(\nabla_t \times \vec{E}_t, \Psi_n \hat{a}_z) \\
&= -\frac{1}{jk_0 Z_0}\oint_c \vec{E}_t \times (\Psi_n \hat{a}_z)^* \cdot \hat{n} dl - \frac{1}{jk_0 Z_0}(\nabla_t \Psi_n \times \hat{a}_z, \vec{E}_t) \\
&= -\frac{1}{jk_0 Z_0}\oint_c M_z \Psi_n^* dl - \frac{1}{jk_0 Z_0} B_n e^{-j\beta z} \\
&= \frac{1}{k_{nTE}} G_n e^{-j\beta z}
\end{aligned} \tag{2.16}
$$

$$
\begin{aligned}
(E_z, \Phi_n) &= -\frac{1}{j\omega\varepsilon_0}(\nabla_t \times \vec{H}_t, \Phi_n \hat{a}_z) \\
&= -\frac{Z_0}{jk_0}\oint_c \vec{H}_t \times (\Phi_n \hat{a}_z)^* \cdot \hat{n} dl - \frac{Z_0}{jk_0}(\hat{a}_z \times \nabla_t \Phi_n, \vec{H}_t) \\
&= -\frac{Z_0}{jk_0} D_n e^{-j\beta z} \\
&= \frac{1}{k_{nTM}} F_n e^{-j\beta z}
\end{aligned} \tag{2.17}
$$

It is convenient to use some abbreviations for the closed loop coupling integrals obtained as a result of the calculations given above for further analysis. So, these integrals can be expressed by:

$$
\begin{aligned}
u_n &= \frac{1}{jk_{nTE}}\oint_c \vec{M}_t \cdot (\nabla_t \Psi_n)^* \cdot dl \\
v_n &= \frac{1}{jk_{nTM}}\oint_c \vec{M}_t \cdot (\hat{a}_z \times \nabla_t \Phi_n)^* \cdot dl \\
w_n &= \oint_c M_z \Psi_n^* dl
\end{aligned} \tag{2.18}
$$

It is possible to obtain two linear and non-homogeneous equality systems by using the equalities given in (2.10) and (2.13)-(2.17). The equalities given by (2.10), (2.15) and (2.16) are related to TE waves and the equalities given by (2.13), (2.14) and (2.17) are related to TM waves.

TE Matrix:

$$\begin{bmatrix} k_0\left[k_{TE}\right]^{-1} & -\beta\left[k_{TE}\right]^{-1} & [0] \\ -\beta\left[k_{TE}\right]^{-1} & k_0\left[k_{TE}\right]^{-1} & [I] \\ [0] & [I] & k_0\left[k_{TE}\right]^{-1} \end{bmatrix} \cdot \begin{bmatrix} \bar{C} \\ \dfrac{1}{Z_0}\bar{B} \\ j\bar{G} \end{bmatrix} = -\frac{1}{Z_0}\begin{bmatrix} \bar{u} \\ \bar{0} \\ \bar{w} \end{bmatrix} e^{j\beta z} \qquad (2.19)$$

TM Matrix:

$$\begin{bmatrix} k_0\left[k_{TM}\right]^{-1} & -\beta\left[k_{TM}\right]^{-1} & [0] \\ -\beta\left[k_{TM}\right]^{-1} & k_0\left[k_{TM}\right]^{-1} & [I] \\ [0] & [I] & k_0\left[k_{TM}\right]^{-1} \end{bmatrix} \cdot \begin{bmatrix} \bar{A} \\ Z_0\bar{D} \\ j\bar{F} \end{bmatrix} = -\begin{bmatrix} \bar{0} \\ \bar{v} \\ \bar{0} \end{bmatrix} e^{j\beta z} \qquad (2.20)$$

Here, [I] is the elementary matrix, [0] is the zero (null) matrix; $[k_{TE}]$ and $[k_{TM}]$ are diagonal matrices with elements k_{nTE} and k_{nTM}; $\bar{A}$, $\bar{B}$, $\bar{C}$, $\bar{D}$, $\bar{F}$ and $\bar{G}$ are the column vectors including field amplitudes A_n, B_n, C_n, D_n, F_n and G_n. Similarly, the column vectors $\bar{u}$, $\bar{v}$ and $\bar{w}$ have the closed loop coupling integrals u_n, v_n and w_n as elements.

TE and TM matrices have the same structure. If the equality systems given in (2.19) and (2.20) are solved with respect to the coefficients of field expansion series;

TE Coefficients:

$$C_n = \frac{1}{Z_0} \frac{\frac{k_{nTE}}{k_0}(k_0^2 - k_{nTE}^2)u_n - \frac{\beta}{k_0}k_{nTE}^2 w_n}{k_{nTE}^2 - (k_0^2 - \beta^2)} e^{j\beta z} \tag{2.21.1}$$

$$B_n = \frac{k_{nTE}(\beta u_n - k_{nTE} w_n)}{k_{nTE}^2 - (k_0^2 - \beta^2)} e^{j\beta z} \tag{2.21.2}$$

$$jG_n = \frac{1}{Z_0} \frac{\frac{\beta}{k_0}k_{nTE}^2 u_n - \frac{k_{nTE}}{k_0}(k_0^2 - \beta^2)w_n}{k_{nTE}^2 - (k_0^2 - \beta^2)} e^{j\beta z} \tag{2.21.3}$$

TM Coefficients:

$$A_n = \frac{\beta k_{nTM} v_n}{k_{nTM}^2 - (k_0^2 - \beta^2)} e^{j\beta z} \tag{2.22.1}$$

$$D_n = \frac{1}{Z_0} \frac{k_0 k_{nTM} v_n}{k_{nTM}^2 - (k_0^2 - \beta^2)} e^{j\beta z} \tag{2.22.2}$$

$$jF_n = \frac{-k_{nTM}^2 v_n}{k_{nTM}^2 - (k_0^2 - \beta^2)} e^{j\beta z} \tag{2.22.3}$$

are obtained.

2.5 Usage of Rotational Symmetry

As a general result of Fourier Transform, a periodic signal transforms to a discrete signal. In our case, the complete structure repeats itself in an interval 2π/N, N is the number of slots. So, it is expected that the spectrum to be spread out by a factor N with respect to an empty circular waveguide.

The field functions of hollow circular waveguide do not have any boundary conditions to satisfy along the azimuthal (θ) direction. Therefore, it is possible to define the angular dependence for the eigenwaves, which rotates to left (p<0) or right (p>0), as $e^{jp\theta}$. Since the boundary conditions are applicable for sector waveguides (for example at ±Θ/2 of the first interval), here, sine and cosine terms must be used to specify the angular dependence. Assuming the azimuthal coordinate at the first interval was given as $\theta^{(1)}$ then, the azimuthal relation between first and the i^{th} interval can be expressed as:

$$\theta^{(i)} = (i-1)\frac{2\pi}{N} + \theta^{(1)} \tag{2.23}$$

It can be seen from the symmetry property of the system that there is a constant phase difference $e^{-j\Delta}$ between adjacent slots. If the system has rotated by 2π/N, the solution and the field intensity change by a phase factor. $(N+1)^{th}$ interval must show the same property as the first interval so, it can be written for the phase factor that:

$$(e^{-j\Delta})^N = 1 \Rightarrow \Delta = q\frac{2\pi}{N} \tag{2.24}$$

Therefore, N linear and independent slot modes are available (q=0, 1,…, N-1). The surface magnetic currents at the slots can be represented by:

$$\vec{M}^{(i)} = \vec{M}^{(1)} e^{-jq(i-1)\frac{2\pi}{N}} \tag{2.25}$$

$1 \leq i \leq N$	: number of related slot
$0 \leq q \leq N-1$	: slot mode (phase difference factor)
N	: number of slots

While the excitation of hollow circular waveguide is seen over the N apertures, only the related sector waveguide is affected.

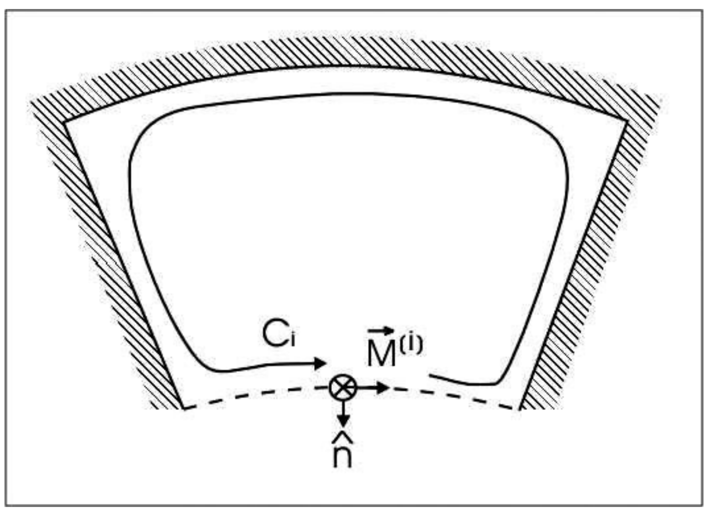

Figure 2.3 Excitation of ith sector waveguide

For the ith sector waveguide, the following expression can be written:

$$
\begin{aligned}
u_n^{(i)} &= \frac{1}{jk_{nTE}} \oint_{c_i} \vec{M}_t^{(i)} \cdot (\nabla_t \Psi_n^{(i)})^* \, dl \\
&= \frac{1}{jk_{nTE}} \int_{L_i} \vec{M}_t^{(i)} \cdot (\nabla_t \Psi_n^{(i)})^* (-dl) \\
&= e^{-jq(i-1)\frac{2\pi}{N}} \left(-\frac{1}{jk_{nTE}} \int_{L_1} \vec{M}_t^{(1)} \cdot (\nabla_t \Psi_n^{(1)})^* \, dl\right)
\end{aligned}
\tag{2.26}
$$

where L_i is the length of the ith slot. Similarly, v_n and w_n can be defined for the ith sector:

$$
u_n^{(i)} = e^{-jq(i-1)\frac{2\pi}{N}} \left(-\frac{1}{jk_{nTE}} \int_{L_1} \vec{M}_t^{(1)} \cdot (\nabla_t \Psi_n^{(1)})^* \, dl\right) \tag{2.27.1}
$$

$$
v_n^{(i)} = e^{-jq(i-1)\frac{2\pi}{N}} \left(-\frac{1}{jk_{nTM}} \int_{L_1} \vec{M}_t^{(1)} \cdot (\hat{a}_z \times \nabla_t \Phi_n^{(1)})^* \, dl\right) \tag{2.27.2}
$$

$$
w_n^{(i)} = e^{-jq(i-1)\frac{2\pi}{N}} \left(-\int_{L_1} \vec{M}^{(1)} \cdot (\Psi_n^{(1)})^* \, dl\right) \tag{2.27.3}
$$

The sign (~) is used to distinguish the expressions for the hollow circular waveguide from the expressions for sector waveguide.

The following relations are used to take out the angular dependence of the field expansion functions of the hollow circular waveguide:

$$
\begin{aligned}
\tilde{\Psi}_n &:= \hat{\Psi}_n \cdot e^{jp_n\theta} \\
\tilde{\Phi}_n &:= \hat{\Phi}_n \cdot e^{jp_n\theta}
\end{aligned}
\tag{2.28}
$$

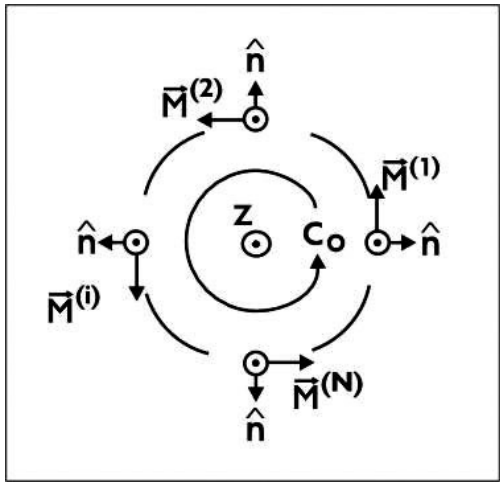

Figure 2.4 Excitation of hollow circular waveguide.

As a result;

$$
\begin{aligned}
\tilde{u}_n &= \frac{1}{jk_{nTE}} \oint_{C_0} \vec{M}_t \cdot (\nabla_t \hat{\Psi}_n)^* e^{-jp_n\theta} dl \\
&= \sum_{i=1}^{N} \frac{1}{jk_{nTE}} \int_{L_i} \vec{M}_t^{(i)} \cdot (\nabla_t \hat{\Psi}_n)^* e^{-jp_n\theta} dl \\
&= \sum_{i=1}^{N} \frac{1}{jk_{nTE}} \int_{L_1} \vec{M}_t^{(i)} \cdot (\nabla_t \hat{\Psi}_n)^* e^{-jp_n(\theta+(i-1)\frac{2\pi}{N})} dl \\
&= \sum_{i=1}^{N} (e^{-j(p_n+q)(i-1)\frac{2\pi}{N}}) \frac{1}{jk_{nTE}} \int_{L_1} \vec{M}_t^{(1)} \cdot (\nabla_t \hat{\Psi}_n)^* e^{-jp_n\theta} dl
\end{aligned}
\tag{2.29}
$$

Substituting the following equality,

$$
\sum_{i=1}^{N} (e^{-j(p_n+q)(i-1)\frac{2\pi}{N}}) = \begin{Bmatrix} N & for \quad p_n = r_n N - q; \quad r_n, p_n \in I \\ 0 & otherwise \end{Bmatrix} \tag{2.30}
$$

into the equation (2.29), the expressions for $\tilde{u}_n$ and similarly for $\tilde{v}_n$ and $\tilde{w}_n$ can be obtained as follows:

$$\tilde{u}_n = \begin{cases} N\dfrac{1}{jk_{nTE}}\displaystyle\int_{L_1} \vec{M}_t^{(1)} \cdot (\nabla_t \hat{\Psi}_n)^* e^{-jp_n\theta} dl & for \quad p_n = r_n N - q \\ 0 & otherwise \end{cases} \tag{2.31.1}$$

$$\tilde{v}_n = \begin{cases} N\dfrac{1}{jk_{nTM}}\displaystyle\int_{L_1} \vec{M}_t^{(1)} \cdot (\hat{a}_z \times \nabla_t \hat{\Phi}_n)^* e^{-jp_n\theta} dl & for \quad p_n = r_n N - q \\ 0 & otherwise \end{cases} \tag{2.31.2}$$

$$\tilde{w}_n = \begin{cases} N\displaystyle\int_{L_1} \vec{M}_z^{(1)} \cdot \hat{\Psi}_n^* e^{-jp_n\theta} dl & for \quad p_n = r_n N - q \\ 0 & otherwise \end{cases} \tag{2.31.3}$$

where r_n and p_n are integer numbers.

So it is obvious that the hollow circular waveguide is excited only at the integer order of N and this is related to the order p and the selected number of the slot mode q (phase difference between slots).

2.6 Expansion Functions of Surface Magnetic Currents

Up to now, the field expansion functions, which are complete and orthogonal, are determined for the field components. It is necessary to determine also the expansion functions of the surface magnetic currents for the numerical analysis of the structure. But, it is not necessary them to be complete and orthogonal. Which is important here, they have to have a good convergence property as far as possible.

In any case, it must be considered to choose functions including the electric and magnetic boundary condition at θ=0.

It can be seen from the equality systems (2.19) and (2.20) that E_t and E_z similarly M_z and M_t have a phase shift by π/2. Therefore, the currents at the first slot can be determined as follows:

$$\vec{M}_t(\theta) = j\sum_m [a_{\theta_m} M_{\theta_m}^{(c)}(\theta) + b_{\theta_m} M_{\theta_m}^{(s)}(\theta)].e^{-j\beta z}\hat{a}_\theta$$
$$M_z(\theta) = \sum_m [a_{z_m} M_{z_m}^{(c)}(\theta) + b_{z_m} M_{z_m}^{(s)}(\theta)].e^{-j\beta z} \tag{2.32}$$

Current terms marked with (c) and (s) contain cosine (represent magnetic wall symmetry) and sine functions (represent electric wall symmetry), respectively (at θ=0).

When the definitions of the closed loop coupling integrals in (2.18) are applied to the current expansions, the integration and summation expressions can be exchanged and the following equations are obtained:

$$\begin{aligned} u_n^{(1)} \cdot e^{j\beta z} &= -(\sum_m a_{\theta_m} R_{nm}^{(c)} + \sum_m b_{\theta_m} R_{nm}^{(s)}) \\ v_n^{(1)} \cdot e^{j\beta z} &= -(\sum_m a_{\theta_m} S_{nm}^{(c)} + \sum_m b_{\theta_m} S_{nm}^{(s)}) \\ w_n^{(1)} \cdot e^{j\beta z} &= -(\sum_m a_{z_m} T_{nm}^{(c)} + \sum_m b_{z_m} T_{nm}^{(s)}) \end{aligned} \tag{2.33}$$

And for the hollow circular waveguide:

$$\begin{aligned} \tilde{u}_n \cdot e^{j\beta z} &= N(\sum_m a_{\theta_m} \tilde{R}_{nm}^{(c)} + \sum_m b_{\theta_m} \tilde{R}_{nm}^{(s)}) \\ \tilde{v}_n \cdot e^{j\beta z} &= N(\sum_m a_{\theta_m} \tilde{S}_{nm}^{(c)} + \sum_m b_{\theta_m} \tilde{S}_{nm}^{(s)}) \\ \tilde{w}_n \cdot e^{j\beta z} &= N(\sum_m a_{z_m} \tilde{T}_{nm}^{(c)} + \sum_m b_{z_m} \tilde{T}_{nm}^{(s)}) \end{aligned} \tag{2.34}$$

For determining the coefficients R_{nm}, S_{nm} and T_{nm} in the equations (2.33) and (2.34), the integral is taken only along the first slot (so it is marked with (^{1})). The closed loop integrals in (2.18), can be converted to the series expressions given in (2.33) and (2.34) by applying the identities given in (2.27) and (2.31).

The following abbreviations are used in (2.33):

$$R_{nm}^{(c)} = \frac{1}{k_{nTE}} \int_{L_1} M_{\theta_m}^{(c)} (\nabla_t \Psi_n)_\theta^* dl$$
$$R_{nm}^{(s)} = \frac{1}{k_{nTE}} \int_{L_1} M_{\theta_m}^{(s)} (\nabla_t \Psi_n)_\theta^* dl \qquad (2.35.1)$$

$$S_{nm}^{(c)} = \frac{1}{k_{nTM}} \int_{L_1} M_{\theta_m}^{(c)} (\hat{a}_z \times \nabla_t \Phi_n)_\theta^* dl$$
$$S_{nm}^{(s)} = \frac{1}{k_{nTM}} \int_{L_1} M_{\theta_m}^{(s)} (\hat{a}_z \times \nabla_t \Phi_n)_\theta^* dl \qquad (2.35.2)$$

$$T_{nm}^{(c)} = \frac{1}{k_{nTE}} \int_{L_1} M_{z_m}^{(c)} \Psi_n^* dl$$
$$T_{nm}^{(s)} = \frac{1}{k_{nTE}} \int_{L_1} M_{z_m}^{(s)} \Psi_n^* dl \qquad (2.35.3)$$

When the sign (~) is added to each related terms in the expressions in eqn. (2.35), they can be used also for the hollow circular waveguide.

2.7 Preparation of Characteristic Matrix

The surface magnetic current amplitudes $a_{z_m}, b_{z_m}, a_{\theta_m}, b_{\theta_m}$ must be calculated together with the related wavenumbers to determine an eigenwave. For this purpose, the continuity of tangential fields at the slots is used. It is enough to satisfy the continuity of tangential components because the normal fields are related to the tangential fields by Maxwell's equations. So, the continuity of normal components will be satisfied automatically.

The continuity of the tangential electric fields was already proved at the previous arrangements. Therefore, only the continuity of the tangential magnetic fields remains to satisfy.

It will be enough to satisfy the continuity of the tangential magnetic fields at the first slot; because the magnetic fields at the other slots are directly related to the magnetic field at the first slot. Hence, the continuity of H_z and H_θ at first slot will be determined.

The problem will be decomposed into TE and TM problems and solved separately. The solutions in terms of TE and TM modes are formulated by equating the related component of tangential magnetic field.

TE Waves:

TE waves do not have E_z. So, M_t cannot be seen at slots. The current coefficients a_θ, b_θ (2.32) and the expressions u_n, v_n disappear related to M_t (2.33 and 2.34). That means TM amplitudes A, D and F disappear by the same way (2.20).

Here, the field components that result a power flow in the normal direction to the slot surface are considered. Since E_z is zero for TE mode, it is not possible to have any power flow at the radial direction related to H_θ. However, E_θ and H_z create a power flow at the radial direction, which is normal to the slot surface.

The boundary condition at the first slot will be focused on. To extend it to the other slot boundaries is straightforward. The continuity relation for H_z can be written using the expression in (2.4.4) as:

$$H_z\big|_{L_1} = \tilde{H}_z\big|_{L_1}$$

$$\sum_{n(q)} k_{nTE} G_n \Psi_n \Big|_{L_1} = \sum_{n(q)} \tilde{k}_{nTE} \tilde{G}_n \tilde{\Psi}_n \Big|_{L_1} \tag{2.36}$$

The direct MoM is the method defined by [13], by outlining a basic principle to implement weighted measures to give precise definitions to the eqn (2.36), which is not properly defined. The method consists of choosing M weighting (testing) functions and then taking an inner (scalar) product on (2.36) with each of the weighting functions, resulting in M precisely defined linear equations, which are then numerically solved by matrix methods for the M unknowns.

The surface magnetic current expansion functions will be used as testing functions (Galerkin's Method). In the case of suitably chosen surface magnetic current expansion functions; they converge rapidly to the exact fields at the slots.

In generalized MoM, the inner product is usually defined as in eqn (2.7). After testing the equality given in (2.36) with $M_{z_m}^{(c)}$ and $M_{z_m}^{(s)}$ (Galerkin's Method)

$$\sum_{n} k_{nTE} G_n \int_{L_1} \Psi_n M_{z_m}{}^* dl = \sum_{n(q)} \tilde{k}_{nTE} \tilde{G}_n \int_{L_1} \tilde{\Psi}_n M_{z_m}{}^* dl \,\forall m \tag{2.37}$$

is obtained. Here M_{z_m} is used in place of $M_{z_m}^{(c)}$ and $M_{z_m}^{(s)}$.

In the case of changing the above integrals with the definitions given in eqns (2.35), the equality becomes:

$$\sum_{n} G_n k_{nTE} T_{nm}^* = \sum_{n(q)} \tilde{G}_n \tilde{k}_{nTE} \tilde{T}_{nm}^* \tag{2.38}$$

Here T_{nm} is used in place of $T_{nm}^{(c)}$ and $T_{nm}^{(s)}$.

Applying eqn (2.21), u_n disappears and;

$$\sum_{n}\frac{k_{nTE}^{2}}{k_{nTE}^{2}-(k_{0}^{2}-\beta^{2})}w_{n}T_{nm}^{*}=\sum_{n(q)}\frac{\tilde{k}_{nTE}^{2}}{\tilde{k}_{nTE}^{2}-(k_{0}^{2}-\beta^{2})}\tilde{w}_{n}\tilde{T}_{nm}^{*} \tag{2.39}$$

is obtained.

Finally, instead of w_n, the series form defined in eqns (2.33) and (2.34) is substituted, and the linear homogeneous equality below is obtained:

$$\left[C^{(TE)}\right]\begin{bmatrix}\overline{a}_z\\ \overline{b}_z\end{bmatrix}=0 \tag{2.40}$$

The element of the matrix here is:

$$C_{nm}^{(TE)}=\sum_{i}\frac{k_{iTE}^{2}}{k_{iTE}^{2}-(k_{0}^{2}-\beta^{2})}T_{im}T_{in}^{*}+N\sum_{i(q)}\frac{\tilde{k}_{iTE}^{2}}{\tilde{k}_{iTE}^{2}-(k_{0}^{2}-\beta^{2})}\tilde{T}_{im}\tilde{T}_{in}^{*} \tag{2.41}$$

When M cosine and M sine terms are substituted instead of M_z, then the matrix $\left[C^{(TE)}\right]$ becomes a square matrix with dimension 2Mx2M. The dimension of the column vectors $\overline{a}_z$ and $\overline{b}_z$ is M. The T_{im} terms in the matrix $\left[C^{(TE)}\right]$ are marked with (c) at the left M columns and with (s) at the right M columns.

TM Waves:

Since H_z is equal to zero for TM waves, G_n is also equal to zero in (2.4.4).

$$G_n = 0 \ \Rightarrow \qquad \beta k_{nTE} u_n = (k_0^2 - \beta^2) w_n$$
$$\tilde{G}_n = 0 \ \Rightarrow \qquad \beta \tilde{k}_{nTE} \tilde{u}_n = (k_0^2 - \beta^2) \tilde{w}_n \tag{2.42}$$

So, it is possible to eliminate one of TE coefficients u_n or w_n. When the equality (2.42) is substituted in (2.21), for example for C_n, then:

$$Z_0 C_n = -\frac{k_0 k_{nTE}}{(k_0^2 - \beta^2)} u_n e^{j\beta z}$$
$$Z_0 \tilde{C}_n = -\frac{k_0 \tilde{k}_{nTE}}{(k_0^2 - \beta^2)} \tilde{u}_n e^{j\beta z} \tag{2.43}$$

For TM case, H_θ and E_z will create a power flow at the radial direction. So, by setting up the equality for H_θ according to (2.8):

$$H_\theta \big|_{L_1} = \tilde{H}_\theta \big|_{L_1}$$

$$[\sum_n C_n (\nabla_t \Psi_n) + \sum_n D_n (\hat{a}_z \times \nabla_t \Phi_n)] \cdot \hat{a}_\theta \bigg|_{L_1} = [\sum_{n(q)} \tilde{C}_n (\nabla_t \tilde{\Psi}_n) + \sum_{n(q)} \tilde{D}_n (\hat{a}_z \times \nabla_t \tilde{\Phi}_n)] \cdot \hat{a}_\theta \bigg|_{L_1} \tag{2.44}$$

In this case, M_{θ_m} will be used as testing functions and with the aid of the equality specified in (2.35) and the inner product (2.7), the expression

$$\sum_n C_n k_{nTE} R_{nm}^* + \sum_n D_n k_{nTM} S_{nm}^* = \sum_{n(q)} \tilde{C}_n \tilde{k}_{nTE} \tilde{R}_{nm}^* + \sum_{n(q)} \tilde{D}_n \tilde{k}_{nTM} \tilde{S}_{nm}^* \tag{2.45}$$

is obtained.

By substituting the equality given in eqn (2.43) in place of C_n and the equality given in eqn (2.22) in place of D_n, it can be reached that:

$$\sum_{n} -\frac{k_{nTE}^{2}}{(k_0^2-\beta^2)} u_n R_{nm}^{*} + \sum_{n} -\frac{k_{nTM}^{2}}{k_{nTM}^{2}-(k_0^2-\beta^2)} v_n S_{nm}^{*} =$$

$$= \sum_{n(q)} -\frac{\tilde{k}_{nTE}^{2}}{(k_0^2-\beta^2)} \tilde{u}_n \tilde{R}_{nm}^{*} + \sum_{n(q)} -\frac{\tilde{k}_{nTM}^{2}}{\tilde{k}_{nTM}^{2}-(k_0^2-\beta^2)} \tilde{v}_n \tilde{S}_{nm}^{*} \tag{2.46}$$

Finally, substituting the series expansions in eqns (2.33) and (2.34), the characteristic matrix for TM waves is obtained as:

$$\left[C^{(TM)} \right] \qquad \begin{bmatrix} \overline{a}_\theta \\ \overline{b}_\theta \end{bmatrix} = 0 \tag{2.47}$$

with the matrix elements:

$$C_{nm}^{(TM)} = -\sum_{i} \frac{k_{iTE}^{2}}{(k_0^2-\beta^2)} R_{im} R_{in}^{*} - N \sum_{i(q)} -\frac{\tilde{k}_{iTE}^{2}}{(k_0^2-\beta^2)} \tilde{R}_{im} \tilde{R}_{in}^{*} +$$

$$+ \sum_{i} \frac{k_{iTM}^{2}}{k_{iTM}^{2}-(k_0^2-\beta^2)} S_{im} S_{in}^{*} + N \sum_{i(q)} \frac{\tilde{k}_{iTM}^{2}}{\tilde{k}_{iTM}^{2}-(k_0^2-\beta^2)} \tilde{S}_{im} \tilde{S}_{in}^{*} \tag{2.48}$$

The same relations are valid for the characteristic matrix dimension and the indexing of the terms S_{im} and R_{im} as TE waves section.

2.8 Properties of Characteristic Matrix

The elements of the characteristic matrices of TE and TM waves have the products of similar types of coefficients such as $R_{im}^{(c)}$ and $R_{in}^{(s)}$. The field and current expansion functions determine these coefficients. The surface magnetic current expansion functions can have magnetic (cosine) and electric (sine) wall symmetry with respect to the point θ=0. Depending on the symmetry of the coefficient, the elements of the characteristic matrices can be real or imaginary or they can vanish.

The structure of the characteristic matrices is as below:

$$\left[C^{(TE/TM)}\right]=\begin{bmatrix}[A] & j[D] \\ -j[D]^T & [B]\end{bmatrix} \tag{2.49}$$

The eqn (2.49) can be rewritten as a real valued eigenvalue equation:

$$\left[C^{(TE/TM)}\right]\begin{bmatrix}\bar{a} \\ j\bar{b}\end{bmatrix}=\begin{bmatrix}[A] & [D] \\ [D]^T & [B]\end{bmatrix}\begin{bmatrix}a \\ jb\end{bmatrix}=0 \tag{2.50}$$

The relation between the free space wavenumber k_0, the cutoff wavenumber k_c (which is the vertical component of the wavenumber vector) and the propagation constant β (which is the longitudinal component of the wavenumber vector) is given by:

$$k_c^2=k_0^2-\beta^2 \tag{2.51}$$

The eigenvalues of k_c^2 are real and positive numbers since the characteristic matrices are Hermitian. The eigenvectors, $\bar{a}$ and $j\bar{b}$, which give the current amplitudes, are also real.

In general, the modes that belong to the slot mode order q and N-q have the same k_c^2 eigenvalues. However, the modes q and N-q are independent from each other. The θ-dependence of q mode in hollow circular waveguide is determined according the equality given in (2.30) by the orders given below:

…-q-2N, -q-N, -q, -q+N, -q+2N…= {p},

and they take the form for N-q mode as:

…-(N-q)-2N, -(N-q)-N, -(N-q), -(N-q)+N, -(N-q)+2N, ...=..., q-2N, q-N, q, q+N, q+2N,… = {-p}

The current-field relations for the orders {p} and {-p} are as follows:

$$\begin{aligned}\tilde{R}_{n(p)m} &= (\tilde{R}_{n(-p)m})^* \\ \tilde{S}_{n(p)m} &= (\tilde{S}_{n(-p)m})^* \\ \tilde{T}_{n(p)m} &= (\tilde{T}_{n(-p)m})^*\end{aligned} \tag{2.52}$$

The characteristic matrices of q and N-q modes are transpose conjugate and their eigenvectors are conjugate.

As special cases, when q=0 (zero phase difference between adjacent slots) or q=N/2 (adjacent slots are excited by inverse phase). In these cases, the transverse blocks of the characteristic matrices ($[D]$) vanish, since the components with the orders p and –p cancel each other according to the equality (2.52). The current coefficients that are related to the magnetic wall symmetry ($\overline{a}_z$ for TE case and $\overline{a}_\theta$ for TM case) and the electric wall symmetry ($\overline{b}_z$ for TE case and $\overline{b}_\theta$ for TM case), are decoupled. Thus, the dimension of the eigenvalue problem decreases to the half of the original one. For these cases, the modes with cosine (vertical) polarization (belonging to the magnetic wall symmetry of the current expansions) and with sine (horizontal) polarization (belonging to the electric wall symmetry of the current expansions) have different cutoff wavenumbers.

For the general case (excluding the same and the inverse phase cases), the addition of q and N-q modes forms standing waves with cosine and sine polarization. These two polarizations are independent of each other.

2.9 Determination of Field Expansion Functions

The elementary wave functions Ψ_n and Φ_n for a homogeneous source free region must satisfy the Helmholtz equation and the necessary boundary conditions.

The tangential component of electric field and the normal component of magnetic field vanish at the surface of a perfect conductor.

$$\hat{n}\times E\big|_c = \hat{n}\cdot H\big|_c = 0 \tag{2.53}$$

For this reason, it is necessary to formulate two different eigenvalue problems for TE and TM waves.

TE Eigenvalue problem (Neumann Problem):

$$\begin{aligned} &\nabla_t^2\Psi + (k_{TE})^2\Psi = 0 \\ &at \quad the \quad boundry: \frac{\partial\Psi}{\partial n}\Big|_C = 0 \end{aligned} \tag{2.54}$$

TM Eigenvalue problem (Dirichlet Problem):

$$\begin{aligned} &\nabla_t^2\Phi + (k_{TM})^2\Phi = 0 \\ &at \quad the \quad boundry: \Phi\big|_C = 0 \end{aligned} \tag{2.55}$$

TE field expansion functions for the hollow circular waveguide:

As a result of the method of separation of variables, the solution of Helmholtz equation can be written as:

$$\tilde{\Psi}_n = \tilde{C}_{TE_n} J_{p_n}(\tilde{k}_{nTE} r) e^{jp_n\theta} \tag{2.56}$$

$\tilde{C}_{TE_n}$ is the normalization constant and will be determined later. The boundary condition given below must be satisfied:

$$J'_{p_n}(\tilde{k}_{nTE} r)\big|_{r=a} = 0 \tag{2.57}$$

The gradient of elementary wave function for TE waves in cylindrical coordinate system is:

$$\begin{aligned}
\nabla_t \tilde{\Psi}_n &= \tilde{C}_{TE_n}(\tilde{k}_{nTE} J'_{p_n}(\tilde{k}_{nTE} r)\hat{a}_r + \frac{jp_n}{r} J_{p_n}(\tilde{k}_{nTE} r)\hat{a}_\theta) e^{jp_n\theta} \\
\nabla_t \tilde{\Psi}_n \times \hat{a}_z &= \tilde{C}_{TE_n}(\frac{jp_n}{r} J_{p_n}(\tilde{k}_{nTE} r)\hat{a}_r - \tilde{k}_{nTE} J'_{p_n}(\tilde{k}_{nTE} r)\hat{a}_\theta) e^{jp_n\theta}
\end{aligned} \tag{2.58}$$

TM field expansion functions for the hollow circular waveguide:

Similarly, the solution of Helmholtz equation can be written as;

$$\tilde{\Phi}_n = \tilde{C}_{TM_n} J_{p_n}(\tilde{k}_{nTM} r) e^{jp_n\theta} \tag{2.59}$$

$\tilde{C}_{TM_n}$ is the normalization constant and will be determined later. The boundary condition given below must be satisfied;

$$J_{p_n}(\tilde{k}_{nTM} r)\Big|_{r=a} = 0 \qquad (2.60)$$

The gradient of elementary wave function for TM waves in cylindrical coordinate system is;

$$\nabla_t \tilde{\Phi}_n = \tilde{C}_{TM_n}(\tilde{k}_{nTM} J'_{p_n}(\tilde{k}_{nTM} r)\hat{a}_r + \frac{jp_n}{r} J_{p_n}(\tilde{k}_{nTM} r)\hat{a}_\theta)e^{jp_n\theta}$$

$$\hat{a}_z \times \nabla_t \tilde{\Phi}_n = \tilde{C}_{TM_n}(-\frac{jp_n}{r} J_{p_n}(\tilde{k}_{nTM} r)\hat{a}_r + \tilde{k}_{nTM} J'_{p_n}(\tilde{k}_{nTM} r)\hat{a}_\theta)e^{jp_n\theta} \qquad (2.61)$$

TE field expansion functions for the first sector waveguide:

The following relation is used for the radial dependence of elementary wave function;

$$F_\mu^{(TE)}(kr) = Y'_\nu(kb)J_\nu(kr) - J'_\nu(kb)Y_\nu(kr) \qquad (2.62)$$

k is any wavenumber and r is any radial distance between the inner radius ‘a’ and the outer radius ‘b’.

TE modes at the first sector waveguide which satisfy the necessary boundary condition are specified by the wave functions

$$\Psi_n^{(1)} = C_{TE_n} F_{\mu_n}^{(TE)}(k_{nTE} r)\cos(\nu_n(\theta - \theta_n)) \qquad (2.63)$$

where C_{TE_n} is the normalization constant and will be determined later.

The values of k_{nTE}, ν_n, θ_n can be extracted using the boundary conditions (Neumann Problem). For the first sector waveguide;

$$\left.\frac{\partial \Psi_n^{(1)}}{\partial \theta}\right|_{\theta=-\frac{\Theta}{2}} = \left.\frac{\partial \Psi_n^{(1)}}{\partial \theta}\right|_{\theta=\frac{\Theta}{2}} = 0 \qquad \forall a \le r \le b$$

$$\left.\frac{\partial \Psi_n^{(1)}}{\partial r}\right|_{r=a} = \left.\frac{\partial \Psi_n^{(1)}}{\partial r}\right|_{r=b} = 0 \qquad \forall |\theta| \le \frac{\Theta}{2} \tag{2.64}$$

Using the conditions above;

$$F_{\mu}^{(TE)'}(k_{nTE} r)\big|_{r=a} = 0 \tag{2.65}$$

and

$$\nu_n = \mu_n \frac{\pi}{\Theta}; \qquad \mu_n \in \mathrm{N}_0$$

$$\nu_n \theta_n = \mu_n \frac{\pi}{2} \tag{2.66}$$

can be written.

The gradient of elementary wave function for TE waves in cylindrical coordinate system is;

$$\nabla_t \Psi_n^{(1)} = C_{TE_n}[k_{nTE} F_{\mu_n}^{(TE)'}(k_{nTE} r)\cos(\nu_n(\theta-\theta_n))\hat{a}_r - \frac{\nu_n}{r} F_{\mu_n}^{(TE)}(k_{nTE} r)\sin(\nu_n(\theta-\theta_n))\hat{a}_\theta]$$

$$\nabla_t \Psi_n^{(1)} \times \hat{a}_z = C_{TE_n}[-\frac{\nu_n}{r} F_{\mu_n}^{(TE)}(k_{nTE} r)\sin(\nu_n(\theta-\theta_n))\hat{a}_r - k_{nTE} F_{\mu_n}^{(TE)'}(k_{nTE} r)\cos(\nu_n(\theta-\theta_n))\hat{a}_\theta] \tag{2.67}$$

TM field expansion functions for the first sector waveguide:

The following relation is used for the radial dependence of elementary wave function;

$$F_{\mu}^{(TM)}(kr) = Y_{\nu}(kb)J_{\nu}(kr) - J_{\nu}(kb)Y_{\nu}(kr) \tag{2.68}$$

TM modes at the first sector waveguide which satisfy the necessary boundary condition are specified by the wave functions

$$\Phi_n^{(1)} = C_{TM_n} F_{\mu_n}^{(TM)}(k_{nTM} r)\sin(\nu_n(\theta - \theta_n)) \tag{2.69}$$

where C_{TM_n} is the normalization constant and will be determined later.

The values of k_{nTE}, ν_n, θ_n can be extracted using the boundary conditions (Dirichlet Problem). For the first sector waveguide;

$$\begin{aligned} &\Phi_n^{(1)}\Big|_{\theta=-\frac{\Theta}{2}} = \Phi_n^{(1)}\Big|_{\theta=\frac{\Theta}{2}} = 0 \qquad \forall a \le r \le b \\ &\Phi_n^{(1)}\Big|_{r=a} = \Phi_n^{(1)}\Big|_{r=b} = 0 \qquad \forall |\theta| \le \frac{\Theta}{2} \end{aligned} \tag{2.70}$$

the boundary conditions result in;

$$F_{\mu}^{(TM)}(k_{nTM} r)\Big|_{r=a} = 0 \tag{2.71}$$

and the expressions for ν_n, θ_n are the same as given in (2.66).

The gradient of elementary wave function for TM waves in cylindrical coordinate system is;

$$\nabla_t \Phi_n^{(1)} = C_{TM_n}(k_{nTM} F_{\mu_n}^{(TM)\prime}(k_{nTM} r)\sin(\nu_n(\theta-\theta_n))\hat{a}_r + \frac{\nu_n}{r} F_{\mu_n}^{(TM)}(k_{nTM} r)\cos(\nu_n(\theta-\theta_n))\hat{a}_\theta)$$

$$\begin{aligned} \hat{a}_z \times \nabla_t \Phi_n^{(1)} = C_{TM_n}(-\frac{\nu_n}{r} F_{\mu_n}^{(TM)}(k_{nTM} r)\cos(\nu_n(\theta-\theta_n))\hat{a}_r + \\ + k_{nTM} F_{\mu_n}^{(TM)\prime}(k_{nTM} r)\sin(\nu_n(\theta-\theta_n))\hat{a}_\theta) \end{aligned} \tag{2.72}$$

Normalizations:

The field expansion functions contain arbitrary amplitude factors and they are normalized using the orthogonality properties. The relations given in (2.5) and (2.6) can be derived with appropriate normalizations:

$$\begin{aligned} &\int_{S_0} \tilde{\Psi}_n \tilde{\Psi}_n^{(*)} dS = \frac{1}{(\tilde{k}_{nTE})^2} \\ &\int_{S_0} \tilde{\Phi}_n \tilde{\Phi}_n^{*} dS = \frac{1}{(\tilde{k}_{nTM})^2} \\ &\int_{S_1} (\Psi_n^{(1)})^2 dS = \frac{1}{(k_{nTM})^2} \\ &\int_{S_1} (\Phi_n^{(1)})^2 dS = \frac{1}{(k_{nTE})^2} \end{aligned} \tag{2.73}$$

These integrals can be solved analytically and the following field normalization constants are obtained [1]:

$$\tilde{C}_{TE_n} = \frac{1}{\sqrt{\pi}} \frac{1}{(\tilde{k}_{nTE} a)} \frac{1}{\sqrt{1-(\frac{p_n}{\tilde{k}_{nTE}})^2} J_{p_n}(\tilde{k}_{nTE} a)} \tag{2.74.1}$$

$$\tilde{C}_{TM_n} = \frac{1}{\sqrt{\pi}} \frac{1}{(\tilde{k}_{nTM} a)} \frac{1}{J'_{p_n}(\tilde{k}_{nTM} a)} \tag{2.74.2}$$

$$C_{TE_n} = \sqrt{2\frac{2-\delta_{\mu_n 0}}{\Theta}} \frac{1}{(k_{nTE} a)} \frac{1}{\sqrt{(\frac{b}{a})^2 (1-(\frac{\nu_n}{(k_{nTE} b)})^2) \frac{4}{\pi^2 (k_{nTE} b)^2} - (1-(\frac{\nu_n}{(k_{nTE} a)})^2)(F_{\mu_n}^{(TE)}(k_{nTE} a))^2}}$$

$$C_{TM_n} = \sqrt{2\frac{2-\delta_{\mu_n 0}}{\Theta}} \frac{1}{(k_{nTM} a)} \frac{1}{\sqrt{\frac{4}{\pi^2 (k_{n_{TM}} a)^2} - (F_{\mu_n}^{(TM)'}(k_{n_{TM}} a))^2}} \tag{2.74.4}$$

δ is the Kronecker delta.

2.10 Edge Condition

In the structure under consideration, there is more than one inner edge. The edge condition is a constraint that is needed for a unique and effective solution whenever a geometric singularity, such as a sharp edge, exists.

The edge condition states that the energy density in the vicinity of an edge, or any geometrical singularity, must be integrable; that is,

$$\iiint_V (\varepsilon_0 E \cdot E^* + \mu_0 H \cdot H^*) dV < \infty \tag{2.75}$$

where V is any volume region containing the corner. The edge condition dictates that the edge shall not radiate any energy because it is not a source.

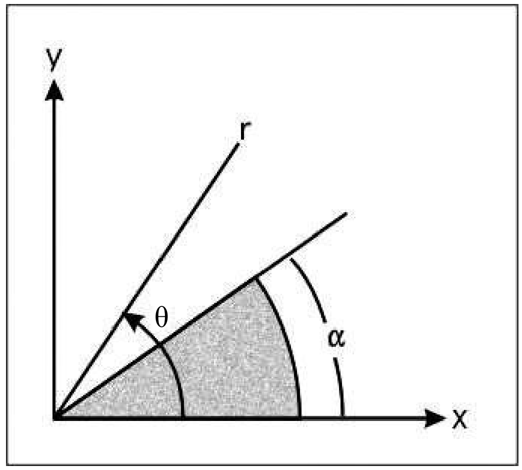

Figure 2.5 Perfectly conducting wedge.

The two-dimensional perfectly-conducting wedge shown in Fig. 2.5 can represent many edge problems. To satisfy the boundary conditions, the transverse components of either E or H fields, denoted by E_t and H_t, respectively, may be singular near the edge along the z-axis, while the rest of the field components are regular.

The fields at the perfectly conducting wedge can be expanded by cylindrical functions. To satisfy the boundary conditions (Dirichlet for E_z and Neumann for H_z) E_z and H_z can be expressed by;

$$\begin{aligned} E_z &\propto J_\nu(kr)\sin(\nu(\theta-\alpha)) \\ H_z &\propto J_\nu(kr)\cos(\nu(\theta-\alpha))+const \end{aligned} \tag{2.76}$$

and

$$\nu=\frac{n\pi}{2\pi-\alpha} \quad ; \quad n\in \mathrm{N} \tag{2.77}$$

For the wedge problem in Fig. 2.5, the edge condition stated in eqn. (2.75) takes the following simple and useful form: as r approaches zero, the field components near the edge cannot be more singular than the following expressions:

$$\begin{aligned} &E_z \propto r^{\nu} && H_z \propto r^{\nu} + const \\ &E_\theta \propto r^{\nu-1} && H_\theta \propto r^{\nu-1} \\ &E_r \propto r^{\nu-1} && H_r \propto r^{\nu-1} \end{aligned} \tag{2.78}$$

And at the edge, the minimum allowed value of ν is:

$$\nu = \frac{\pi}{2\pi - \alpha} \tag{2.79}$$

For waveguides and periodic structures having edges, the edge condition is used to truncate the number of modes and, in particular, to achieve relative convergence, which is essential to numerical accuracy.

2.11 Selection of Current Expansion Functions

In the structure in Fig.2.1, the inner edges with the angle of 90^{o} are appeared at the boundary between hollow circular and sector waveguide parts. According to eqn (2.79), the characteristic exponent ν gives the result of ν =2/3 for the edge condition. This means that the transverse field components become singular at the edges, and that the longitudinal components remain regular. If r is taken as distance from the associated edge, according to eqn (2.78), near the edges E_z and E_θ become:

$$\begin{aligned} &E_z \propto r^{2/3} \\ &E_\theta \propto r^{-1/3} \end{aligned} \tag{2.80}$$

To guarantee numerical efficiency, the basis functions should include the singular nature of the transverse electric field at the sharp metallic edges of the discontinuity. In the present situation, the component of the electric field perpendicular to the metallic edge becomes infinite since it is related to $r^{-1/3}$ where r is the radial distance from the edge where as the component parallel to the edge vanishes as r goes to zero since it is related to $r^{2/3}$.

According to eqns (2.1), E_z and E_θ are proportional to the surface magnetic current components M_t and M_z, respectively, at the slots. To optimize the convergence of the current expansion functions, it is required to specify the current expansion functions to satisfy the edge condition by taking into account the field behaviour at the slot edges. The dimensions of characteristic matrices relatively become smaller and the current expansions converge well with the edge conditioned basis functions. So, the calculation process becomes easier.

The possible complete series for current expansions can be specified by the modified cosine half-waves (cos-symmetry regarding the edges at ±Θ/2) and modified sine half-waves (sin-symmetry regarding the edges). Cosine and Sine functions constitute a complete set. The basis functions are modified by appropriate edge condition.

The modification function is chosen as:

$$
\begin{aligned}
&m(\theta) = \sqrt[3]{(\frac{\Theta}{2})^2 - \theta^2} \\
&\lim_{\theta \to \pm\frac{\Theta}{2}} (m(\theta)) \propto (\frac{\Theta}{2} - \theta)^{-1/3}
\end{aligned}
\tag{2.81}
$$

Therefore, the following series expansions fulfil the boundary and edge conditions at the slot interfaces [1]:

$$M_z = \sum_{m=0,2,4...} a_{z_m} k_{z_m}^{(c)} \frac{\cos(m\frac{\pi}{\Theta}\theta)}{((\frac{\Theta}{2})^2 - \theta^2)^{1/3}} + \sum_{m=1,3,5,...} b_{z_m} k_{z_m}^{(s)} \frac{\sin(m\frac{\pi}{\Theta}\theta)}{((\frac{\Theta}{2})^2 - \theta^2)^{1/3}}$$

(2.82)

$$M_\theta = j(\sum_{m=1,3,5,...} a_{\theta_m} k_{\theta_m}^{(c)} \frac{\cos(m\frac{\pi}{\Theta}\theta)}{((\frac{\Theta}{2})^2 - \theta^2)^{1/3}} + \sum_{m=2,4,6,...} b_{\theta_m} k_{\theta_m}^{(s)} \frac{\sin(m\frac{\pi}{\Theta}\theta)}{((\frac{\Theta}{2})^2 - \theta^2)^{1/3}})$$

It is obvious that the current expansion functions corresponding to M_z (or E_θ) tend to infinity at the slot edges, whereas the ones corresponding to M_θ (E_z) vanish at $\theta=\pm\Theta/2$.

Current Normalizations:

The current expansion functions are required to be normalized to the same vector length to improve the behaviour of the characteristic matrices and to obtain equal current amplitudes.

The expressions below will be used as the normalization condition:

$$\int_{L_1} (M_{z_m}^{(c)})^2 dl = \frac{1}{\Theta a} \qquad \forall m$$

$$\int_{L_1} (M_{z_m}^{(s)})^2 dl = \frac{1}{\Theta a} \qquad \forall m$$

(2.83)

$$\int_{L_1} (M_{\theta_m}^{(c)})^2 dl = \frac{1}{\Theta a} \qquad \forall m$$

$$\int_{L_1} (M_{\theta_m}^{(s)})^2 dl = \frac{1}{\Theta a} \qquad \forall m$$

Θa is the integration length (slot length).

These integrals can be solved analytically. Using the following definition:

$$J_n(x) = \frac{(\frac{x}{2})^n}{\sqrt{\pi}\Gamma(n+\frac{1}{2})} \int_{-1}^{1} (1-t^2)^{n-1/2} \cos(xt)dt \tag{2.84}$$

and substituting n=-1/6, the following current normalizations are obtained [17]:

$$k_{z_m}^{(c)} = \frac{1}{a}(\frac{\Theta}{2})^{-\frac{1}{3}} \sqrt{\frac{\Gamma(\frac{5}{6})}{\sqrt{\pi}\Gamma(\frac{1}{3})}} \left\{ \begin{array}{lll} \dfrac{1}{\sqrt{1+\Gamma(\frac{5}{6})(\frac{m\pi}{2})^{\frac{1}{6}} J_{-1/6}(m\pi)}} & for & m = 2,4,6,... \\ \dfrac{1}{\sqrt{2}} & for & m = 0 \end{array} \right\}$$

$$k_{z_m}^{(s)} = \frac{1}{a}(\frac{\Theta}{2})^{-\frac{1}{3}} \sqrt{\frac{\Gamma(\frac{5}{6})}{\sqrt{\pi}\Gamma(\frac{1}{3})}} \frac{1}{\sqrt{1-\Gamma(\frac{5}{6})(\frac{m\pi}{2})^{\frac{1}{6}} J_{-1/6}(m\pi)}} \qquad for \quad m = 1,3,5,..$$

$$k_{\theta_m}^{(c)} = \frac{1}{a}(\frac{\Theta}{2})^{-\frac{1}{3}} \sqrt{\frac{\Gamma(\frac{5}{6})}{\sqrt{\pi}\Gamma(\frac{1}{3})}} \frac{1}{\sqrt{1+\Gamma(\frac{5}{6})(\frac{m\pi}{2})^{\frac{1}{6}} J_{-1/6}(m\pi)}} \qquad for \quad m = 1,3,5,..$$

$$k_{\theta_m}^{(s)} = \frac{1}{a}(\frac{\Theta}{2})^{-\frac{1}{3}} \sqrt{\frac{\Gamma(\frac{5}{6})}{\sqrt{\pi}\Gamma(\frac{1}{3})}} \frac{1}{\sqrt{1-\Gamma(\frac{5}{6})(\frac{m\pi}{2})^{\frac{1}{6}} J_{-1/6}(m\pi)}} \qquad for \quad m = 2,4,6,..$$

(2.85)

where $\Gamma(x)$ is the gamma function.

2.12 Determination of Current-Field Coupling

It is necessary to solve the line integrals specified in (2.35). The integrands are the products of the current and field expansion functions and the integration length is one slot length (Θa). It will be done along the first slot.

The Euler Identity gives a relationship between real sinusoidal functions and the complex exponential functions.

$$e^{j\theta} = \cos(\theta) + j\sin(\theta) \tag{2.86}$$

By using this relationship, it is possible to express the θ-dependency of the field expansion functions by sine and cosine functions. Also, it is known that the θ-dependent terms of the current expansion functions are composed of modified cosine and modified sine functions. Considering the orthogonality relation between sinusoidal functions, it can be seen that the integral of the product of sine and cosine functions along θ will vanish [17]. So, the current functions are related only to the field functions, which have the same wall symmetry. Through the equation (2.84), the integrals of θ-dependent terms are as follows [17]:

$$\begin{Bmatrix} I_{z_c}(\mu,m) \\ I_{\theta_c}(\mu,m) \end{Bmatrix} = \int_{-\frac{\Theta}{2}}^{\frac{\Theta}{2}} \frac{\cos(\mu\frac{\pi}{\Theta}\theta)\cos(m\frac{\pi}{\Theta}\theta)}{\sqrt[3]{(\frac{\Theta}{2})^2-\theta^2}}\,d\theta$$

$$= \frac{\sqrt{\pi}}{2}(\frac{\Theta}{2})^{\frac{1}{3}}\Gamma(\frac{2}{3})\begin{Bmatrix} \dfrac{J_{1/6}(|m-\mu|\frac{\pi}{2})}{\sqrt[6]{|m-\mu|\frac{\pi}{4}}}+\dfrac{J_{1/6}(|m+\mu|\frac{\pi}{2})}{\sqrt[6]{|m+\mu|\frac{\pi}{4}}} & for \quad m\neq\mu \\ \dfrac{1}{\Gamma(\frac{7}{6})}+\dfrac{J_{1/6}(|m+\mu|\frac{\pi}{2})}{\sqrt[6]{|m+\mu|\frac{\pi}{4}}} & for \quad m=\mu\neq 0 \\ \dfrac{2}{\Gamma(\frac{7}{6})} & for \quad m=\mu=0 \end{Bmatrix}$$

(2.87)

$$\begin{Bmatrix} I_{z_s}(\mu,m) \\ I_{\theta_s}(\mu,m) \end{Bmatrix} = \int_{-\frac{\Theta}{2}}^{\frac{\Theta}{2}} \frac{\sin(\mu\frac{\pi}{\Theta}\theta)\sin(m\frac{\pi}{\Theta}\theta)}{\sqrt[3]{(\frac{\Theta}{2})^2-\theta^2}}\,d\theta$$

$$= \frac{\sqrt{\pi}}{2}(\frac{\Theta}{2})^{\frac{1}{3}}\Gamma(\frac{2}{3})\begin{Bmatrix} \dfrac{J_{1/6}(|m-\mu|\frac{\pi}{2})}{\sqrt[6]{|m-\mu|\frac{\pi}{4}}}-\dfrac{J_{1/6}(|m+\mu|\frac{\pi}{2})}{\sqrt[6]{|m+\mu|\frac{\pi}{4}}} & for \quad m\neq\mu \\ \dfrac{1}{\Gamma(\frac{7}{6})}-\dfrac{J_{1/6}(|m+\mu|\frac{\pi}{2})}{\sqrt[6]{|m+\mu|\frac{\pi}{4}}} & for \quad m=\mu\neq 0 \end{Bmatrix}$$

(2.88)

$$\begin{Bmatrix} \tilde{I}_{z_c}(p,m) \\ \tilde{I}_{\theta_c}(p,m) \end{Bmatrix} = \int_{-\frac{\Theta}{2}}^{\frac{\Theta}{2}} \frac{\cos(p\theta)\cos(m\frac{\pi}{\Theta}\theta)}{\sqrt[3]{(\frac{\Theta}{2})^2-\theta^2}} d\theta$$

$$= \frac{\sqrt{\pi}}{2}(\frac{\Theta}{2})^{\frac{1}{3}}\Gamma(\frac{2}{3}) \begin{Bmatrix} \dfrac{J_{1/6}(\frac{|m\pi-|p|\Theta|}{2})}{\sqrt[6]{\frac{|m\pi-|p|\Theta|}{4}}} + \dfrac{J_{1/6}(\frac{|m\pi+|p|\Theta|}{2})}{\sqrt[6]{\frac{|m\pi+|p|\Theta|}{4}}} & for \quad m\pi \neq |p|\Theta \\ \dfrac{1}{\Gamma(\frac{7}{6})} + \dfrac{J_{1/6}(|p|\Theta)}{\sqrt[6]{|p|\frac{\Theta}{2}}} & for \quad m\pi = |p|\Theta \neq 0 \\ \dfrac{2}{\Gamma(\frac{7}{6})} & for \quad m\pi = |p|\Theta = 0 \end{Bmatrix}$$

(2.89)

$$\begin{Bmatrix} \tilde{I}_{z_s}(p,m) \\ \tilde{I}_{\theta_s}(p,m) \end{Bmatrix} = \int_{-\frac{\Theta}{2}}^{\frac{\Theta}{2}} \frac{\sin(p\theta)\sin(m\frac{\pi}{\Theta}\theta)}{\sqrt[3]{(\frac{\Theta}{2})^2-\theta^2}} d\theta$$

$$= \mathrm{sgn}(p)\frac{\sqrt{\pi}}{2}(\frac{\Theta}{2})^{\frac{1}{3}}\Gamma(\frac{2}{3}). \begin{Bmatrix} \dfrac{J_{1/6}(\frac{|m\pi-|p|\Theta|}{2})}{\sqrt[6]{\frac{|m\pi-|p|\Theta|}{4}}} - \dfrac{J_{1/6}(\frac{|m\pi+|p|\Theta|}{2})}{\sqrt[6]{\frac{|m\pi+|p|\Theta|}{4}}} & for \quad m\pi \neq |p|\Theta \\ \dfrac{1}{\Gamma(\frac{7}{6})} - \dfrac{J_{1/6}(|p|\Theta)}{\sqrt[6]{|p|\frac{\Theta}{2}}} & for \quad m\pi = |p|\Theta \neq 0 \end{Bmatrix}$$

(2.90)

The field expansion functions defined in Section 2.8 are inserted instead of current-field relations specified in equation (2.35) and then, it is found out that:

$$
\begin{aligned}
R_{nm}^{(c)} &= -\frac{\nu_n}{(k_{nTE}a)} C_{TE_n} k_{\theta_m}^{(c)} a F_{\mu_n}^{(TE)}(k_{nTE}a) I_{\theta_c}(\mu_n, m) \sin(\mu_n \frac{\pi}{2}) \\
R_{nm}^{(s)} &= -\frac{\nu_n}{(k_{nTE}a)} C_{TE_n} k_{\theta_m}^{(s)} a F_{\mu_n}^{(TE)}(k_{nTE}a) I_{\theta_s}(\mu_n, m) \cos(\mu_n \frac{\pi}{2}) \\
\tilde{R}_{nm}^{(c)} &= -j \frac{p_n}{(\tilde{k}_{nTE}a)} \tilde{C}_{TE_n} k_{\theta_m}^{(c)} a J_{p_n}(\tilde{k}_{nTE}a) \tilde{I}_{\theta_c}(p_n, m) \\
\tilde{R}_{nm}^{(s)} &= -\frac{p_n}{(\tilde{k}_{nTE}a)} \tilde{C}_{TE_n} k_{\theta_m}^{(s)} a J_{p_n}(\tilde{k}_{nTE}a) \tilde{I}_{\theta_s}(p_n, m)
\end{aligned}
\tag{2.91}
$$

$$
\begin{aligned}
S_{nm}^{(c)} &= C_{TM_n} k_{\theta_m}^{(c)} a F_{\mu_n}^{(TM)\prime}(k_{nTM}a) I_{\theta_c}(\mu_n, m) \sin(\mu_n \frac{\pi}{2}) \\
S_{nm}^{(s)} &= C_{TM_n} k_{\theta_m}^{(s)} a F_{\mu_n}^{(TM)\prime}(k_{nTM}a) I_{\theta_s}(\mu_n, m) \cos(\mu_n \frac{\pi}{2}) \\
\tilde{S}_{nm}^{(c)} &= \tilde{C}_{TM_n} k_{\theta_m}^{(c)} a J'_{p_n}(\tilde{k}_{nTM}a) \tilde{I}_{\theta_c}(p_n, m) \\
\tilde{S}_{nm}^{(s)} &= -j\tilde{C}_{TM_n} k_{\theta_m}^{(s)} a J'_{p_n}(\tilde{k}_{nTM}a) \tilde{I}_{\theta_s}(p_n, m)
\end{aligned}
\tag{2.92}
$$

$$
\begin{aligned}
T_{nm}^{(c)} &= C_{TE_n} k_{z_m}^{(c)} a F_{\mu_n}^{(TE)}(k_{nTE}a) I_{z_c}(\mu_n, m) \cos(\mu_n \frac{\pi}{2}) \\
T_{nm}^{(s)} &= -C_{TE_n} k_{z_m}^{(s)} a F_{\mu_n}^{(TE)}(k_{nTE}a) I_{z_s}(\mu_n, m) \sin(\mu_n \frac{\pi}{2}) \\
\tilde{T}_{nm}^{(c)} &= \tilde{C}_{TE_n} k_{z_m}^{(c)} a J_{p_n}(\tilde{k}_{nTE}a) \tilde{I}_{z_c}(p_n, m) \\
\tilde{T}_{nm}^{(s)} &= -j\tilde{C}_{TE_n} k_{z_m}^{(s)} a J_{p_n}(\tilde{k}_{nTE}a) \tilde{I}_{z_s}(p_n, m)
\end{aligned}
\tag{2.93}
$$

2.13 Field Coefficients and Polarizations

In this section, the relation between the expansion coefficients of the transverse fields for both TE and TM waves will be shown.

Substituting the expressions given in (2.42) into the equality (2.21) eliminates the terms 'w_n' at the field amplitudes and the following equalities are obtained:

TM waves:

$$A_n = \frac{\beta k_{nTM} v_n}{k_{nTM}^2 - (k_0^2 - \beta^2)} e^{j\beta z} \qquad D_n = \frac{1}{Z_0} \frac{k_0 k_{nTM} v_n}{k_{nTM}^2 - (k_0^2 - \beta^2)} e^{j\beta z}$$

$$B_n = -\frac{\beta k_{nTE} u_n}{(k_0^2 - \beta^2)} e^{j\beta z} \qquad C_n = -\frac{1}{Z_0} \frac{k_0 k_{nTE} u_n}{(k_0^2 - \beta^2)} e^{j\beta z} \qquad (2.94)$$

$$jF_n = \frac{-k_{nTM}^2 v_n}{k_{nTM}^2 - (k_0^2 - \beta^2)} e^{j\beta z} \qquad jG_n = 0$$

TE waves:

$$A_n = 0 \qquad D_n = 0$$

$$B_n = -\frac{k_{nTE}^2 w_n}{k_{nTE}^2 - (k_0^2 - \beta^2)} e^{j\beta z} \qquad C_n = -\frac{1}{Z_0} \frac{\frac{\beta}{k_0} k_{nTE}^2 w_n}{k_{nTE}^2 - (k_0^2 - \beta^2)} e^{j\beta z}$$

$$jF_n = 0 \qquad jG_n = \frac{1}{Z_0} \frac{\frac{k_{nTE}}{k_0} (k_0^2 - \beta^2) w_n}{k_{nTE}^2 - (k_0^2 - \beta^2)} e^{j\beta z}$$

$$(2.95)$$

The relation between transverse field amplitudes of a TM wave can be expressed as:

$$B_n = \frac{\beta}{k_0} Z_0 C_n = Z_{TM} C_n$$
$$A_n = \frac{\beta}{k_0} Z_0 D_n = Z_{TM} D_n \tag{2.96}$$

The transverse fields are related to each other in the same way as in the case of uniform plane waves propagating in the z- direction, that is, they are perpendicular to each other and their cross product points in the z-direction and they satisfy:

$$E_t^{(TM)} = Z_{TM} \cdot (H_t^{(TM)} \times \hat{a}_z) \tag{2.97}$$

where Z_{TM} is the transverse wave impedance and equal to

$$Z_{TM} = \frac{\beta}{k_0} Z_0 \tag{2.98}$$

Similarly, the relation between the transverse field amplitudes of TE waves can be expressed as:

$$C_n = \frac{\beta}{k_0 Z_0} B_n = Y_{TE} B_n$$
$$A_n = D_n = 0 \tag{2.99}$$

And the relation between the transverse field components of TE waves is:

$$H_t^{(TE)} = Y_{TE} \cdot (\hat{a}_z \times E_t^{(TE)}) \tag{2.100}$$

where Y_{TE} is the transverse wave admittance and can be expressed as:

$$Y_{TE} = \frac{\beta}{k_0}\frac{1}{Z_0} \tag{2.101}$$

The field components will be examined in the following sections. As it is shown in section (2.7), the modes related to the phase factor q are complex conjugates of the modes related to the phase factor (N-q) at the slots. The field components related to q and N-q modes can be explained as the waves moving forward and backward at the azimuthal direction. When they are added to each other, a real valued standing wave is obtained and when they are subtracted, at this time, a fully imaginary standing wave is coming up. In this manner, two different types of polarizations (cosine and sine) that a hollow cylindrical waveguide can have are obtained.

So, it can be concluded that the field components with cosine polarization are the real parts of a q mode and the field components with sine polarization are the imaginary part of a q mode. Only for the same and inverse phase cases, field components become fully real ($\vec{b} = 0; \vec{a} \neq 0$) or imaginary ($\vec{a} = 0; \vec{b} \neq 0$). That means in these special cases, a single polarization is available for the related modes of the slotted waveguide.

2.14 Determination of the Elements of the Characteristic Matrices

The elements of the characteristic matrices for TE and TM modes can be expressed by substituting the equations (2.91), (2.92) and (2.93) into the equations (2.41) and (2.48) as follows:

TE Waves:

The summation term for hollow circular waveguide is:

$$\sum_i \frac{\tilde{k}_{iTE}^2}{\tilde{k}_{iTE}^2 - k_c^2} \tilde{T}_{im} \tilde{T}_{in}^* =$$
$$= \sum_i \frac{\tilde{k}_{iTE}^2}{\tilde{k}_{iTE}^2 - k_c^2} \begin{Bmatrix} k_{z_m}^{(c)} a \tilde{I}_{z_c}(p_i, m) \\ -jk_{z_m}^{(s)} a \tilde{I}_{z_s}(p_i, m) \end{Bmatrix} \begin{Bmatrix} k_{z_n}^{(c)} a \tilde{I}_{z_c}(p_i, n) \\ jk_{z_n}^{(s)} a \tilde{I}_{z_s}(p_i, n) \end{Bmatrix} . (\tilde{C}_{TE_i})^2 J_{p_i}^2(\tilde{k}_{iTE} a)$$

$$= \begin{Bmatrix} k_{z_m}^{(c)} a \\ -jk_{z_m}^{(s)} a \end{Bmatrix} \begin{Bmatrix} k_{z_n}^{(c)} a \\ jk_{z_n}^{(s)} a \end{Bmatrix} \sum_{p(q)} \begin{Bmatrix} \tilde{I}_{z_c}(p, m) \\ \tilde{I}_{z_s}(p, m) \end{Bmatrix} \begin{Bmatrix} \tilde{I}_{z_c}(p, n) \\ \tilde{I}_{z_s}(p, n) \end{Bmatrix} . \sum_{i(p)} \frac{\tilde{k}_{iTE}^2}{\tilde{k}_{iTE}^2 - k_c^2} (\tilde{C}_{TE_i})^2 J_p^2(\tilde{k}_{iTE} a)$$

(2.102)

And for sector waveguide:

$$\sum_i \frac{k_{iTE}^2}{k_{iTE}^2 - k_c^2} T_{im} T_{in} =$$
$$= \sum_i \frac{k_{iTE}^2}{k_{iTE}^2 - k_c^2} \begin{Bmatrix} k_{z_m}^{(c)} a I_{z_c}(\mu_i, m) \cos(\mu_i \frac{\pi}{2}) \\ -k_{z_m}^{(s)} a I_{z_s}(\mu_i, m) \sin(\mu_i \frac{\pi}{2}) \end{Bmatrix} \begin{Bmatrix} k_{z_n}^{(c)} a I_{z_c}(\mu_i, n) \cos(\mu_i \frac{\pi}{2}) \\ -k_{z_n}^{(s)} a I_{z_s}(\mu_i, n) \sin(\mu_i \frac{\pi}{2}) \end{Bmatrix} .$$
$$. (C_{TE_i})^2 (F_{\mu_i}^{(TE)}(k_{iTE} a))^2$$

$$= \begin{Bmatrix} k_{z_m}^{(c)} a \\ k_{z_m}^{(s)} a \end{Bmatrix} \begin{Bmatrix} k_{z_n}^{(c)} a \\ k_{z_n}^{(s)} a \end{Bmatrix} \sum_{\mu} \begin{Bmatrix} I_{z_c}(\mu, m) \cos(\mu \frac{\pi}{2}) \\ I_{z_s}(\mu, m) \sin(\mu \frac{\pi}{2}) \end{Bmatrix} \begin{Bmatrix} I_{z_c}(\mu, n) \cos(\mu \frac{\pi}{2}) \\ I_{z_s}(\mu, n) \sin(\mu \frac{\pi}{2}) \end{Bmatrix} .$$
$$. \sum_{i(\mu)} \frac{k_{iTE}^2}{k_{iTE}^2 - k_c^2} (C_{TE_i})^2 (F_{\mu_i}^{(TE)}(k_{iTE} a))^2$$

(2.103)

TM waves:

The summation term for hollow circular waveguide is:

$$-\sum_i \frac{\tilde{k}_{iTE}^2}{k_c^2} \tilde{R}_{im}\tilde{R}_{in}^* + \sum_i \frac{\tilde{k}_{iTM}^2}{\tilde{k}_{iTM}^2 - k_c^2} \tilde{S}_{im}\tilde{S}_{in}^* =$$

$$= -\sum_i \frac{\tilde{k}_{iTE}^2}{k_c^2} \begin{Bmatrix} -jk_{\theta_m}^{(c)} a\tilde{I}_{\theta_c}(p_i,m) \\ -k_{\theta_m}^{(s)} a\tilde{I}_{\theta_s}(p_i,m) \end{Bmatrix} \begin{Bmatrix} k_{\theta_n}^{(c)} a\tilde{I}_{\theta_c}(p_i,n) \\ jk_{\theta_n}^{(s)} a\tilde{I}_{\theta_s}(p_i,n) \end{Bmatrix}.$$

$$.(\tilde{C}_{TE_i})^2 \frac{p_i^2}{\tilde{k}_{iTE}^2} J_{p_i}^2(\tilde{k}_{iTE}a)$$

$$+\sum_i \frac{\tilde{k}_{iTM}^2}{\tilde{k}_{iTM}^2 - k_c^2} \begin{Bmatrix} k_{\theta_m}^{(c)} a\tilde{I}_{\theta_c}(p_i,m) \\ -jk_{\theta_m}^{(s)} a\tilde{I}_{\theta_s}(p_i,m) \end{Bmatrix} \begin{Bmatrix} k_{\theta_n}^{(c)} a\tilde{I}_{\theta_c}(p_i,n) \\ jk_{\theta_n}^{(s)} a\tilde{I}_{\theta_s}(p_i,n) \end{Bmatrix}.$$

$$.(\tilde{C}_{TM_i})^2 (J'_{p_i}(\tilde{k}_{iTM}a))^2$$

$$= \begin{Bmatrix} k_{\theta_m}^{(c)} a \\ -jk_{\theta_m}^{(s)} a \end{Bmatrix} \begin{Bmatrix} k_{\theta_n}^{(c)} a \\ jk_{\theta_n}^{(s)} a \end{Bmatrix} \sum_{p(q)} \begin{Bmatrix} \tilde{I}_{\theta_c}(p,m) \\ \tilde{I}_{\theta_s}(p,m) \end{Bmatrix} \begin{Bmatrix} \tilde{I}_{\theta_c}(p,n) \\ \tilde{I}_{\theta_s}(p,n) \end{Bmatrix}.$$

$$\cdot \sum_{i(p)} [-\frac{p^2}{(k_c a)^2} (\tilde{C}_{TE_i})^2 J_p^2(\tilde{k}_{iTE}a) + \frac{\tilde{k}_{iTM}^2}{\tilde{k}_{iTM}^2 - k_c^2} (\tilde{C}_{TM_i})^2 (J'_p(\tilde{k}_{iTM}a))^2]$$

(2.104)

And for sector waveguide:

$$-\sum_i \frac{k_{iTE}^2}{k_c^2} R_{im} R_{in} + \sum_i \frac{k_{iTM}^2}{k_{iTM}^2 - k_c^2} S_{im} S_{in} =$$

$$= -\sum_i \frac{k_{iTE}^2}{k_c^2} \frac{\nu_i^2}{(k_{iTE} a)^2} \begin{Bmatrix} k_{\theta_m}^{(c)} a I_{\theta_c}(\mu_i, m) \sin(\mu_i \frac{\pi}{2}) \\ k_{\theta_m}^{(s)} a I_{\theta_s}(\mu_i, m) \cos(\mu_i \frac{\pi}{2}) \end{Bmatrix} \begin{Bmatrix} k_{\theta_n}^{(c)} a I_{\theta_c}(\mu_i, n) \sin(\mu_i \frac{\pi}{2}) \\ k_{\theta_n}^{(s)} a I_{\theta_s}(\mu_i, n) \cos(\mu_i \frac{\pi}{2}) \end{Bmatrix}.$$

$$.(C_{TE_i})^2 (F_{\mu_i}^{(TE)}(k_{iTE} a))^2$$

$$+\sum_i \frac{k_{iTM}^2}{k_{iTM}^2 - k_c^2} \begin{Bmatrix} k_{\theta_m}^{(c)} a I_{\theta_c}(\mu_i, m) \sin(\mu_i \frac{\pi}{2}) \\ k_{\theta_m}^{(s)} a I_{\theta_s}(\mu_i, m) \cos(\mu_i \frac{\pi}{2}) \end{Bmatrix} \begin{Bmatrix} k_{\theta_n}^{(c)} a I_{\theta_c}(\mu_i, n) \sin(\mu_i \frac{\pi}{2}) \\ k_{\theta_n}^{(s)} a I_{\theta_s}(\mu_i, n) \cos(\mu_i \frac{\pi}{2}) \end{Bmatrix}.$$

$$.(C_{TM_i})^2 (F_{\mu_i}^{(TM)\prime}(k_{iTM} a))^2$$

$$= \begin{Bmatrix} k_{\theta_m}^{(c)} a \\ k_{\theta_m}^{(s)} a \end{Bmatrix} \begin{Bmatrix} k_{\theta_n}^{(c)} a \\ k_{\theta_n}^{(s)} a \end{Bmatrix} \sum_{\mu} \begin{Bmatrix} I_{\theta_c}(\mu, m) \sin(\mu \frac{\pi}{2}) \\ I_{\theta_s}(\mu, m) \cos(\mu \frac{\pi}{2}) \end{Bmatrix} \begin{Bmatrix} I_{\theta_c}(\mu, n) \sin(\mu \frac{\pi}{2}) \\ I_{\theta_s}(\mu_i, n) \cos(\mu \frac{\pi}{2}) \end{Bmatrix}$$

$$\cdot \sum_{i(\mu)} [-\frac{\nu^2}{(k_c a)^2} (C_{TE_i})^2 (F_{\mu}^{TE}(k_{iTE} a))^2 + \frac{k_{iTM}^2}{k_{iTM}^2 - k_c^2} (C_{TM_i})^2 (F_{\mu}^{(TM)\prime}(k_{iTM} a))^2] \tag{2.105}$$

When the elements of characteristic matrices for TE and TM modes derived in the equations (2.41) and (2.48) respectively are examined, it can be seen that infinite number of solutions exist for every μ and p values.

For TE as well as for TM modes, each element of the characteristic matrix contains a doubly infinite sum, which has to be summed with respect to the azimuthal and the radial indices corresponding to the modes of the circular and the sector waveguides. It has been found that the summations over the index corresponding to the direction normal to the surface current have closed-form expressions [8] [19] [20]. The detailed analysis can be found in Appendix-A.

This increases the numerical efficiency of the technique significantly. Furthermore the cutoff wavenumbers k_{nTM} and k_{nTE} of the modes corresponding to the individual waveguides need not to be determined after substituting the infinite sums by closed-form expressions given in Appendix A.

Substituting the closed form expressions into the equations (2.102)-(2.105) by replacing $k_{nTM}^{(2)}$ and $k_{nTE}^{(2)}$ with the cutoff wavenumber k_c ($k_c^{(TE)}$ and $k_c^{(TM)}$) leads to:

For hollow circular waveguide;

$$\sum_i \frac{\tilde{k}_{iTE}^2}{\tilde{k}_{iTE}^2 - k_c^2} \tilde{T}_{im} \tilde{T}_{in}^* = \tag{2.106}$$
$$= \frac{1}{2\pi} \begin{Bmatrix} k_{z_m}^{(c)} a \\ -jk_{z_m}^{(s)} a \end{Bmatrix} \begin{Bmatrix} k_{z_n}^{(c)} a \\ jk_{z_n}^{(s)} a \end{Bmatrix} \sum_{p(q)} \begin{Bmatrix} \tilde{I}_{z_c}(p,m) \\ \tilde{I}_{z_s}(p,m) \end{Bmatrix} \begin{Bmatrix} \tilde{I}_{z_c}(p,n) \\ \tilde{I}_{z_s}(p,n) \end{Bmatrix} \frac{1}{k_c a} \frac{J_p(k_c a)}{J'_p(k_c a)}$$

$$-\sum_i \frac{\tilde{k}_{iTE}^2}{k_c^2} \tilde{R}_{im} \tilde{R}_{in}^* + \sum_i \frac{\tilde{k}_{iTM}^2}{\tilde{k}_{iTM}^2 - k_c^2} \tilde{S}_{im} \tilde{S}_{in}^* = \tag{2.107}$$
$$= \frac{1}{2\pi} \begin{Bmatrix} k_{\theta_m}^{(c)} a \\ -jk_{\theta_m}^{(s)} a \end{Bmatrix} \begin{Bmatrix} k_{\theta_n}^{(c)} a \\ jk_{\theta_n}^{(s)} a \end{Bmatrix} \sum_{p(q)} \begin{Bmatrix} \tilde{I}_{\theta_c}(p,m) \\ \tilde{I}_{\theta_s}(p,m) \end{Bmatrix} \begin{Bmatrix} \tilde{I}_{\theta_c}(p,n) \\ \tilde{I}_{\theta_s}(p,n) \end{Bmatrix} \frac{1}{k_c a} \frac{J'_p(k_c a)}{J_p(k_c a)}$$

For sector waveguide;

$$\sum_i \frac{k_{iTE}^2}{k_{iTE}^2 - k_c^2} T_{im} T_{in} =$$
$$= \begin{Bmatrix} k_{z_m}^{(c)} a \\ k_{z_m}^{(s)} a \end{Bmatrix} \begin{Bmatrix} k_{z_n}^{(c)} a \\ k_{z_n}^{(s)} a \end{Bmatrix} \sum_{\mu} \begin{Bmatrix} I_{z_c}(\mu,m) \cos(\mu \frac{\pi}{2}) \\ -I_{z_s}(\mu,m) \sin(\mu \frac{\pi}{2}) \end{Bmatrix} \begin{Bmatrix} I_{z_c}(\mu,n) \cos(\mu \frac{\pi}{2}) \\ -I_{z_s}(\mu,n) \sin(\mu \frac{\pi}{2}) \end{Bmatrix} \frac{2}{(1+\delta_{\mu 0})(k_c a)\Theta} \frac{F_{\mu}^{(TE)}(k_c a)}{F_{\mu}^{(TE)\prime}(k_c a)}$$

$$\tag{2.108}$$

$$-\sum_i \frac{k_{iTE}^2}{k_c^2} R_{im} R_{in} + \sum_i \frac{k_{iTM}^2}{k_{iTM}^2 - k_c^2} S_{im} S_{in} =$$

$$= \begin{Bmatrix} k_{\theta_m}^{(c)} a \\ k_{\theta_m}^{(s)} a \end{Bmatrix} \begin{Bmatrix} k_{\theta_n}^{(c)} a \\ k_{\theta_n}^{(s)} a \end{Bmatrix} \sum_{\mu \geq 1} \begin{Bmatrix} I_{\theta_c}(\mu, m) \sin(\mu \frac{\pi}{2}) \\ I_{\theta_s}(\mu, m) \cos(\mu \frac{\pi}{2}) \end{Bmatrix} \begin{Bmatrix} I_{\theta_c}(\mu, n) \sin(\mu \frac{\pi}{2}) \\ I_{\theta_s}(\mu, n) \cos(\mu \frac{\pi}{2}) \end{Bmatrix} \frac{2}{(k_c a)\Theta} \frac{F_\mu^{(TM)\prime}(k_c a)}{F_\mu^{(TM)}(k_c a)}$$

(2.109)

2.15 Determination of Magnetic and Electric Field Components

The following expressions for each field components of TE and TM waves can be obtained as a result of substituting the field expansion functions given in section 2.9 into the equations (2.4), setting the field amplitudes derived in section 2.13 separately for TE and TM waves and using the series forms of u_n, v_n and w_n given in the equations (2.33) and (2.34) by replacing the terms R_{nm}, S_{nm} and T_{nm} with the expressions derived in the equations (2.91), (2.92) and (2.93):

TE waves in i^{th} sector waveguide;

$$\begin{aligned} E_t^{(TE)} = e^{-jq(i-1)\frac{2\pi}{N}} \sum_m [a_{z_m} k_{z_m}^{(c)} a \sum_\mu I_{z_c}(\mu, m) \cos(\mu \frac{\pi}{2}) + j(jb_{z_m}) k_{z_m}^{(s)} a \sum_\mu I_{z_s}(\mu, m) \sin(\mu \frac{\pi}{2})] \\ \cdot \sum_{n(\mu)} \frac{k_{nTE}^2}{k_{nTE}^2 - (k_0^2 - \beta^2)} C_{TE_n}^2 F_\mu^{(TE)}(k_{nTE} a) [-\frac{\nu}{r} F_\mu^{(TE)}(k_{nTE} r) \sin(\nu(\theta - \theta_n)) \hat{a}_r \\ - k_{nTE} F_\mu^{(TE)}(k_{nTE} r) \cos(\nu(\theta - \theta_n)) \hat{a}_\theta] \end{aligned}$$

(2.110)

$$jH_z = -\frac{k_0^2-\beta^2}{k_0 Z_0} e^{-jq(i-1)\frac{2\pi}{N}} \sum_m [a_{z_m} k_{z_m}^{(c)} a \sum_\mu I_{z_c}(\mu,m)\cos(\mu\frac{\pi}{2})$$

$$+ j(jb_{z_m})k_{z_m}^{(s)} a \sum_\mu I_{z_s}(\mu,m)\sin(\mu\frac{\pi}{2})]$$

$$\cdot \sum_{n(\mu)} \frac{k_{nTE}^2}{k_{nTE}^2-(k_0^2-\beta^2)} C_{TE_n}^2 F_\mu^{(TE)}(k_{nTE}a) F_\mu^{(TE)}(k_{nTE}r)\cos(\nu(\theta-\theta_n))$$

(2.111)

TM waves in i[th] sector waveguide;

$$H_t^{(TM)} = -\frac{k_0}{Z_0} e^{-jq(i-1)\frac{2\pi}{N}} \sum_m [a_{\theta_m} k_{\theta_m}^{(c)} a \sum_\mu I_{\theta_c}(\mu,m)\sin(\mu\frac{\pi}{2})$$

$$- j(jb_{\theta_m})k_{\theta_m}^{(s)} a \sum_\mu I_{\theta_s}(\mu,m)\cos(\mu\frac{\pi}{2})]$$

$$\cdot(\sum_{n(\mu)} \frac{\nu}{(k_0^2-\beta^2)a^2} C_{TE_n}^2 F_\mu^{(TE)}(k_{nTE}a)[k_{nTE}aF_\mu^{(TE)'}(k_{nTE}r)\cos(\nu(\theta-\theta_n))\hat{a}_r$$

$$-\frac{\nu}{r/a} F_\mu^{(TE)}(k_{nTE}r)\sin(\nu(\theta-\theta_n))\hat{a}_\theta]$$

$$+\frac{k_{nTM}a}{(k_{nTM}^2-(k_0^2-\beta^2))a^2} C_{TM_n}^2 F_\mu^{(TM)'}(k_{nTM}a)[-\frac{\nu}{r/a} F_\mu^{(TM)}(k_{nTM}r)\cos(\nu(\theta-\theta_n))\hat{a}_r$$

$$+k_{nTM}aF_\mu^{(TM)'}(k_{nTM}r)\sin(\nu(\theta-\theta_n))\hat{a}_\theta])$$

(2.112)

$$E_z = e^{-jq(i-1)\frac{2\pi}{N}} \sum_m [a_{\theta_m} k_{\theta_m}^{(c)} a \sum_\mu I_{\theta_c}(\mu,m)\sin(\mu\frac{\pi}{2}) - j(jb_{\theta_m} k_{\theta_m}^{(s)} a \sum_\mu I_{\theta_s}(\mu,m)\cos(\mu\frac{\pi}{2})]$$

$$\cdot \sum_{n(\mu)} \frac{k_{nTM}^3}{k_{nTM}^2-(k_0^2-\beta^2)} C_{TM_n}^2 F_\mu^{(TM)'}(k_{nTM}a) F_\mu^{(TM)}(k_{nTM}r)\sin(\nu(\theta-\theta_n))$$

(2.113)

TE waves in hollow circular waveguide;

$$E_t^{(TE)} = N\sum_m [a_{z_m} k_{z_m}^{(c)} a \sum_{p(q)} \tilde{I}_{z_c}(p,m) - (jb_{z_m}) k_{z_m}^{(s)} a \sum_{p(q)} \tilde{I}_{z_s}(p,m)]$$
$$\cdot e^{jp\varphi} \sum_{n(p)} \frac{\tilde{k}_{nTE}^2}{\tilde{k}_{nTE}^2 - (k_0^2 - \beta^2)} \tilde{C}_{TE_n}^2 J_p(\tilde{k}_{nTE} a)[-\frac{jp}{r} J_p(\tilde{k}_{nTE} r)\hat{a}_r + \tilde{k}_{nTE} J'_p(\tilde{k}_{nTE} r)\hat{a}_\theta] \tag{2.114}$$

$$jH_z = N\frac{k_0^2 - \beta^2}{k_0 Z_0} \sum_m [a_{z_m} k_{z_m}^{(c)} a \sum_{p(q)} \tilde{I}_{z_c}(p,m) - (jb_{z_m}) k_{z_m}^{(s)} a \sum_{p(q)} \tilde{I}_{z_s}(p,m)]$$
$$\cdot e^{jp\theta} \sum_{n(p)} \frac{\tilde{k}_{nTE}^2}{\tilde{k}_{nTE}^2 - (k_0^2 - \beta^2)} \tilde{C}_{TE_n}^2 J_p(\tilde{k}_{nTE} a) J_p(\tilde{k}_{nTE} r) \tag{2.115}$$

TM waves in hollow circular waveguide;

$$H_t^{(TM)} = N\frac{k_0}{Z_0} \sum_m [a_{\theta_m} k_{\theta_m}^{(c)} a \sum_{p(q)} \tilde{I}_{\theta_c}(p,m) - (jb_{\theta_m}) k_{\theta_m}^{(s)} a \sum_{p(q)} \tilde{I}_{\theta_s}(p,m)]$$
$$\cdot e^{jp\theta} (\sum_{n(p)} \frac{jp}{(k_0^2 - \beta^2)a^2} \tilde{C}_{TE_n}^2 J_p(\tilde{k}_{nTE} a)[\tilde{k}_{nTE} a J'_p(\tilde{k}_{nTE} r)\hat{a}_r + \frac{jp}{r/a} J_p(\tilde{k}_{nTE} r)\hat{a}_\theta]$$
$$+ \frac{\tilde{k}_{nTM} a}{(\tilde{k}_{nTM}^2 - (k_0^2 - \beta^2))a^2} \tilde{C}_{TM_n}^2 J'_p(\tilde{k}_{nTM} a)[-\frac{jp}{r/a} J_p(\tilde{k}_{nTM} r)\hat{a}_r + \tilde{k}_{nTM} a J'_p(\tilde{k}_{nTM} r)\hat{a}_\theta]) \tag{2.116}$$

$$E_z = N\sum_m [a_{\theta_m} k_{\theta_m}^{(c)} a \sum_{p(q)} \tilde{I}_{\theta_c}(p,m) - (jb_{\theta_m}) k_{\theta_m}^{(s)} a \sum_{p(q)} \tilde{I}_{\theta_s}(p,m)]$$
$$\cdot e^{jp\theta} \sum_{n(p)} - \frac{\tilde{k}_{nTM}^3}{\tilde{k}_{nTM}^2 - (k_0^2 - \beta^2)} \tilde{C}_{TM_n}^2 J'_p(\tilde{k}_{nTM} a) J_p(\tilde{k}_{nTM} r) \tag{2.117}$$

Since the phase factor θ_n is related to the index μ, it will be more convenient to use the term θ_μ for the phase factor and to avoid the radial summations belonging to the orders other than μ.

After setting for the wavenumbers in the relations given in Appendix A2 that:

$$\begin{Bmatrix} k_{nTE}^{(2)} \\ k_{nTM}^{(2)} \end{Bmatrix} = \begin{Bmatrix} \tilde{k}_{nTE}^{(2)} \\ \tilde{k}_{nTM}^{(2)} \end{Bmatrix} = k_c = \sqrt{k_0^2 - \beta^2} \tag{2.118}$$

The field components can be expressed by substituting the relations derived in Appendix A2 as:

TE waves in ith sector waveguide;

$$\begin{aligned} E_t^{(TE)} &= e^{-jq(i-1)\frac{2\pi}{N}} \sum_m [a_{z_m} k_{z_m}^{(c)} a \sum_\mu I_{z_c}(\mu,m)\cos(\mu\frac{\pi}{2}) + j(jb_{z_m}) k_{z_m}^{(s)} a \sum_\mu I_{z_s}(\mu,m)\sin(\mu\frac{\pi}{2})] \\ &\quad \cdot \frac{2-\delta_{\mu 0}}{\Theta a}[\frac{\nu}{r/a}\frac{1}{k_c a}\frac{F_\mu^{(TE)}(k_c r)}{F_\mu^{(TE)\prime}(k_c a)}\sin(\nu(\theta-\theta_\mu)\hat{a}_r + \frac{F_\mu^{(TE)\prime}(k_c r)}{F_\mu^{(TE)\prime}(k_c a)}\cos(\nu(\theta-\theta_\mu))\hat{a}_\theta] \\ &= \frac{j\beta Z_{TE}}{k_c^2}\cdot(\hat{a}_z \times \nabla_t H_z) \end{aligned} \tag{2.119}$$

$$\begin{aligned} jH_z &= \frac{k_c}{k_0}\frac{1}{Z_0} e^{-jq(i-1)\frac{2\pi}{N}} \\ &\quad \cdot \sum_m [a_{z_m} k_{z_m}^{(c)} a \sum_\mu I_{z_c}(\mu,m)\cos(\mu\frac{\pi}{2}) + j(jb_{z_m}) k_{z_m}^{(s)} a \sum_\mu I_{z_s}(\mu,m)\sin(\mu\frac{\pi}{2})] \\ &\quad \cdot \frac{2-\delta_{\mu 0}}{\Theta a}\frac{F_\mu^{(TE)}(k_c r)}{F_\mu^{(TE)\prime}(k_c a)}\cos(\nu(\theta-\theta_\mu)) \end{aligned} \tag{2.120}$$

TM waves in ith sector waveguide;

$$jH_t^{(TM)} = -\frac{k_0}{k_c}\frac{1}{Z_0}e^{-jq(i-1)\frac{2\pi}{N}}\cdot$$
$$\cdot\sum_m [a_{\theta_m} k_{\theta_m}^{(c)} a \sum_{\mu\geq 1} I_{\theta_c}(\mu,m)\sin(\mu\frac{\pi}{2}) - j(jb_{\theta_m})k_{\theta_m}^{(s)} a \sum_{\mu\geq 1} I_{\theta_s}(\mu,m)\cos(\mu\frac{\pi}{2})]$$
$$\cdot\frac{2}{\Theta a}[\frac{\nu}{r/a}\frac{1}{k_c a}\frac{F_\mu^{(TM)}(k_c r)}{F_\mu^{(TM)}(k_c a)}\cos(\nu(\theta-\theta_\mu))\hat{a}_r - \frac{F_\mu^{(TM)\prime}(k_c r)}{F_\mu^{(TM)}(k_c a)}\sin(\nu(\theta-\theta_\mu))\hat{a}_\theta]$$

$$= \frac{-\beta Y_{TM}}{k_c^2}\cdot(\nabla_t E_z \times \hat{a}_z)$$

(2.121)

$$E_z = e^{-jq(i-1)\frac{2\pi}{N}}\sum_m [a_{\theta_m} k_{\theta_m}^{(c)} a \sum_{\mu\geq 1} I_{\theta_c}(\mu,m)\sin(\mu\frac{\pi}{2}) - j(jb_{\theta_m})k_{\theta_m}^{(s)} a \sum_{\mu\geq 1} I_{\theta_s}(\mu,m)\cos(\mu\frac{\pi}{2})]$$
$$\cdot\frac{2}{\Theta a}\frac{F_\mu^{(TM)}(k_c r)}{F_\mu^{(TM)}(k_c a)}\sin(\nu(\theta-\theta_\mu))$$

(2.122)

TE waves in hollow circular waveguide;

$$E_t^{(TE)} = -N\sum_m [a_{z_m} k_{z_m}^{(c)} a \sum_{p(q)} \tilde{I}_{z_c}(p,m) - (jb_{z_m})k_{z_m}^{(s)} a \sum_{p(q)} \tilde{I}_{z_s}(p,m)]$$
$$\cdot e^{jp\theta}\frac{1}{2\pi a}[\frac{jp}{r/a}\frac{1}{k_c a}\frac{J_p(k_c r)}{J_p'(k_c a)}\hat{a}_r - \frac{J_p'(k_c r)}{J_p'(k_c a)}\hat{a}_\theta] \tag{2.123}$$

$$= \frac{j\beta Z_{TE}}{k_c^2}\cdot(\hat{a}_z \times \nabla_t H_z)$$

$$jH_z = -N\frac{k_c}{k_0}\frac{1}{Z_0}\sum_m [a_{z_m} k_{z_m}^{(c)} a \sum_{p(q)} \tilde{I}_{z_c}(p,m) - (jb_{z_m}) k_{z_m}^{(s)} a \sum_{p(q)} \tilde{I}_{z_s}(p,m)] \\ \cdot e^{jp\theta}\frac{1}{2\pi a}\frac{J_p(k_c r)}{J'_p(k_c a)} \tag{2.124}$$

TM waves in hollow circular waveguide;

$$jH_t^{(TM)} = -N\frac{k_0}{k_c}\frac{1}{Z_0}\sum_m [a_{\theta_m} k_{\theta_m}^{(c)} a \sum_{p(q)} \tilde{I}_{\theta_c}(p,m) - (jb_{\theta_m}) k_{\theta_m}^{(s)} a \sum_{p(q)} \tilde{I}_{\theta_s}(p,m)] \\ \cdot e^{jp\theta}\frac{1}{2\pi a}[\frac{jp}{r/a}\frac{1}{k_c a}\frac{J_p(k_c r)}{J_p(k_c a)}\hat{a}_r - \frac{J'_p(k_c r)}{J_p(k_c a)}\hat{a}_\theta] \tag{2.125}$$

$$= \frac{-\beta Y_{TM}}{k_c^2}\cdot(\nabla_t E_z \times \hat{a}_z)$$

$$E_z = N\sum_m [a_{\theta_m} k_{\theta_m}^{(c)} a \sum_{p(q)} \tilde{I}_{\theta_c}(p,m) - (jb_{\theta_m}) k_{\theta_m}^{(s)} a \sum_{p(q)} \tilde{I}_{\theta_s}(p,m)] \\ \cdot e^{jp\theta}\frac{1}{2\pi a}\frac{J_p(k_c r)}{J_p(k_c a)} \tag{2.126}$$

The transverse components $H_t^{(TE)}$ and $E_t^{(TM)}$ of the field expressions can easily be obtained from the equations (2.97) and (2.100). Finally, the field distributions at all over the waveguide can be seen by taking the real and the imaginary parts (cosine and sine polarized fields) as it is explained also in section 2.12.

2.16 Power

The total power carried by the fields along the guide direction is calculated by integrating the z-component of the Poynting vector over the cross sectional area of the guide;

$$P=\frac{1}{2}\mathrm{Re}\iint_S E\times H^*.a_z dS=\frac{1}{2}\mathrm{Re}\iint_S E_t\times H_t^*.a_z dS$$
$$=\frac{1}{2}\mathrm{Re}\iint_S (E_{t_r}H_{t_\theta}^*-E_{t_\theta}H_{t_r}^*)dS=\frac{1}{2}Y_{TE/TM}\iint_S |E_t|^2\,dS=\frac{1}{2}Z_{TE/TM}\iint_S |H_t|^2\,dS \tag{2.127}$$

Transverse components of electric and magnetic fields that are required to find the Poynting vector can be derived as follows:

TE Waves in ith sector waveguide;

Substituting the equation (2.119) into equation (2.100) gives

$$\begin{aligned}H_t^{(TE)}=&\frac{\beta}{k_0}\frac{1}{Z_0}e^{-jq(i-1)\frac{2\pi}{N}}.\\&.\sum_m[a_{z_m}k_{z_m}^{(c)}a\sum_\mu I_{z_c}(\mu,m)\cos(\mu\frac{\pi}{2})+j(jb_{z_m})k_{z_m}^{(s)}a\sum_\mu I_{z_s}(\mu,m)\sin(\mu\frac{\pi}{2})]\\&\cdot\frac{2-\delta_{\mu 0}}{\Theta a}[\frac{\nu}{r/a}\frac{1}{k_c a}\frac{F_\mu^{(TE)}(k_c r)}{F_\mu^{(TE)'}(k_c a)}\sin(\nu(\theta-\theta_\mu))\hat{a}_\theta-\frac{F_\mu^{(TE)'}(k_c r)}{F_\mu^{(TE)'}(k_c a)}\cos(\nu(\theta-\theta_\mu))\hat{a}_r]\end{aligned} \tag{2.128}$$

TE Waves in hollow circular waveguide;

Inserting the equation (2.123) into equation (2.100) yields

$$\begin{aligned}H_t^{(TE)}=N\frac{\beta}{k_0}\frac{1}{Z_0}&\sum_m[a_{z_m}k_{z_m}^{(c)}a\sum_{p(q)}\tilde{I}_{z_c}(p,m)-(jb_{z_m})k_{z_m}^{(s)}a\sum_{p(q)}\tilde{I}_{z_s}(p,m)]\\&\cdot e^{jp\theta}\frac{1}{2\pi a}[-\frac{jp}{r/a}\frac{1}{k_c a}\frac{J_p(k_c r)}{J_p'(k_c a)}\hat{a}_\theta-\frac{J_p'(k_c r)}{J_p'(k_c a)}\hat{a}_r]\end{aligned} \tag{2.129}$$

TM Waves in i[th] sector waveguide;

Substituting the equation (2.121) into equation (2.97) leads to

$$E_t^{(TM)} = -\frac{\beta}{k_c} e^{-jq(i-1)\frac{2\pi}{N}} \sum_m [a_{\theta_m} k_{\theta_m}^{(c)} a \sum_{\mu \geq 1} I_{\theta_c}(\mu, m) \sin(\mu \frac{\pi}{2}) - j(jb_{\theta_m}) k_{\theta_m}^{(s)} a \sum_{\mu \geq 1} I_{\theta_s}(\mu, m) \cos(\mu \frac{\pi}{2})]$$
$$\cdot \frac{2}{\Theta a} [\frac{F_\mu^{(TM)\prime}(k_c r)}{F_\mu^{(TM)}(k_c a)} \sin(\nu(\theta - \theta_\mu)) \hat{a}_r + \frac{\nu}{r/a} \frac{1}{k_c a} \frac{F_\mu^{(TM)}(k_c r)}{F_\mu^{(TM)}(k_c a)} \cos(\nu(\theta - \theta_\mu) \hat{a}_\theta]$$

(2.130)

TM Waves in hollow circular waveguide;

Inserting the equation (2.125) into equation (2.97) yields

$$E_t^{(TM)} = \frac{N\beta}{k_c} \sum_m [a_{\theta_m} k_{\theta_m}^{(c)} a \sum_{p(q)} \tilde{I}_{\theta_c}(p, m) - (jb_{\theta_m}) k_{\theta_m}^{(s)} a \sum_{p(q)} \tilde{I}_{\theta_s}(p, m)]$$
$$.e^{jp\theta} \frac{1}{2\pi a} [-\frac{jp}{r/a} \frac{1}{k_c a} \frac{J_p(k_c r)}{J_p(k_c a)} \hat{a}_\theta - \frac{J_p'(k_c r)}{J_p(k_c a)} \hat{a}_r] \tag{2.131}$$

So, the analytical derivations are completed for numerical evaluation.

CHAPTER 3

SIMULATION RESULTS AND DISCUSSIONS

3.1 Introduction

The formulation of the matrix eigenvalue problem is done in the previous chapter. In this chapter, the numerical approach to the eigenvalues of the system of homogeneous equations and the results of computer program are explained and presented.

The convergence study is realized for the triple ridged waveguide and the behaviours of the cutoff eigenvalues and corresponding eigenvectors are analyzed with recpect to the numbers of field and surface magnetic current expansion functions.

Power handling capacities and modal field distributions for quadruple ridged waveguides are presented with different ridge penetration depth and angular width at the end of the chapter.

3.2 Solution of the Matrix Eigenvalue Problem

A graphical user Interface is developed to make it simple to manage and a brief description about GUI is given in Appendix B. The program is written in MATLAB. The parameters that have to be defined before starting to the analysis are as follows:

N : Number of slots

a : Inner radius of waveguide

b : Outer radius of waveguide

ϴ : Angular width of a slot

M : Number of surface magnetic current expansion functions (specifies also the dimension of the characteristic matrix)

N_s : Number of field expansion functions in sector waveguide

N_c : Number of field expansion functions in hollow circular waveguide

q : Phase difference factor between adjacent slots (defines different class of modes)

The eigenvalues of the matrix eigenvalue problem derived in equations (2.40) and (2.47) with the matrix element given through the equations (2.106) and (2.109) are calculated by the program. The truncated summations in each element of the characteristic matrix are computed by separate sub routines.

The analysis is started first to find the cutoff wavenumbers within the specified interval if there is any. The multiplication of inner radius of waveguide and the cutoff wavenumber ($k_c a$) is used as the output parameter of the cutoff analysis. The program computes the determinant of the matrix by back substituting the cutoff wavenumber. The eigenvalue is determined by noting a change of sign between successive determinant values by using bisection method [21]. With the use of this method, it is easy to find very accurate results when the axis of frequency is sampled sufficiently.

If there is one or more cutoff within the specified search interval, they are listed in the 'Select kca' box of GUI and the determinant versus kca graph is displayed. Using this graph, it is easy to recognize zero crossings and asymptotes.

Finally, it is possible to find and plot the field components Ez (for TM mode) or Hz (for TE mode) within the activated 'Field Evaluation Panel' for any selected kca.

The Bessel Functions of the first and second kind available in MATLAB are used for the orders smaller than 100. For the orders greater than 100, the following approximation defined in [22] is used and a sub function is written for the high orders of Bessel functions.

$$
\begin{aligned}
&J_\nu(z) \sim \frac{1}{\sqrt{2\pi\nu}}\left(\frac{ez}{2\nu}\right)^{\nu} \\
&N_\nu(z) \sim -\sqrt{\frac{2}{\pi\nu}}\left(\frac{ez}{2\nu}\right)^{-\nu}
\end{aligned}
\tag{3.1}
$$

3.3 Convergence of Eigenvalues and Eigenvectors

Cutoff wavenumber is a characteristic quantity for an eigenmode. For this reason, it can be used for making a decision about the convergence property of a method.

The amplitudes of current expansion functions are the eigenvectors of the characteristic equation system. Especially at low cutoff wavenumbers, it is expected that the large part of the fields will be constituted by the small indexed current terms. Since the amplitudes of current expansion functions normalized to the same length, the current spectrum must converge rapidly. To make a decision about the convergence behaviour of the solution, it is important to test that the higher order components of eigenvectors are damped while the orders of the current and the field expansion functions increase.

3.4 Convergence Behaviour with Increasing Field Expansion Order

The highest degree of the current expansion functions will be kept constant and the convergence behaviour of the eigenvalues and eigenvectors will be examined by increasing the degree of the field expansion functions.

The field expansion functions at the highest degree must be approximately the same for whether the hollow circular or the sector waveguide parts so that the fields could converge with the same ratio at both sides. So, it can be written for the degree of the field expansion functions that:

$$\max_{(p)}(p) = \max_{\mu}(\nu) \tag{3.2}$$

If the highest degree of the current expansion functions is chosen too large (or the highest degree of the field expansion functions is chosen too small), the equivalent surface magnetic currents cannot be formed again correctly because the degree of eigenfunctions remains too small. Thus, the higher degree current terms remain indefinite. By this reason, the highest degree of the field expansion functions must be chosen larger than the highest degree of the current expansion functions. Satisfying this condition, it is possible to define the ratio below as a parameter:

$$\eta = \frac{\mu_{\max}}{m_{\max}} = \frac{\mu_{\max}}{2M} \geq 1 \tag{3.3}$$

Here, M is the number of sine and cosine terms composing the surface magnetic current.

The variation of $k_c a$ eigenvalues and the convergence behaviour of eigenvectors of TE and TM waves for the case of the smallest cosine polarized waves (TE01 and TM01) with the same phase over the slots are presented in the two tables below,

Table 3-1 TM Eigen Vector for TM01 Mode (N=3, b/a=2, ϴ=60)

M/Ns/Nc	10/20/60	10/50/150	10/100/300	10/150/450	10/300/900
$k_c a$	2.14012	2.14113	2.14122	2.14125	2.14125
$V_1(a_{\theta 1})$	1.00000	1.00000	1.00000	1.00000	1.00000
$V_2(a_{\theta 3})$	-0.03332	-0.03229	-0.03220	-0.03217	-0.03215
$V_3(a_{\theta 5})$	0.00904	0.00822	0.00815	0.00813	0.00811
$V_4(a_{\theta 7})$	-0.00426	-0.00354	-0.00347	-0.00345	-0.00344
$V_5(a_{\theta 9})$	0.00268	0.00200	0.00193	0.00191	0.00190
$V_6(a_{\theta 11})$	-0.00203	-0.00135	-0.00128	-0.00126	-0.00125
$V_7(a_{\theta 13})$	0.00179	0.00104	0.00097	0.00095	0.00094
$V_8(a_{\theta 15})$	-0.00182	-0.00090	-0.00083	-0.00081	-0.00080
$V_9(a_{\theta 17})$	0.00226	0.00089	0.00081	0.00079	0.00077
$V_{10}(a_{\theta 19})$	-0.00490	-0.00111	-0.00100	-0.00097	-0.00094

Table 3-2 TE Eigen Vector for TE01 Mode (N=3, b/a=2, ϴ=60)

M/Ns/Nc	10/20/60	10/50/150	10/100/300	10/150/450	10/300/900
$k_c a$	1.58361	1.58297	1.58292	1.58290	1.58287
$V_1(a_{z0})$	1.00000	1.00000	1.00000	1.00000	1.00000
$V_2(a_{z2})$	0.08256	0.08002	0.07987	0.07983	0.07978
$V_3(a_{z4})$	-0.02756	-0.02639	-0.02638	-0.02637	-0.02636
$V_4(a_{z6})$	0.01347	0.01332	0.01340	0.01342	0.01344
$V_5(a_{z8})$	-0.00684	-0.00769	-0.00786	-0.00790	-0.00794
$V_6(a_{z10})$	0.00245	0.00449	0.00475	0.00483	0.00489
$V_7(a_{z12})$	0.00139	-0.00227	-0.00264	-0.00275	-0.00283
$V_8(a_{z14})$	-0.00586	0.00041	0.00093	0.00107	0.00119
$V_9(a_{z16})$	0.01311	0.00152	0.00079	0.00060	0.00044
$V_{10}(a_{z18})$	-0.03359	-0.00462	-0.00341	-0.00310	-0.00283

The facts below can be concluded when the results on both tables (3.1) and (3.2) examined:

- The cutoff wavenumbers ($k_c a$) converge too rapid, especially for TM case. Even if small numbers of high order field expansion functions (η=1) are used, it can be reached the correct value.

- The coefficients of higher order components show a rising behaviour in the case of small number of field expansion order (especially for η=1).

- The coefficients of low and medium order components are quite accurate even for the η values that are not so large (i.e. η=5).

Therefore, it can be seen that it is not necessary to use very high order current components at the beginning since the higher order current expansion coefficients can be calculated correctly only with a huge amount of field expansion order.

3.5 Convergence Behaviour with Increasing Current Expansion Order

The convergence behaviour for the increasing current expansion order will be examined. The numbers of field expansion functions for individual waveguides must be chosen as constant and sufficiently large values so that they will not effect the convergence behaviour (i.e. Ns=150, Nc=450). The obtained results are listed at the following tables:

Table 3-3 TM Eigen Vector for TM01 Mode (N=3, b/a=2, ϴ=60)

M/Ns/Nc	1/150/450	3/150/450	5/150/450	8/150/450
$k_c a$	2.14269	2.14135	2.14127	2.14125
V_1	1.00000	1.00000	1.00000	1.00000
V_2		-0.03292	-0.03232	-0.03219
V_3		0.00997	0.00836	0.00816
V_4			-0.00384	-0.00350
V_5			0.00278	0.00198
V_6				-0.00137
V_7				0.00113
V_8				-0.00123

Table 3-4 TE eigenvector for TE01 mode (N=3, b/a=2, ϴ=60)

M/Ns/Nc	1/150/450	3/150/450	5/150/450	8/150/450
$k_c a$	1.58021	1.58285	1.58290	1.58290
V_1	1.00000	1.00000	1.00000	1.00000
V_2		0.08281	0.08008	0.07973
V_3		-0.03312	-0.02674	-0.02626
V_4			0.01408	0.01329
V_5			-0.00967	-0.00774
V_6				0.00460
V_7				-0.00238
V_8				0.00027

The coefficients of current components show a decreasing tendency. The amplitudes of the first current components decrease while the values of M increase; since the higher harmonics also affect the spectrum.

Since the dimension of calculation is proportional to the number of maximum current degree (matrix dimension), the maximum current expansion degree has to be chosen not too large (i.e. M=3) taking into account that the maximum number of field expansion functions specifies only the number of summation terms.

3.6 Comparison of the Results for Triple Ridged Waveguide

Table 3-5 Comparison of the first ten cutoff wavenumber, kca, (N=3, ϴ=60, b/a=2, M=4, Ns=30, Nc=90)

	Type	q	Polarization	kca in [1]	kca
1	TE	1	Cos	0.794	0.7965
2	TE	1	Sin	0.794	0.7965
3	TE	0	Cos	1.583	1.5831
4	TE	1	Cos	2.076	2.0542
5	TE	1	Sin	2.076	2.0542
6	TE	0	Sin	2.128	2.0887
7	TM	0	Cos	2.142	2.1410
8	TE	1	Cos	2.373	2.4052
9	TE	1	Sin	2.373	2.4052
10	TM	1	Sin	2.933	2.9322

The comparison with the eigenvalues of the first ten modes published in [1] is tabulated in Table 3.5. The agreement between results is good.

3.7 Field Distributions of Triple Ridged Waveguide

Some field plots for the first TE and TM modes found according to the phase difference between adjacent slots are presented at the following figures with parameters b/a=2 and ϴ=60^{o}. The accuracy of the plots can be controlled by the continuity property of the fields across the slots and also compared with results given in [1].

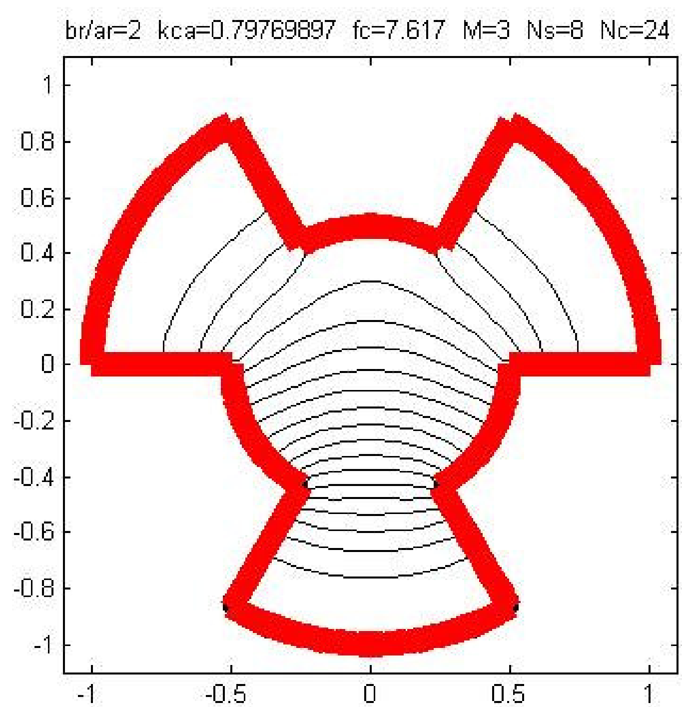

Figure 3.1 Electric Field Lines for the first TE Mode with N=3, q=1, cos pol.

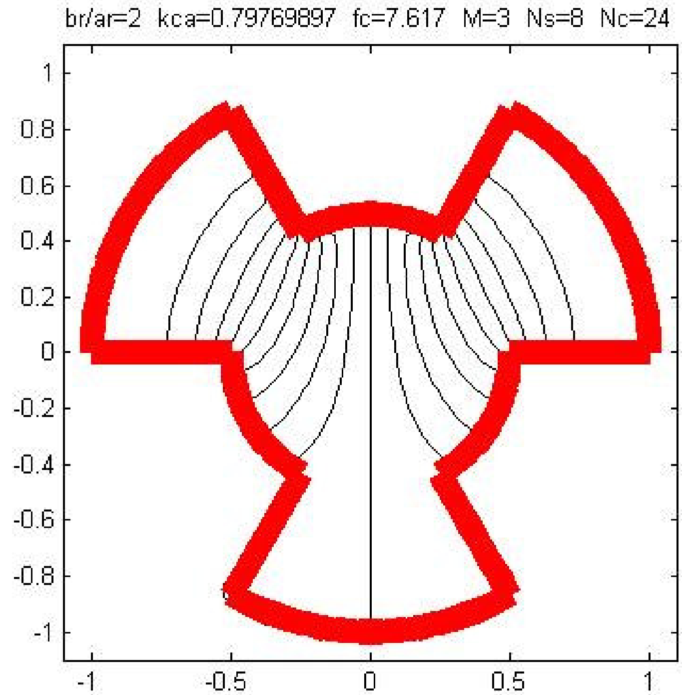

Figure 3.2 Electric Field Lines for the first TE Mode with N=3, q=1, sin pol.

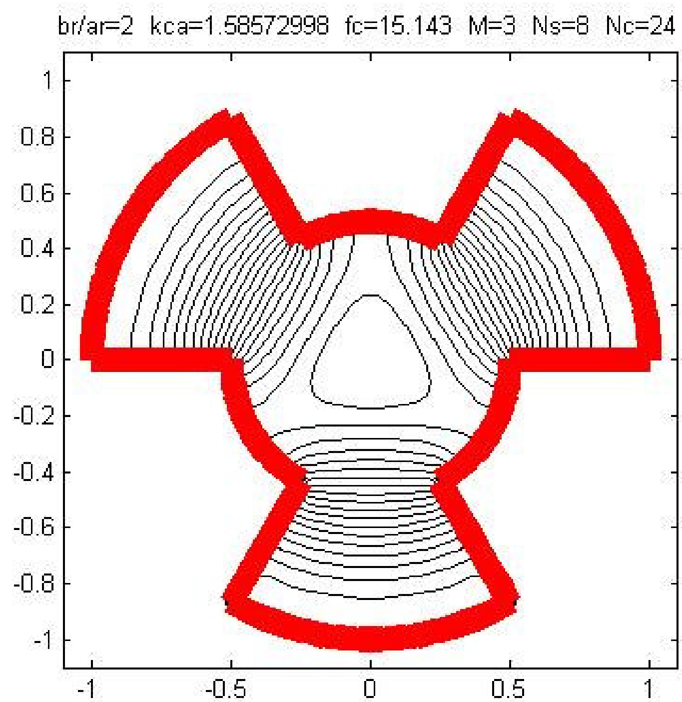

Figure 3.3 Electric Field Lines for the first TE Mode with N=3, q=0, cos pol.

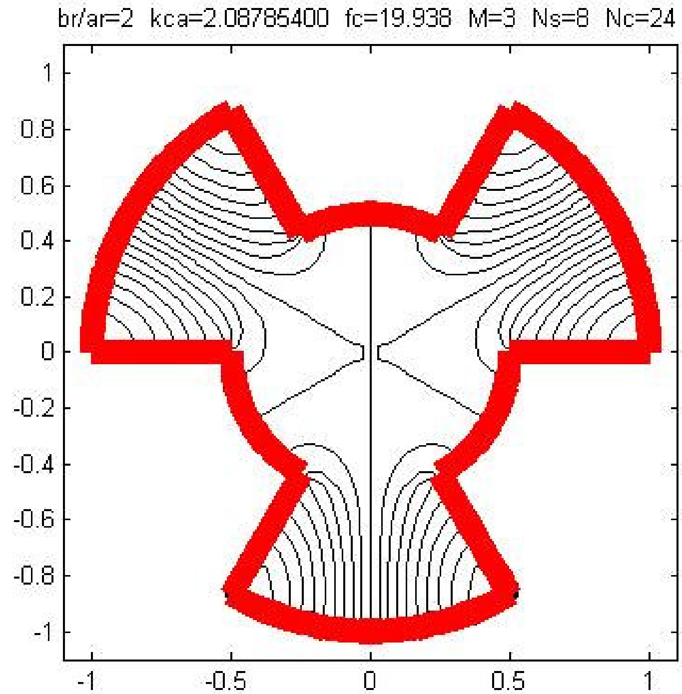

Figure 3.4 Electric Field Lines for the first TE Mode with N=3, q=0, sin pol.

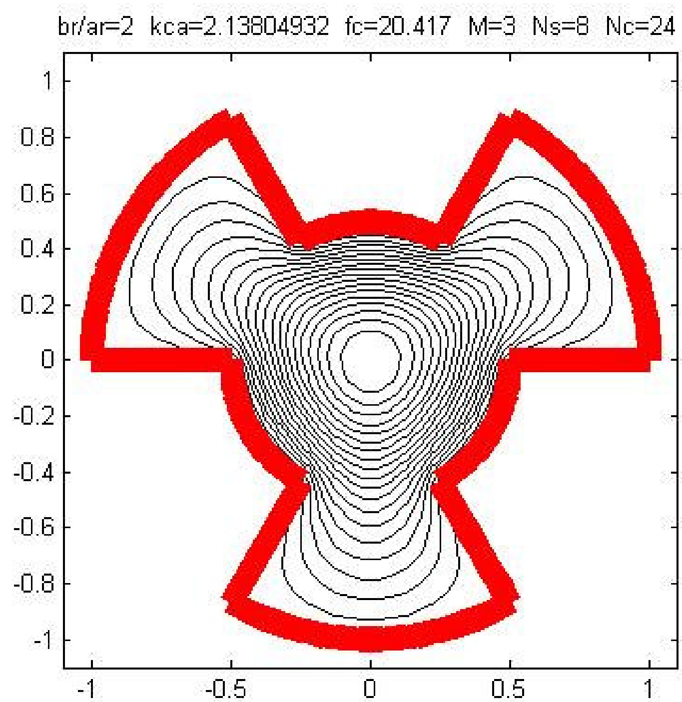

Figure 3.5 Magnetic Field Lines for the first TM Mode with N=3, q=0, cos pol.

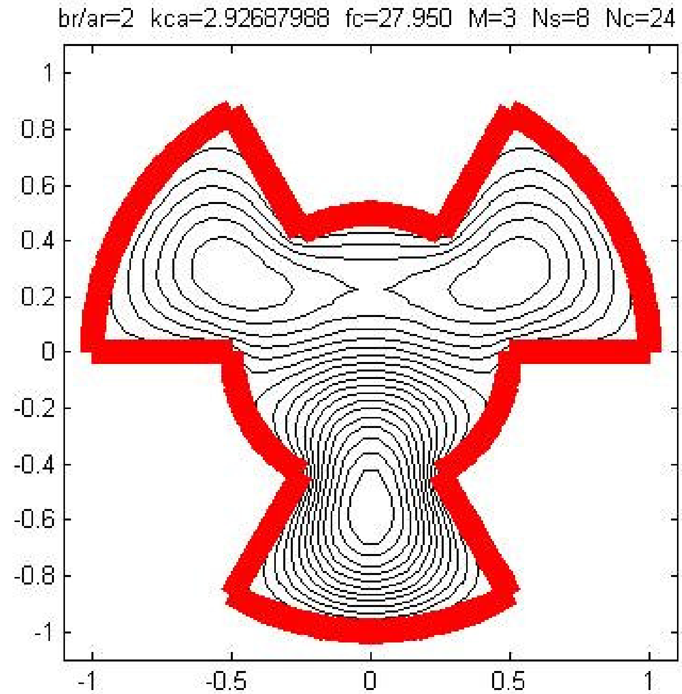

Figure 3.6 Magnetic Field Lines for the first TM Mode with N=3, q=1, cos pol.

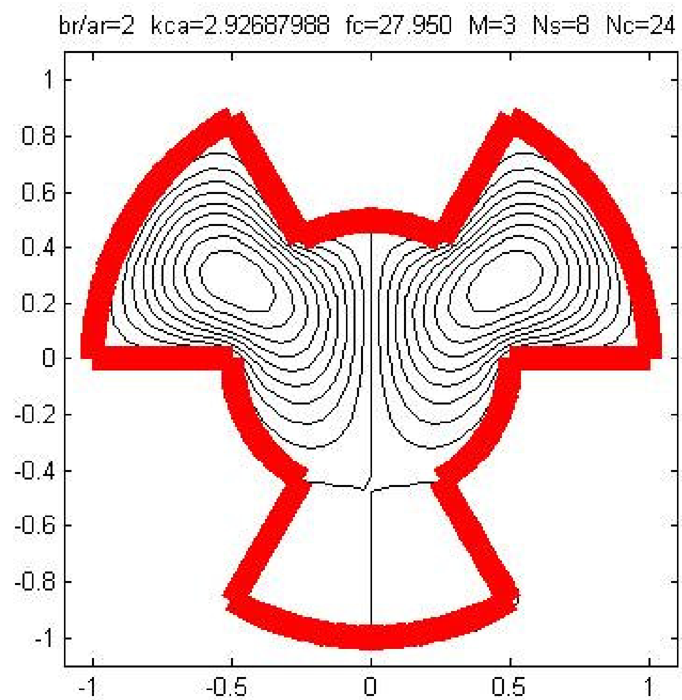

Figure 3.7 Magnetic Field Lines for the first TM Mode with N=3, q=1, sin pol.

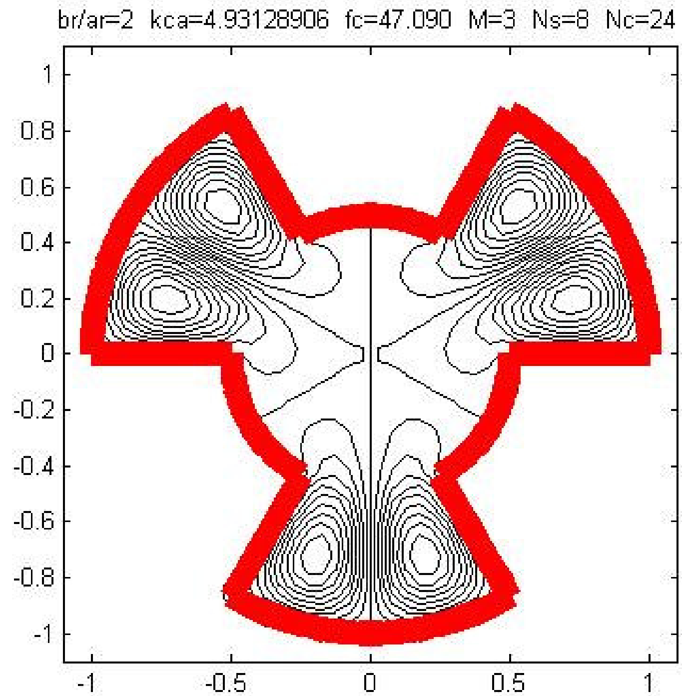

Figure 3.8 Magnetic Field Lines for the first TM Mode with N=3, q=0, sin pol.

3.8 Cutoff Characteristics of Quadruple Ridged Waveguide

Cutoff characteristics of quadruple ridged waveguide are investigated by changing slot angle and ridge penetration depth separately and the results for TE and TM modes are listed at the Tables 3-8 through 3-11. The corresponding plots showing the cutoff behaviours are illustrated in Figures 3.20 through 3.24 to see the bandwidth characteristics more clearly.

Table 3-6 Cutoff characteristics of quadruple ridged waveguide for TE modes with varying slot angle (b=1 cm, b/a=2, M=3, Ns=8, Nc=24)

Slot Angle	cos pol q=0	cos/sin pol q=1	cos pol q=2	sin pol q=0	sin pol q=2
ϴ	kca	kca	kca	kca	kca
10^o	1.34876709	1.05465820	1.12086914	5.39972656	3.08384766
20^o	1.41712646	0.94187622	1.02612305	5.35353125	3.15716797
30^o	1.50032959	0.87686157	0.97281738	3.74732422	3.25144043
40^o	1.58582764	0.83380737	0.93950684	2.92791016	2.90685547
50^o	1.67005615	0.80547485	0.92083496	2.43001953	2.40802734
60^o	1.74969727	0.78747559	0.91292114	2.09740234	2.06585693
70^o	1.82030029	0.77788696	0.9147644	1.86368164	1.81622314
80^o	1.87725830	0.77872925	0.92981567	1.69891602	1.62496338
85^o	1.89954834	0.78499146	0.94491577	1.63958008	1.54476318

Table 3-7 Cutoff characteristics of quadruple ridged waveguide for TM modes with varying slot angle (b=1 cm, b/a=2, M=3, Ns=8, Nc=24)

Slot Angle	cos pol q=0	cos/sin pol q=1	cos pol q=2	sin pol q=0	sin pol q=2
ϴ	kca	kca	kca	kca	kca
10o	2.39615479	3.81716797	5.09584961	7.58768750	5.13555000
20o	2.37154541	3.77396484	4.97094727	7.58031250	5.13425000
30o	2.32884521	3.68493652	4.61765137	7.54527344	5.12855469
40o	2.26419678	3.49318848	3.90407715	6.66832031	5.11238281
50o	2.17393799	3.18513184	3.39650879	5.63847656	5.06941406
60o	2.06279297	2.89490234	3.06060547	4.93785156	4.84933594
70o	1.93870850	2.66882324	2.83020020	4.43137207	4.37893066
80o	1.80645752	2.49499512	2.67165527	4.05192871	3.98808594
85o	1.73712158	2.42156982	2.61291504	3.89768066	3.82106934

Table 3-8 Cutoff Frequencies of Quadruple Ridged Waveguide for TE Modes with Ridge Depth (b=1 cm, ϴ=60^o, M=3, Ns=8, Nc=24)

	cos pol q=0	cos/sin pol q=1	cos pol q=2	sin pol q=0	sin pol q=2
(b-a)/b	fc (TE01)	fc (TE11)	fc (TE21L)	fc	fc (TE21U)
0.01	18.34607	8.859233	14.5187	25.06768	14.84615
0.10	18.68129	9.144062	13.77127	22.53372	16.38547
0.20	18.52333	9.087117	12.57327	20.99313	17.58277
0.30	17.89518	8.742911	11.22422	20.31963	18.55489
0.50	16.70166	7.516812	8.714247	20.02066	19.71938
0.60	16.56064	6.801777	7.633698	20.03112	19.9456
0.80	17.37536	5.320991	5.69922	20.05046	20.04907

Table 3-9 Cutoff Frequencies of Quadruple Ridged Waveguide for TM Modes with Ridge Depth (b=1 cm, Θ=60°, M=3, Ns=8, Nc=24)

	cos pol q=0	cos/sin pol q=1	cos pol q=2	sin pol q=0	sin pol q=2
(b-a)/b	fc (TM01)	fc	fc (TM21L)	fc	fc (TM21U)
0.01	11.52004	18.35944	24.52915	36.43153	24.71443
0.10	12.07556	19.20745	24.84838	38.67548	26.85937
0.20	13.07268	20.58483	25.56509	41.6819	29.98359
0.30	14.54495	22.46788	26.64282	44.56183	34.09966
0.50	19.6903	27.63316	29.21487	47.13404	46.28912
0.60	24.21064	29.62423	30.03392	47.38097	47.36885
0.80	45.49961	46.43551	46.4961	64.85726	64.85726

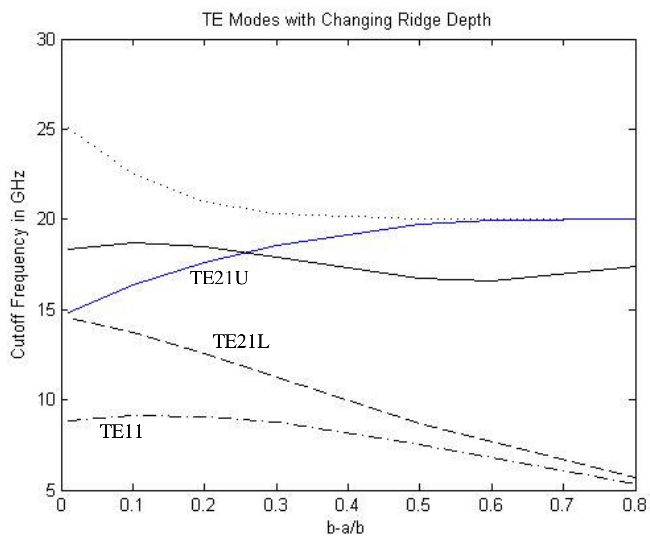

Figure 3.9 Cutoff Frequencies of TE modes versus the ridge depth, b=1cm and Θ=60°.

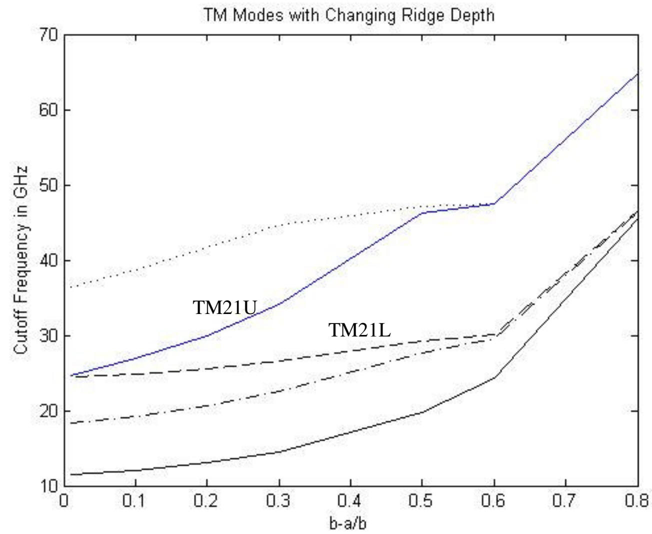

Figure 3.10 Cutoff Frequencies of TM modes versus the ridge depth, b=1cm and $\Theta=60^o$.

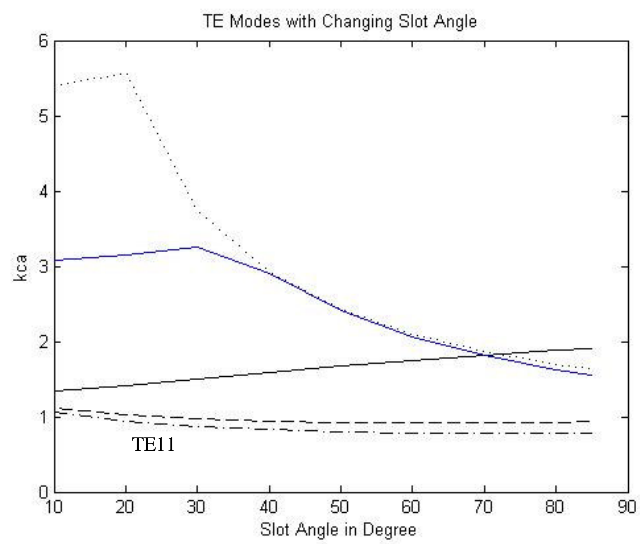

Figure 3.11 Cutoff frequencies of TE modes versus the slot angle, b/a=2 and b=1cm.

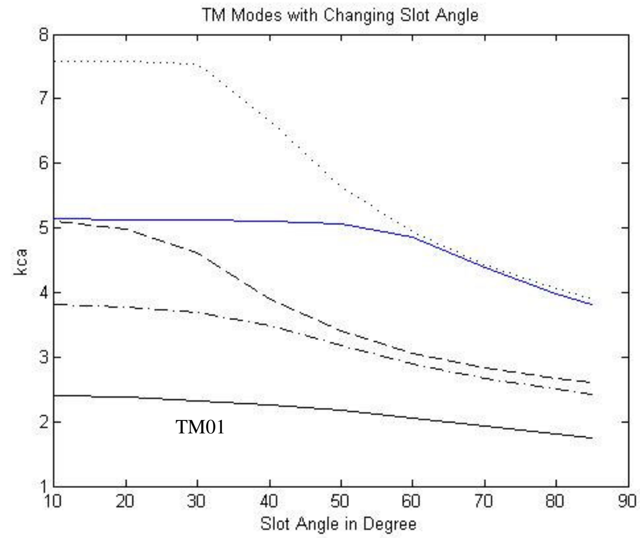

Figure 3.12 Cutoff frequencies of TM modes versus the slot angle, b/a=2 and b=1cm.

The usage of the same nomenclature of TE and TM modes of the empty circular waveguide means only that the new perturbed modes for ridged (distorted) waveguide can be traced back to the original ones.

In quadruple ridged waveguide, the ridge loading lowers the cutoff frequency of TE11 mode and raises the cutoff frequency of TM01. In the cutoff curves of the quadruple ridged waveguide in the Figures 3.9 and 3.10, it can be seen that at the small ridge depth, the bandwidth is determined by TE11 and TM01 modes, but increasing the ridge load the bandwith is determined by TE11 and TE21 modes.

It is clear to find out that the dominant mode (TE11) has a cutoff frequency very close to that of the second lowest mode (TE21). As a result of this behaviour, the single mode operation bandwidth is very small especially with the increasing ridge penetration depth. A wide bandwidth characteristic can be achieved only when the second lowest mode (TE21) is suppressed or not excited.

Although the single mode operation bandwidth is not affected so much by the variation of the ridge angular width, it must be considered to determine the maximum bandwith.

The splitting of TE21 and TM21 modes as a result of ridge loading can also be observed from the Figures 3.9 and 3.10. Mode-splitting behaviour comes out as a result of symmetry of the structure and transverse mode of the waveguides.

3.9 Field Distributions of Quadruple Ridged Waveguide

The transverse field distributions of quadruple ridged waveguide belonging to the first TE and TM modes for different q factors and polarization are obtained. Firstly, the plots of each mode are presented at the following figures for various ridge penetration depths. The parameters b and Θ are fixed to 1 cm and 60° respectively and (b-a)/b ratio is varied to 0.01, 0.3, 0.5 and 0.8.

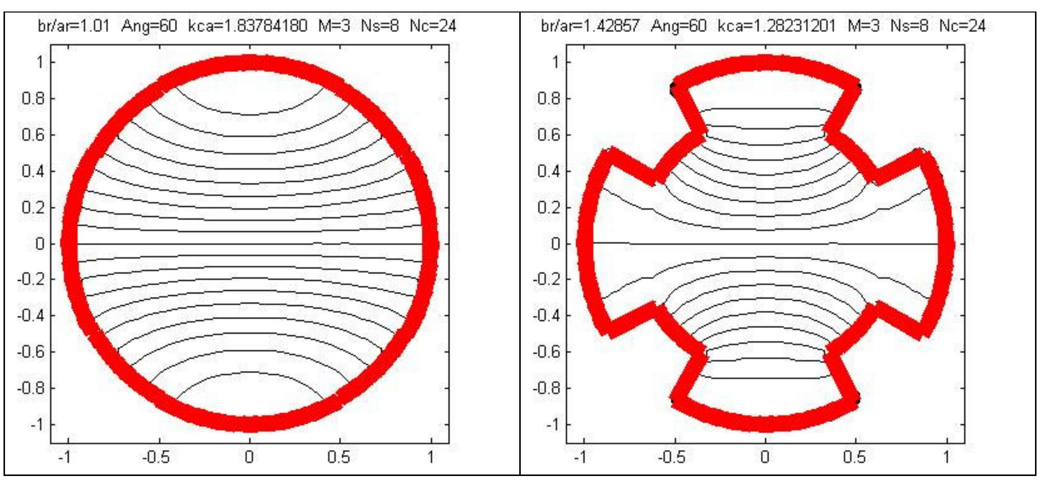

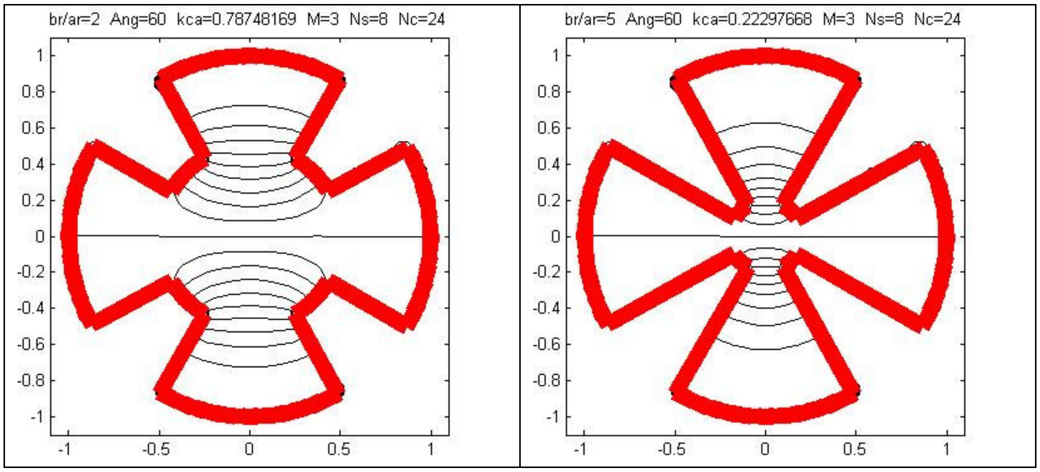

Figure 3.13 Electric field lines for the first TE mode with N=4, q=1, cos pol.

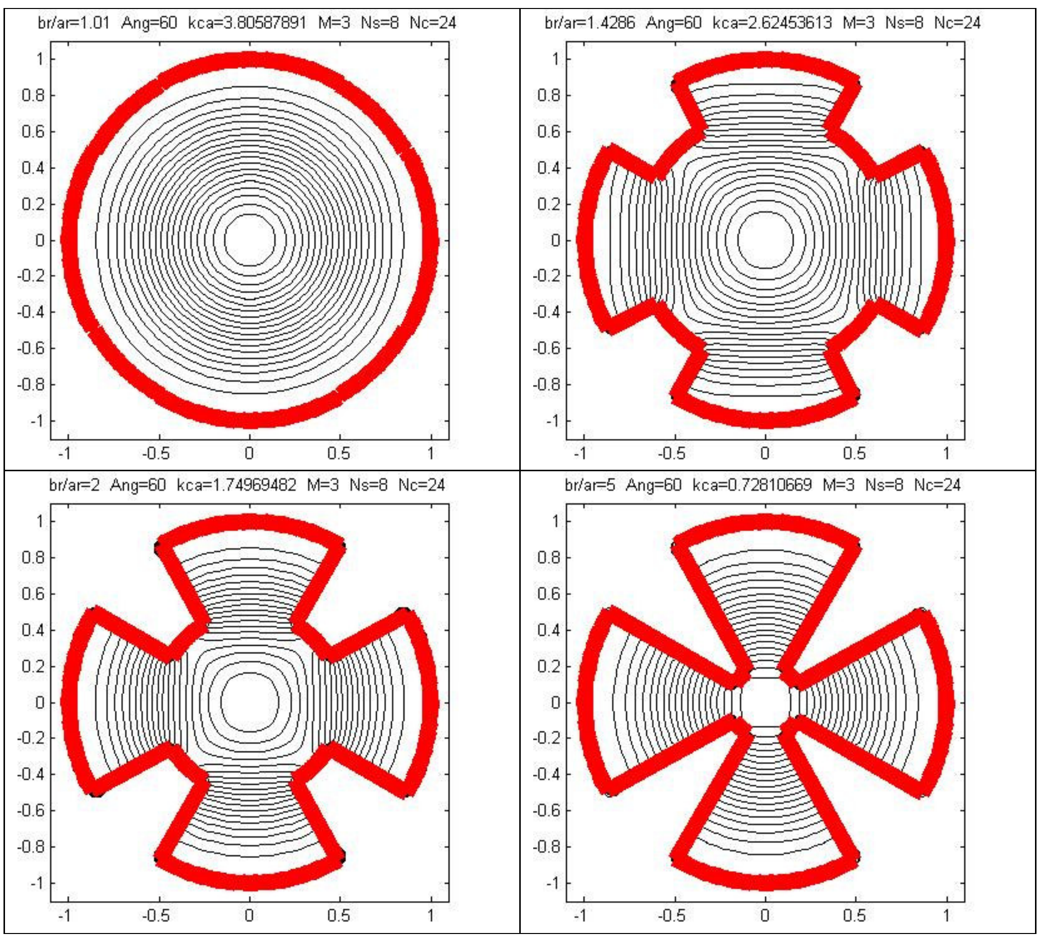

Figure 3.14 Electric field lines for the first TE mode with N=4, q=0, cos pol.

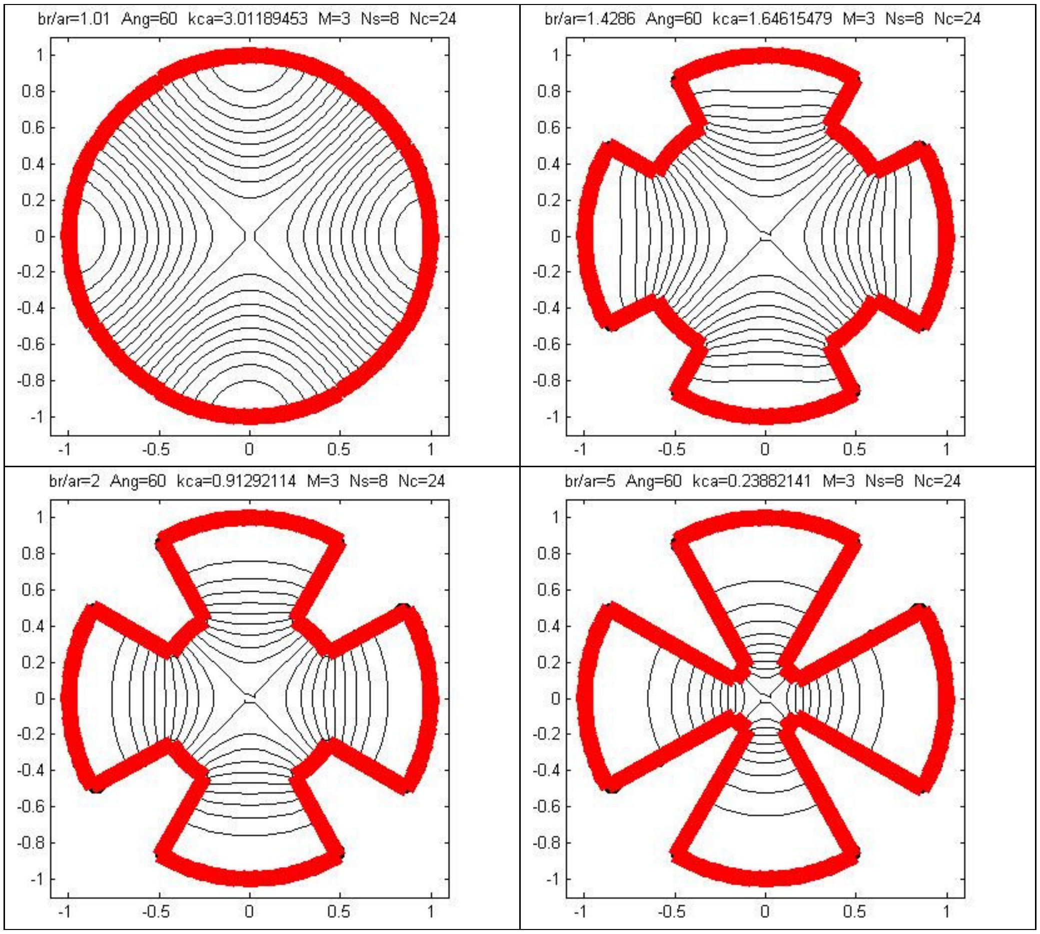

Figure 3.15 Electric field lines for the first TE mode with N=4, q=2, cos pol.

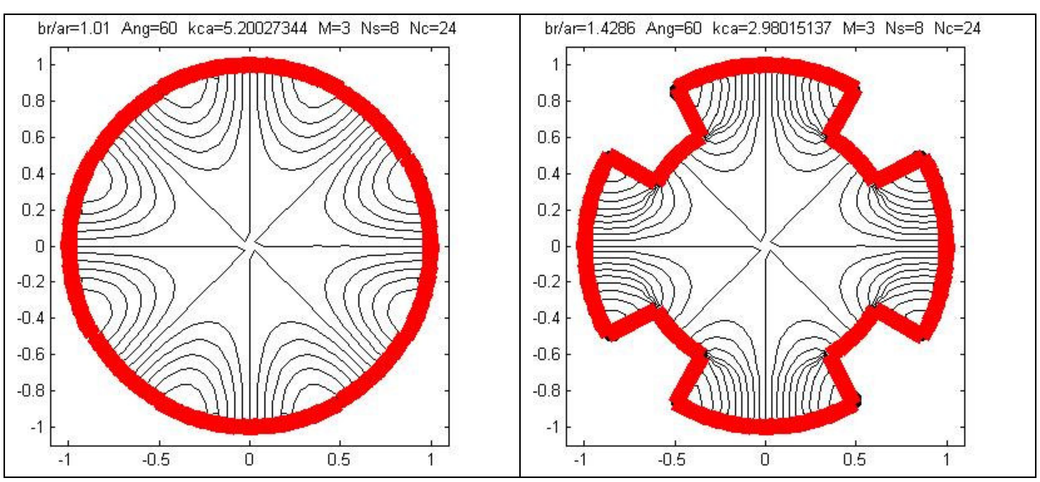

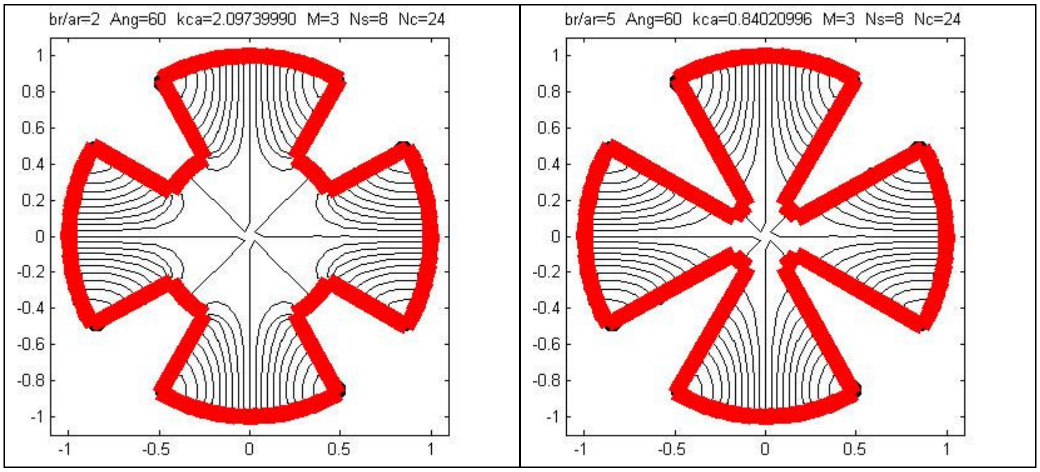

Figure 3.16 Electric field lines for the first TE mode with N=4, q=0, sin pol.

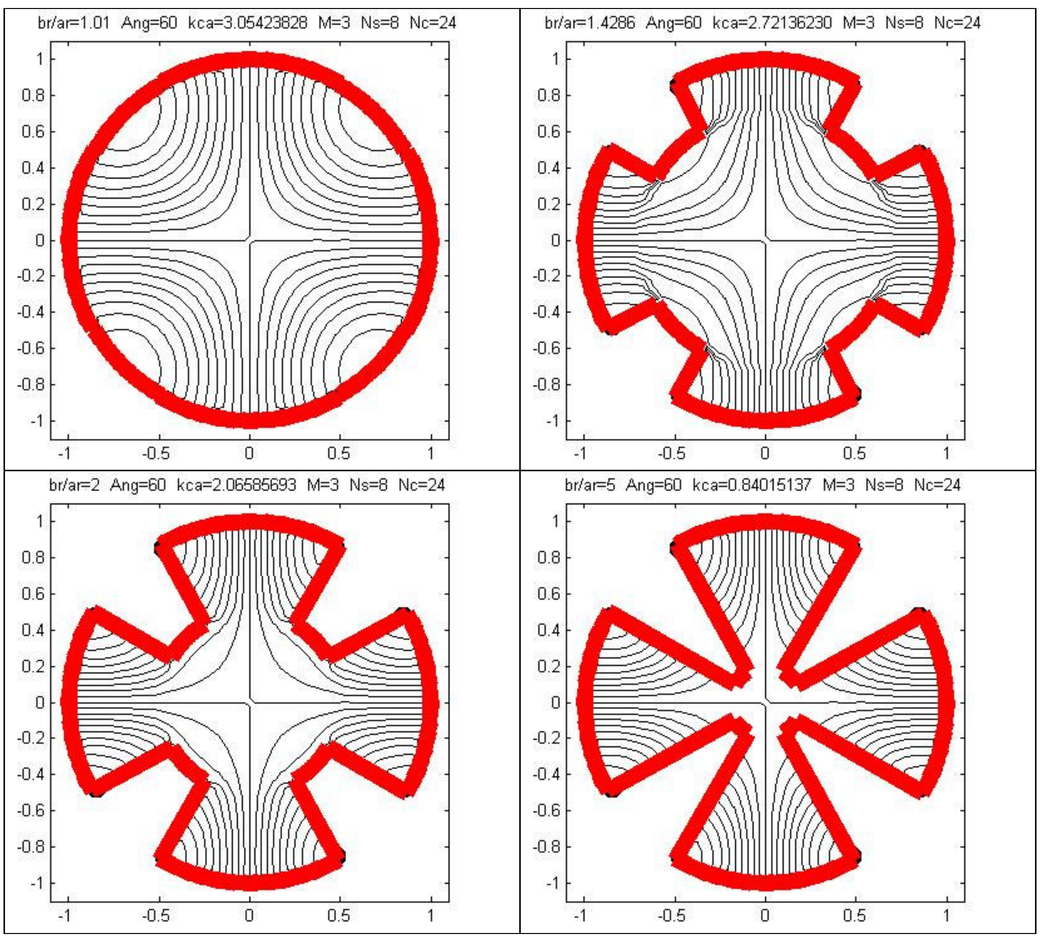

Figure 3.17 Electric field lines for the first TE mode with N=4, q=2, sin pol.

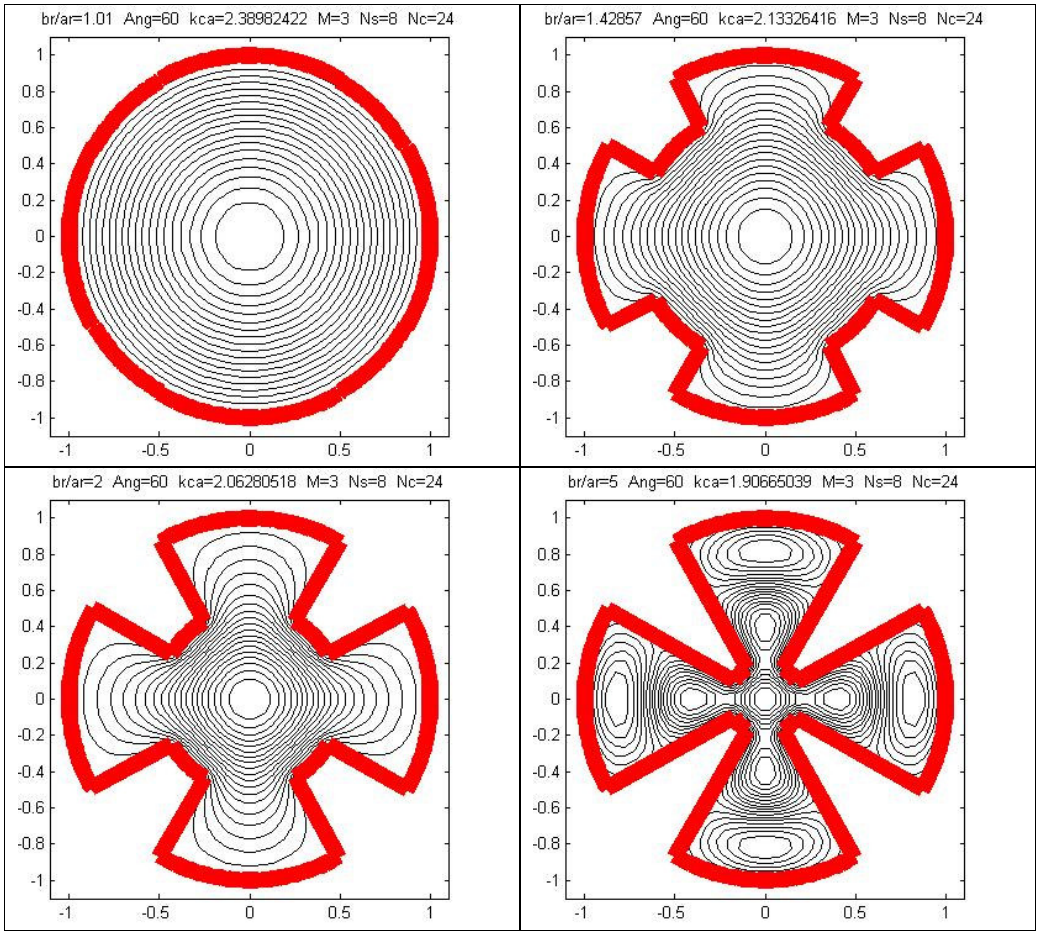

Figure 3.18 Magnetic field lines for the first TM mode with N=4, q=0, cos pol.

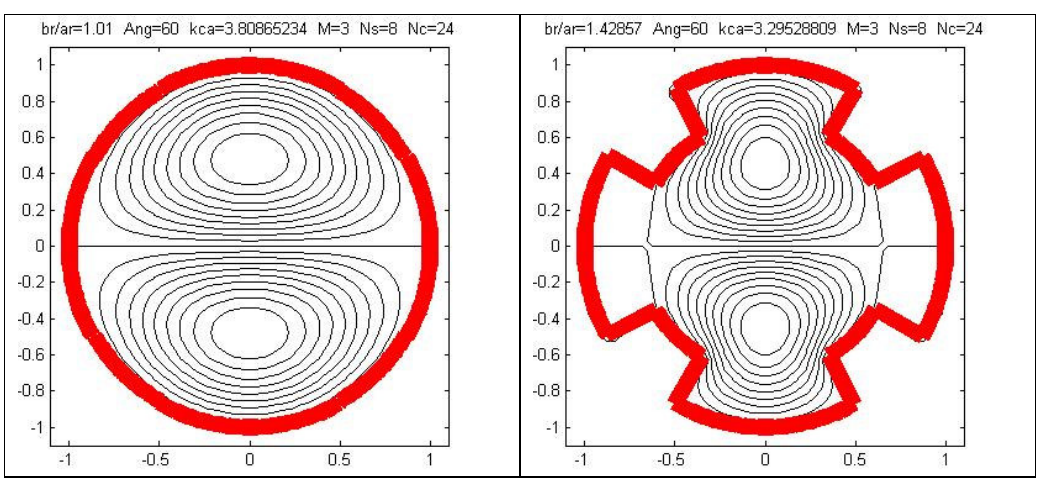

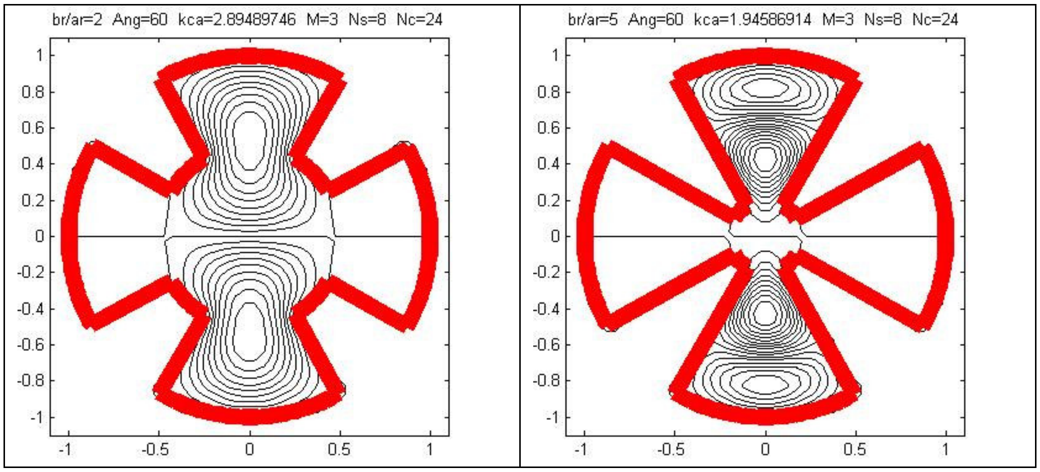

Figure 3.19 Magnetic field lines for the first TM mode with N=4, q=1, cos pol.

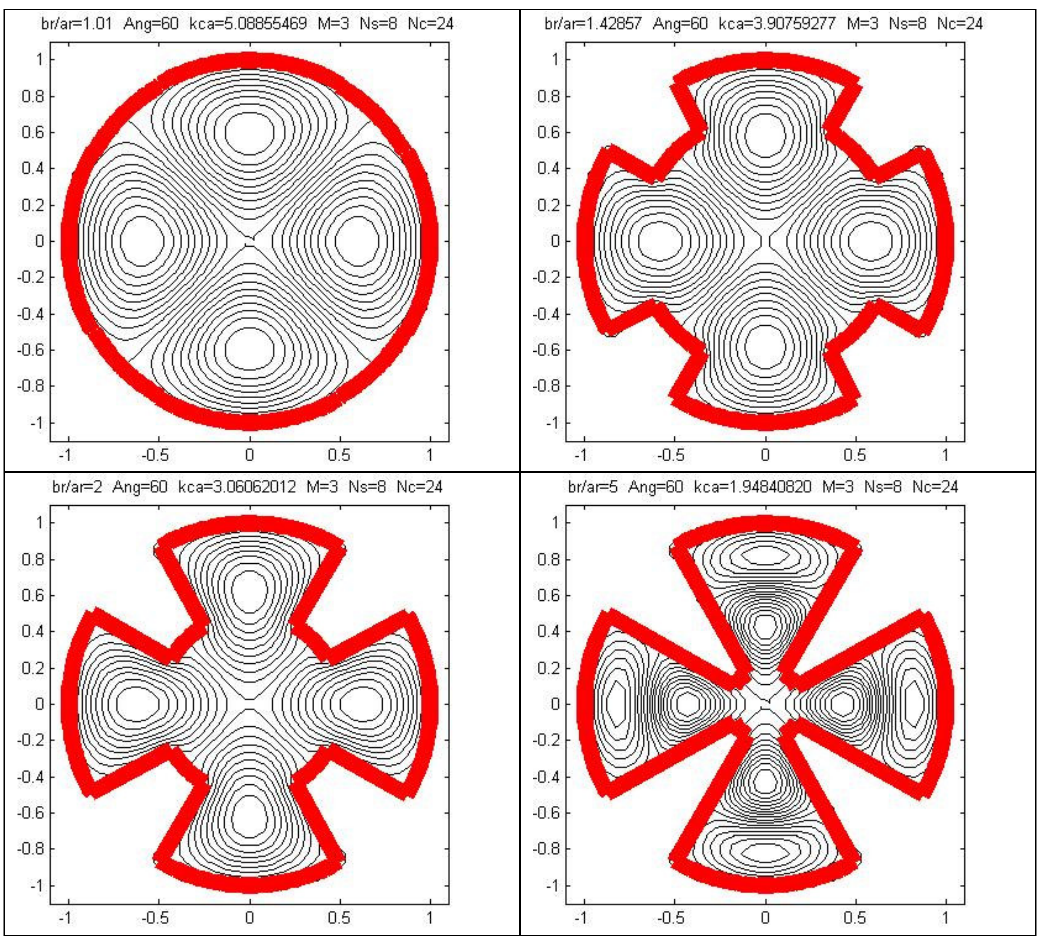

Figure 3.20 Magnetic field lines for the first TM mode with N=4, q=2, cos pol.

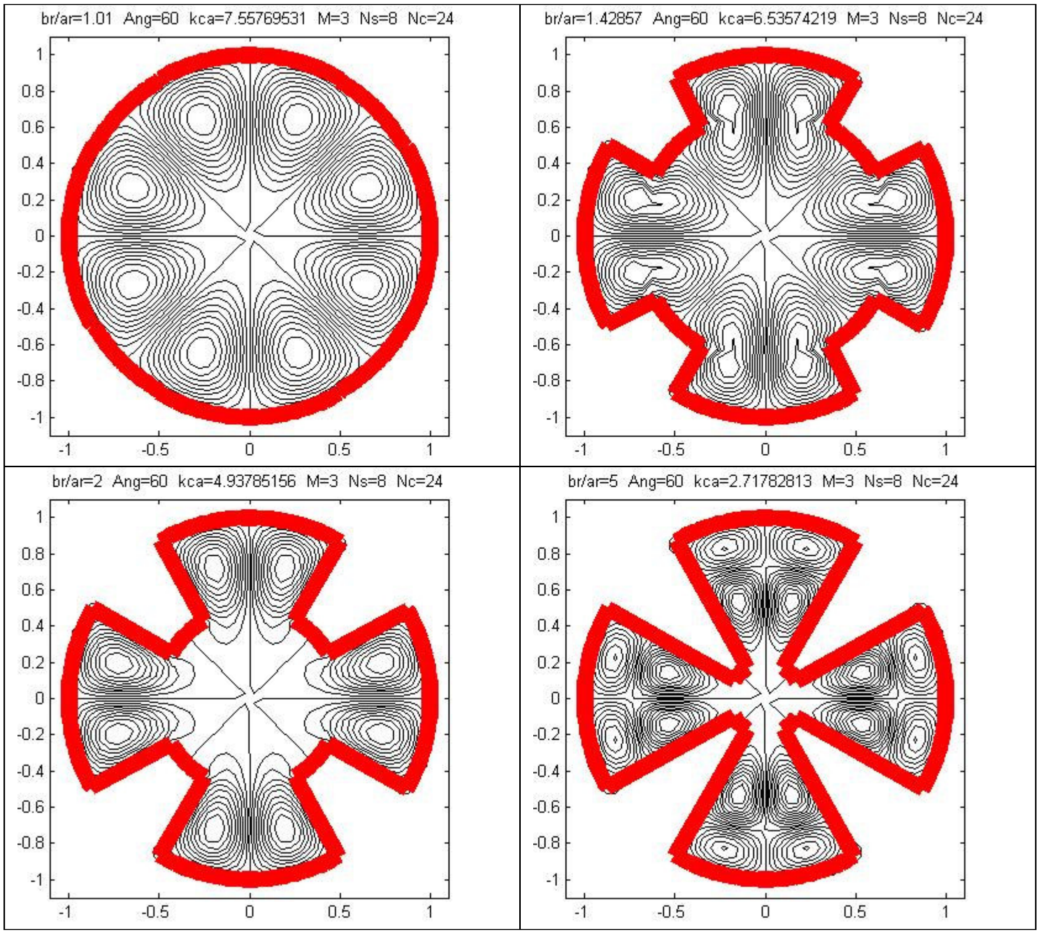

Figure 3.21 Magnetic field lines for the first TM mode with N=4, q=0, sin pol.

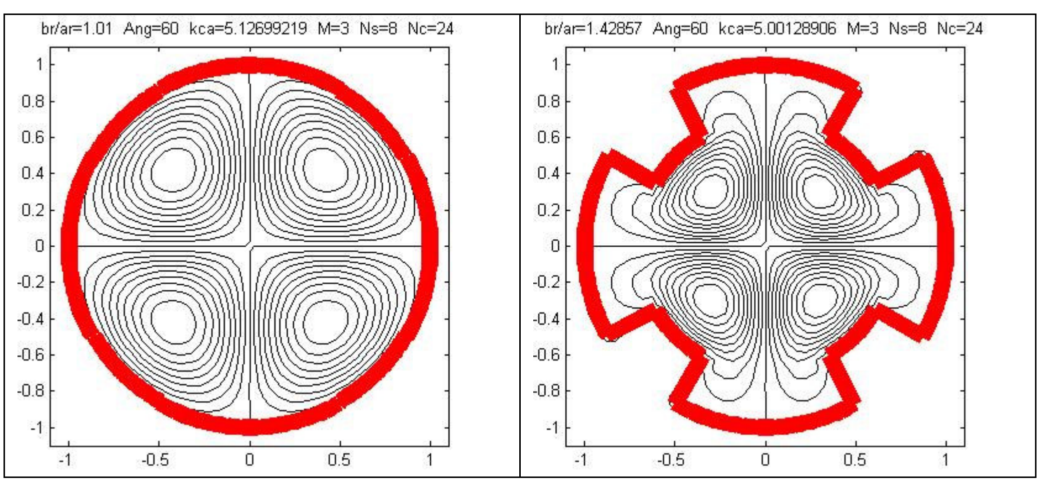

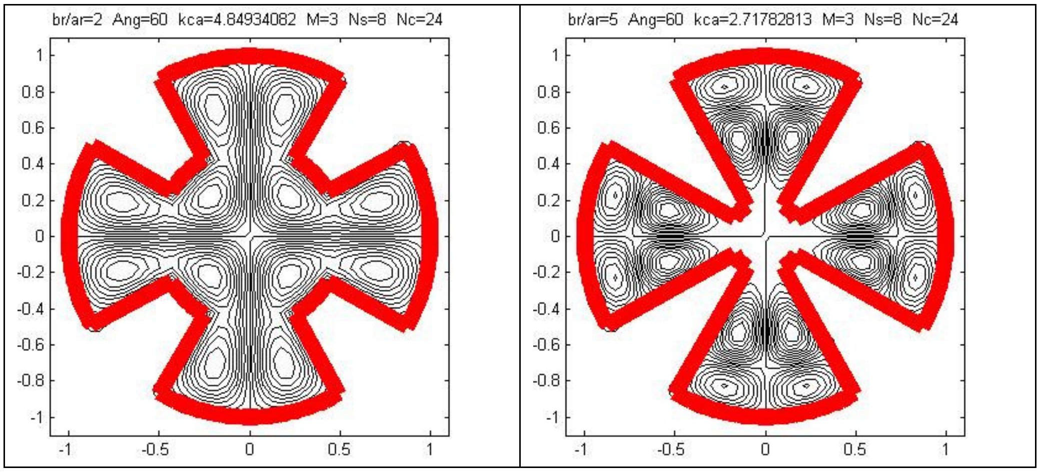

Figure 3.22 Magnetic field lines for the first TM mode with N=4, q=2, sin pol.

As seen from the Figure 3.21, it is curious to notice that the first mode found for the circular waveguide happens to be TM_{41} mode. This is the first circular mode which has sine polarized and zero phased quadruple symmetry enforced.

Finally, the plots of TE and TM modes are presented at the following figures for various angular widths of slots. The parameters b and b/a ratio are fixed to 1 cm and 2 respectively and Θ is varied to 20, 40, 70 and 85 degrees.

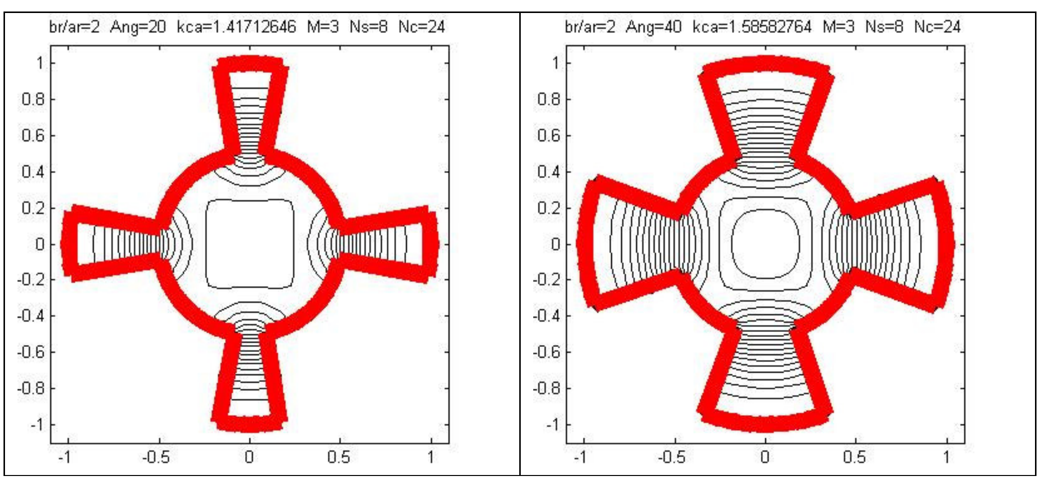

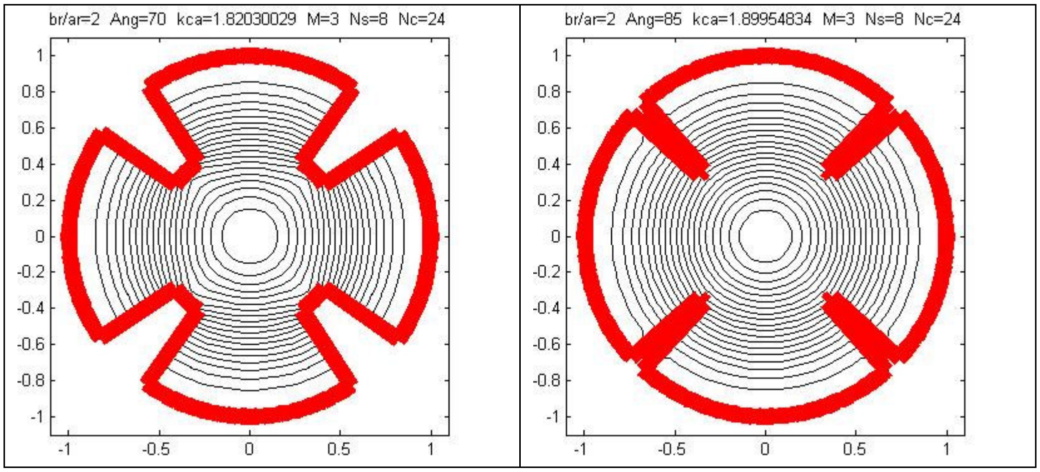

Figure 3.23 Electric field lines for the first TE mode with N=4, q=0, cos pol.

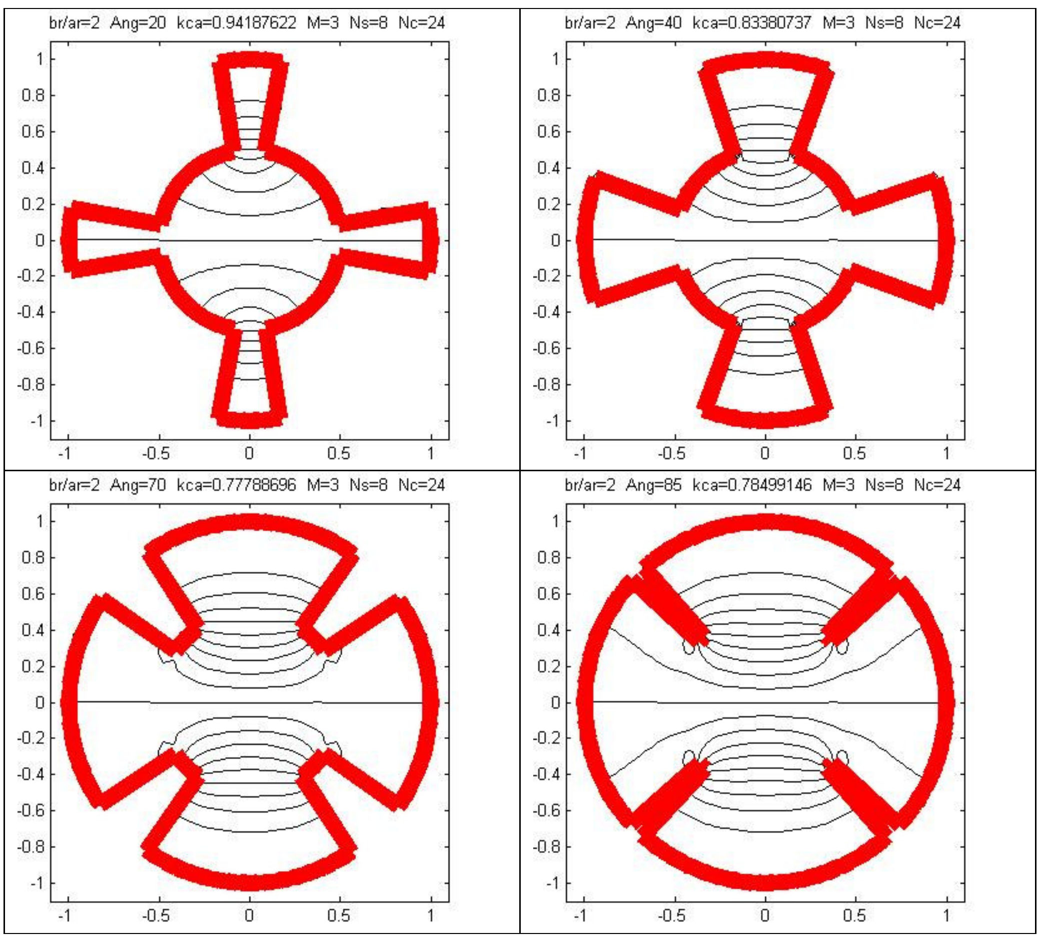

Figure 3.24 Electric field lines for the first TE mode with N=4, q=1, cos pol.

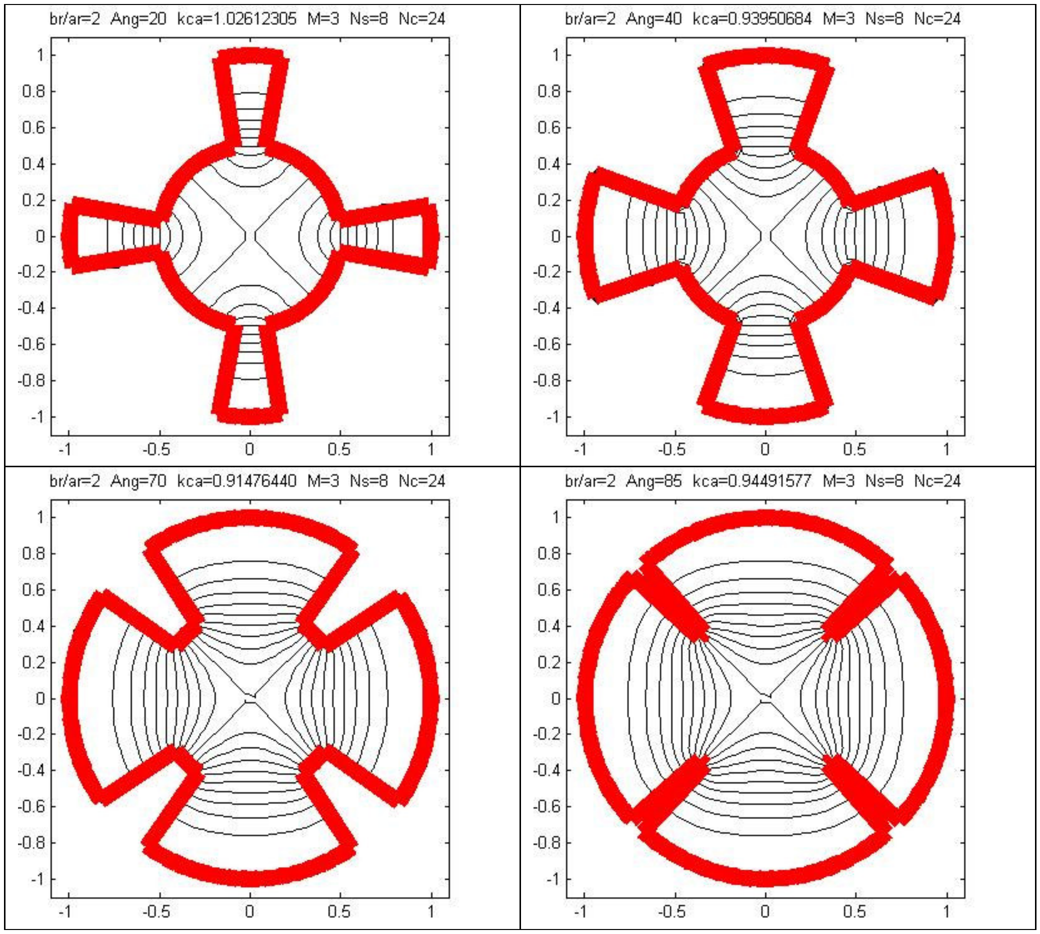

Figure 3.25 Electric field lines for the first TE mode with N=4, q=2, cos pol.

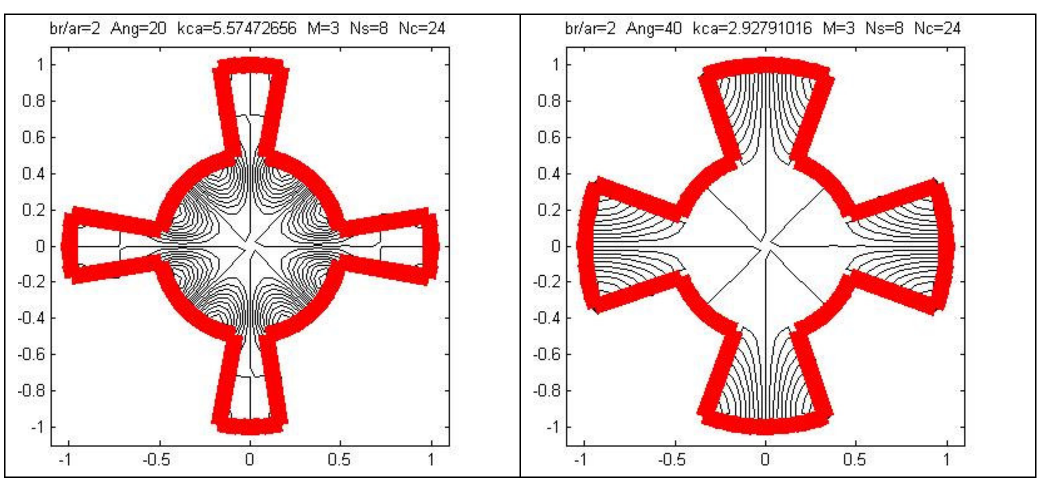

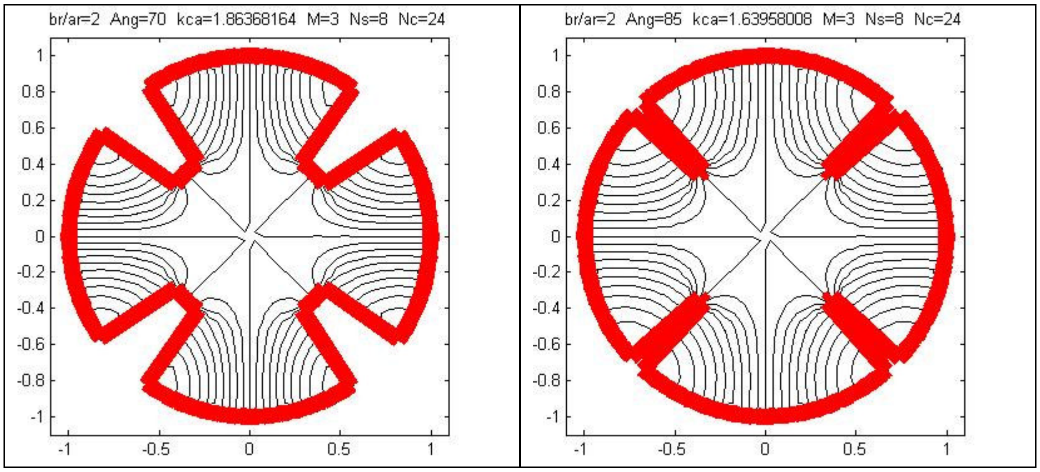

Figure 3.26 Electric field lines for the first TE mode with N=4, q=0, sin pol.

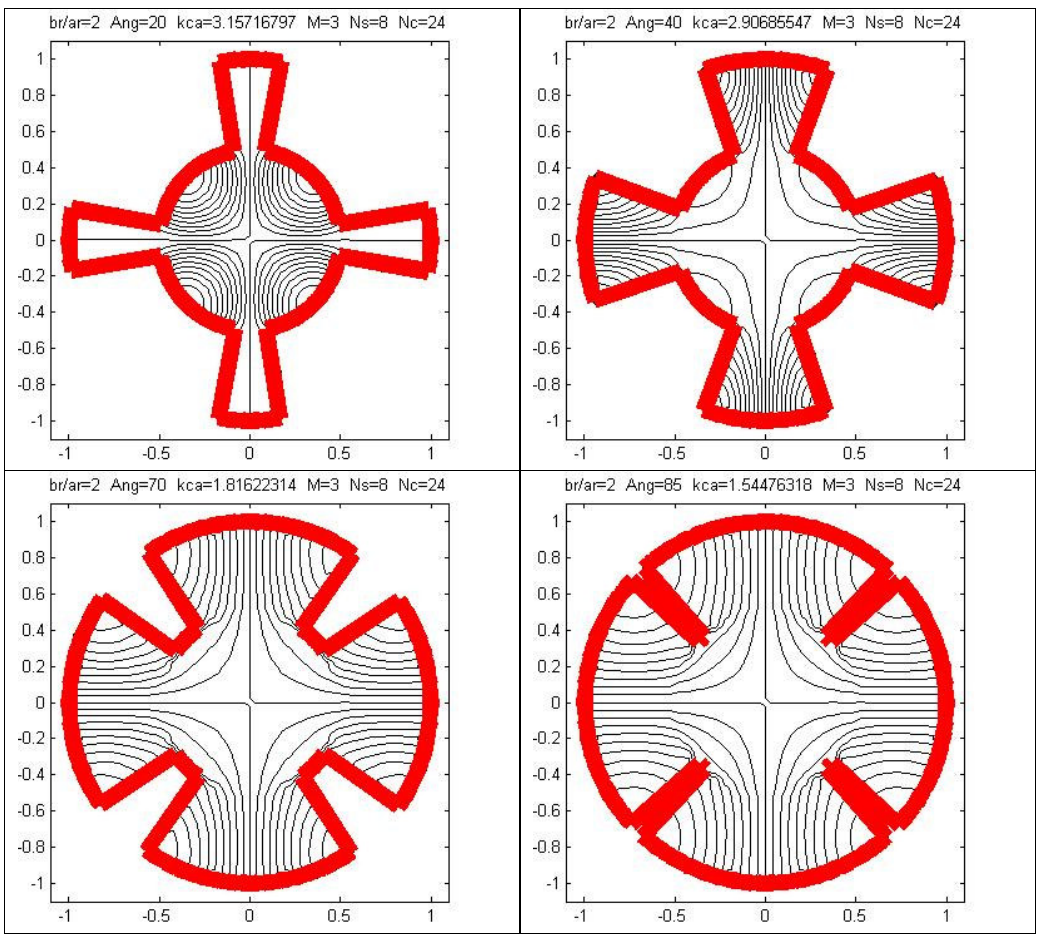

Figure 3.27 Electric field lines for the first TE mode with N=4, q=2, sin pol.

3.10 Variation of Power Handling Capacity with Dimensions

The maximum power that may pass through a waveguide will depend on the maximum electric field strength that can exist without breakdown. Experimental data on allowable field strengths at ultra high frequencies indicates a value of 30 000 V/cm applicable for air filled waveguides under standard sea level pressure, temperature and humidity conditions.

Supposing that the maximum electric field strength is E_{max} then the upper limit of the transmitted power P_{max} in the waveguide can be computed through the following relation:

$$\begin{aligned} P_{\max} &= \left(\frac{30000}{E_{\max}}\right)^2 \cdot \left[\frac{1}{2} \mathrm{Re} \iint_S (E_{t_r} H_{t_\theta}^* - E_{t_\theta} H_{t_r}^*) dS\right] \\ &= \left(\frac{30000}{E_{\max}}\right)^2 \cdot P \end{aligned} \tag{3.4}$$

With this maximum allowable field strength specified, the variation of power handling capacities of the slotted waveguides for N=3 and N=4 with changing azimuthal and radial dimensions are computed and the results are presented at the following tables.

Table 3-10 Power handling capacity of dominant mode (TE11) for triple ridge waveguide (b=1 cm, $\Theta=60^o$, M=3, Ns=8, Nc=24 and f_0=10 GHz)

(b-a)/b	kca(TE11)	Cutoff Frequency (GHz)	Maximum Power (watt)	Waveguide Surface (cm^2)
0.01	1.83840820	8.86641674	813,507.393	3.110
0.10	1.73668213	9.21338485	547,697.314	2.843
0.20	1.54390869	9.21452624	369,670.193	2.576
0.30	1.30252686	8.88443950	227,969.091	2.340
0.50	0.79769897	7.61746405	186,234.443	1.963
0.60	0.57622375	6.87816436	160,722.575	1.822
0.80	0.22450867	5.35974969	84,825.281	1.634

Table 3-11 Power handling capacity of dominant mode (TE11) for quadruple ridge waveguide (b=1 cm, ϴ=60^o, M=3, Ns=8, Nc=24 and f_0=10 GHz)

(b-a)/b	kca(TE11)	Cutoff Frequency (GHz)	Maximum Power (watt)	Waveguide Surface (cm^2)
0.01	1.83784180	8.86368506	814,753.267	3.121
0.10	1.72432617	9.14783445	648,330.257	2.943
0.20	1.52315674	9.09067216	420,708.501	2.765
0.30	1.28231201	8.74655550	322,325.515	2.608
0.50	0.78748169	7.51989621	255,031.679	2.356
0.60	0.57004700	6.80443484	220,449.573	2.262
0.80	0.22297668	5.32317612	112,115.869	2.136

As seen from the Tables 3.12 and 3.13, the power handling capacities are decreasing since the ridges are closer to each other and also the surface of the waveguides are decreasing.

The quadruple ridge waveguide has better power handling capability than triple ridge waveguide. But its bandwidth characteristic is poor because of mode splitting. The power handling at infinite frequency and dominant mode wavelength characteristics of the triple and quadruple ridged waveguides are shown in Figure 3.28 by rearranging the results given in Table 3.10 and 3.11. A good agreement with the results of [23] is observed.

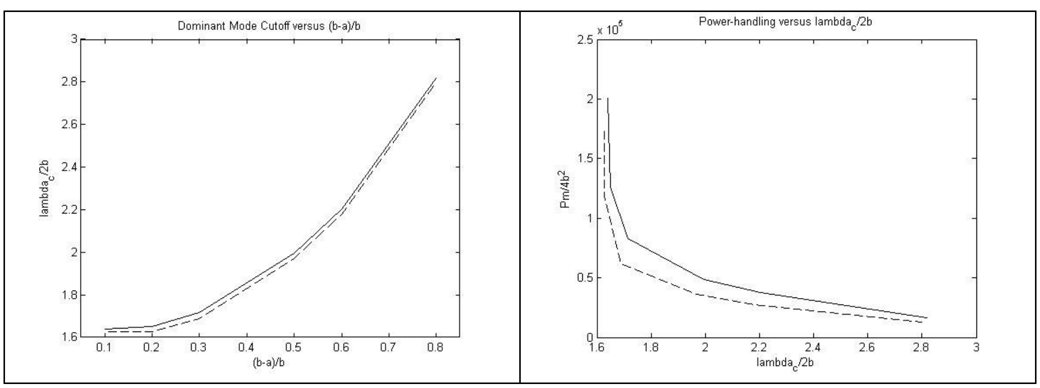

Figure 3.28 Dominant mode cutoff wavelength and Power handling for N=4 and N=3 (dashed line).

CHAPTER 4

CONCLUSION

The aim of the study was to derive the details of the application of generalized spectral domain approach to the analysis of slot-coupled waveguides and to check the validity.

The method has been presented and applied to the slotted circular waveguides. It is shown that the method is very effective to calculate the eigenwaves of a slotted circular waveguide. The results obtained show good agreement with the ones that exist in the literature.

The method used here is based on decomposing the structure into two separate waveguides by short-circuiting the coupling slots to make it more familiar: a hollow circular waveguide and N sector waveguides. Two surface magnetic currents at both sides of the slot replace the non-vanishing slot tangential electric field. These two surface magnetic currents are equal in magnitude and opposite in direction; so the continuity of the tangential electric field is satisfied. Both of them behave as sources over the related waveguide regions. The field components for each individual region were expanded according to their eigenfunctions. In addition, the surface magnetic currents at the slots are expanded in terms of suitable basis functions, which satisfy the edge condition at the 90^{o} slot edges.

The elements of the characteristic matrix for each individual waveguide contain doubly infinite sums over radial and azimuthal indices of the related eigenmodes. It has been found that the summations over the index corresponding to the direction normal to the surface current can be solved analytically and have closed form expressions. This increases the numerical efficiency of the method significantly.

The inclusion of the edge condition in the basis functions makes the numerical approach very efficient as shown by the convergence study. This allows keeping the number of basis functions, which determines the characteristic matrix dimension, lower.

The electric and magnetic field lines corresponding to the dominant as well as a number of higher order modes in the transverse plane are graphed for triple and quadruple ridged waveguides. Computer output plots of electric and magnetic field lines that satisfy the boundary conditions prove the results to be perfectly true.

It is found that the quadruple ridged waveguide has a second lowest cutoff frequency very close to the dominant mode. Thus the single mode operating bandwidth is very small. A large bandwidth can be achieved if and only if the second lowest mode is sufficiently suppressed or not excited.

The technique is easily applicable to situations where more ridges are present. The presented method is very efficient and can calculate all kinds of existing field behaviours over the structure in an acceptable time.

REFERENCES

[1] A.S. Omar, “Application of the GSD Technique to The Analysis of Slot-Coupled Waveguides”, *IEEE Trans. Microwave Theory and Tech,* vol.-42,no.11, pp.2139-2148, 1994

[2] P.Dally, “Polar Geometry Waveguides by Finite-Element Methods”, *IEEE Trans. Microwave Theory and Tech,* vol.MTT-22, pp.202-209, 1974.

[3] F.Canatan, “Cutoff Wavenumbers of Ridged Circular Waveguides via Ritz-Galerkin Approach”, *Electronic Lett.,* vol.25, pp.1036-614, 1989.

[4] S.Aygün, “Ritz-Galerkin Study of Circular Waveguides with Double T-Septa”, *M.Sc. Thesis in Electrical and Electronics Engineering,* METU, 1990.

[5] T.Koçak, “Ritz-Galerkin Analysis of a Circular Waveguide with a Thin Metallic Septum”, *M.Sc. Thesis in Electrical and Electronics Engineering,* METU, 1993.

[6] H.GUO, “Special Complex Open-Cavity and Low-Magnetic Field High Power Gyrotron”, *IEEE Trans. Plasma Sci.,* Vol.PS-18, pp.326-333, 1990.

[7] Spira-Hakkarainen, S.Kreischer and K. Temkin, “Slotted –resonator gyrotron experiments”, *IEEE Trans. Electron Devices,* Vol. ED-38, pp.1544-1552, 1991.

[8] A.Jöstingmeier, “Closed-Form Expressions for a Number of Fourier-Bessel Series Encountered in the GSD Method”, *IEEE Trans. Microwave and Guided wave lett.,* vol.-2, no.10, pp.391,1992

[9] U.Balaji, “Radial Mode Matching Analysis of Ridged Circular Waveguides”, *IEEE Trans. Microwave Theory and Tech,* vol.44, pp.1183-1186, 1996.

[10] W.Sun, “Analysis and Design of Quadruple-Ridged Waveguides”, *IEEE Trans. Microwave Theory and Tech,* vol.42, pp.2201-2207, 1994.

[11] S.Amari, “A Comparative Study of Two Integral Equation Formulations of TE Modes in Circular Ridged Waveguide”, *J.of Electromagnetic Waves and App*, Vol.11, pp.1057-1072, 1997

[12] R.A. Waldron, *The Theory of Waveguides and Cavities*, New York: Gordon and Breach Science Publishers, 1967.

[13] R. Harrington, *Time-Harmonic Electromagnetic Fields*, New York: McGraw-Hill, 1966.

[14] Johnson J.H. Wang, *“Generalized Moment Methods in Electromagnetics”,* New York: John Wiley & Sons Inc, 1991.

[15] R.E. Collin, *Field Theory of Guided Waves*, New York: McGraw-Hill, 1960.

[16] A.S.Omar, “Scattering By Material and Conducting Bodies Inside Waveguides, Part I: Theoretical Formulations”, *IEEE Trans. Microwave Theory and Tech,* vol. MTT-34, no.2, pp.266-272, 1986.

[17] I.S.Gradshteyn, *Table of Integrals, Series and Products*, New York: Dover 1972.

[18] R.A. Waldron, *Theory of Guided Electromagnetic Waves*, London: Van Nostrand Reinhold Company, 1969.

[19] A.S.Omar, “Application of the generalized spectral domain technique to the analysis of rectangular waveguides with rectangular and circular metal inserts”, *IEEE Trans. Microwave Theory and Tech,* vol.-39, pp.944-952, 1991.

[20] J.A. Cochran, “Unusual identities for special functions from waveguide propagation analysis”, *IEEE Trans. Microwave Theory and Tech,* vol.MTT-36, pp.611-614, 1988.

[21] S.Chapra, *Numerical Methods for Engineers*, New York: McGraw-Hill, 1988.

[22] M.Abramowitz and Stegun, *Handbook of mathematical Functions*, New York: Dover 1972.

[23] Y.Rong, “Chareacteristics of Generalized Rectangular and Circular Ridge Waveguide”, *IEEE Trans. Microwave Theory and Tech,* vol.48, No.2, pp.258-265, 2000.

APPENDIX-A

ANALYTICAL SUMMATIONS OF INFINITE SERIES OVER THE RADIAL INDEX

A1 Closed-Form Expressions for Characteristic Matrices

The eigenmodes of one waveguide can be expanded with respect to the eigenmodes of another waveguide in a similar manner with the analysis presented in [8] and [20]. Use of the orthogonality property of the eigenmodes is made in order to yield some identities. The closed-form expressions of the infinite sums under consideration can consequently be obtained by suitable linear combinations of these identities.

Considering two waveguides of cross section S_1 and S_2, with $S_1 \subset S_2$, which are joined in the plane z=constant (i.e. =0), where z denotes the longitudinal coordinate.

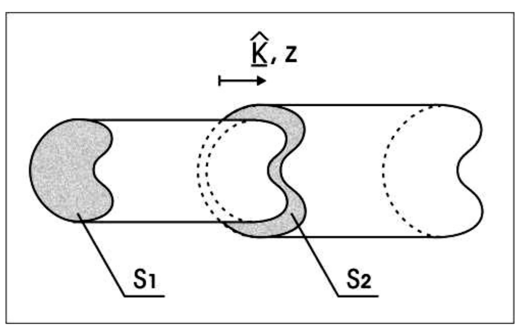

Figure A1 Transition of Waveguide Cross Sections

The fields for separate waveguides (i=1, 2) can be obtained according to (2.4). The field expansion functions of the first waveguide are shown with index (1), and the field expansion functions of the second waveguide as (2). The transverse and longitudinal components of the eigenmodes corresponding to the waveguide (2) can be expanded with respect to the eigenmodes of waveguide (1) on the common cross section S_1.

$$\nabla_t \Phi_q^{(2)} = \sum_p c_{pq} \nabla_t \Phi_p^{(1)} + \sum_p a_{pq} (\nabla_t \Psi_p^{(1)} \times \hat{k}) \tag{A1.1.1}$$

$$(\nabla_t \Psi_q^{(2)} \times \hat{k}) = \sum_p d_{pq} \nabla_t \Phi_p^{(1)} + \sum_p b_{pq} (\nabla_t \Psi_p^{(1)} \times \hat{k}) \tag{A1.1.2}$$

$$\Phi_q^{(2)} = \sum_p f_{pq} (k_{pTM}^{(1)})^2 \Phi_p^{(1)} \tag{A1.1.3}$$

Making use of the orthogonality relations (2.5) and (2.6) results in:

$$\begin{aligned}
a_{pq} &= \int_{(S_1)} (\nabla_t \Psi_p^{(1)} \times \hat{k})^* \cdot (\nabla_t \Phi_q^{(2)}) dS \\
b_{pq} &= \int_{(S_1)} (\nabla_t \Psi_p^{(1)})^* \cdot (\nabla_t \Psi_q^{(2)}) dS \\
c_{pq} &= \int_{(S_1)} (\nabla_t \Phi_p^{(1)})^* \cdot (\nabla_t \Phi_q^{(2)}) dS \\
d_{pq} &= \int_{(S_1)} (\nabla_t \Phi_p^{(1)})^* \cdot (\nabla_t \Psi_q^{(2)} \times \hat{k}) dS \\
f_{pq} &= \int_{(S_1)} (\Phi_p^{(1)})^* \cdot (\Phi_q^{(2)}) dS
\end{aligned} \tag{A1.2}$$

Testing the expansions (A1.1) with respect to the expansion functions of the waveguide (2), the following equalities are obtained:

$$\sum_p c_{pq} c_{pq}^* + \sum_p a_{pq} a_{pq}^* = \int_{(S_2 - S_1)} (\nabla_t \Phi_q^{(2)}) \cdot (\nabla_t \Phi_p^{(2)})^* dS \tag{A1.3.1}$$

$$\sum_p c_{pq} d_{pq}^* + \sum_p a_{pq} b_{pq}^* = \int_{(S_2 - S_1)} (\nabla_t \Phi_q^{(2)}) \cdot (\nabla_t \Psi_p^{(2)} \times \hat{k})^* dS \tag{A1.3.2}$$

$$\sum_p d_{pq}d_{pq}^* + \sum_p b_{pq}b_{pq}^* = \int_{(S_2-S_1)} (\nabla_t\Psi_q^{(2)})\cdot(\nabla_t\Psi_p^{(2)})^* dS \qquad \text{(A1.3.3)}$$

$$\sum_p (k_{pTM}^{(1)})^2 f_{pq}f_{pq}^* = \int_{(S_2-S_1)} (\Phi_q^{(2)})\cdot(\Phi_p^{(2)})^* dS \qquad \text{(A1.3.4)}$$

Applying the Stoke's theorem, the coefficients a_{pq}, b_{pq}, c_{pq}, d_{pq} and f_{pq} can be written as:

$$\begin{aligned}
a_{pq} &= \int_{(C_1)} (\nabla_t\Psi_p^{(1)})^* \cdot (\Phi_q^{(2)}))dl \\
b_{pq} &= (k_{pTE}^{(1)})^2 \int_{(S_1)} (\Psi_p^{(1)})^* \cdot (\Psi_p^{(2)})dS \\
c_{pq} &= (k_{qTM}^{(2)})^2 \int_{(S_1)} (\Phi_p^{(1)})^* \cdot (\Phi_q^{(2)})dS \qquad \text{(A1.4)} \\
d_{pq} &= 0 \\
f_{pq} &= \tfrac{1}{(k_{qTM}^{(2)})^2} c_{pq}
\end{aligned}$$

The formulation above is used for the transition of two hollow circular waveguides.

All identities here will be shown with tilda (~) prefixed to distinguish from the others. Assuming the radius of the first hollow circular waveguide as 'a' and the radius of the second waveguide as 'b'>'a', and using the expressions (2.56) and (2.59) as field expansion functions; the surface integrals in (A1.4) will be simple integrals with Bessel functions that can be calculated analytically. Considering that the first waveguide satisfies the boundary conditions specified in (2.57) and (2.60),

$$\tilde{a}_{mn} = -j2\pi \tilde{C}^{(2)}_{TM_n}\tilde{C}^{(1)}_{TE_m} pJ_p(\tilde{k}^{(2)}_{nTM}a)J_p(\tilde{k}^{(1)}_{mTE}a)$$

$$\tilde{b}_{mn} = 2\pi \tilde{C}^{(2)}_{TE_n}\tilde{C}^{(1)}_{TE_m} \frac{(\tilde{k}^{(2)}_{nTE}a)}{1-(\frac{\tilde{k}^{(2)}_{nTE}}{\tilde{k}^{(1)}_{mTE}})^2} J_p(\tilde{k}^{(1)}_{mTE}a)J_p'(\tilde{k}^{(2)}_{nTE}a) \tag{A1.5}$$

$$\tilde{c}_{mn} = 2\pi \tilde{C}^{(2)}_{TM_n}\tilde{C}^{(1)}_{TM_m} \frac{(\tilde{k}^{(1)}_{mTM}a)}{1-(\frac{\tilde{k}^{(1)}_{mTM}}{\tilde{k}^{(2)}_{nTM}})^2} J_p(\tilde{k}^{(2)}_{nTM}a)J_p'(\tilde{k}^{(1)}_{mTM}a)$$

The relations between different orders vanish because of the orthogonality property of the complex exponential functions, and only the expressions with the common radial orders p are considered ($p_n=p_m=p$).

The expression given in (A1.3.1) can be written after some manipulations as:

$$\begin{aligned} &p^2\sum_m(\tilde{C}^{(1)}_{TE_m}J_p(\tilde{k}^{(1)}_{mTE}a))^2 + \sum_m[(\tilde{k}^{(2)}_{nTM})^2\frac{\tilde{C}^{(1)}_{TM_m}\tilde{k}^{(1)}_{mTM}a}{(\tilde{k}^{(2)}_{nTM})^2-(\tilde{k}^{(1)}_{mTM})^2}J_p'(\tilde{k}^{(1)}_{mTM}a)]^2 \\ &= \frac{(\tilde{k}^{(2)}_{nTM}a)^2}{4\pi}[(1-(\frac{p}{\tilde{k}^{(2)}_{nTM}a})^2)+\frac{2}{\tilde{k}^{(2)}_{nTM}a}\frac{J_p'(\tilde{k}^{(2)}_{nTM}a)}{J_p(\tilde{k}^{(2)}_{nTM}a)}+(\frac{J_p'(\tilde{k}^{(2)}_{nTM}a)}{J_p(\tilde{k}^{(2)}_{nTM}a)})^2] \end{aligned} \tag{A1.6}$$

In the same way the equality given in (A1.3.4) can be written as:

$$\begin{aligned} &\sum_m[\tilde{C}^{(1)}_{TM_m}\frac{(\tilde{k}^{(1)}_{mTM})^2}{(\tilde{k}^{(2)}_{nTM})^2-(\tilde{k}^{(1)}_{mTM})^2}J_p'(\tilde{k}^{(1)}_{mTM}a)]^2 \\ &= \frac{1}{4\pi}(1-(\frac{p}{\tilde{k}^{(2)}_{nTM}a})^2)+\frac{1}{4\pi}(\frac{J_p'(\tilde{k}^{(2)}_{nTM}a)}{J_p(\tilde{k}^{(2)}_{nTM}a)})^2 \end{aligned} \tag{A1.7}$$

The linear combination of (A1.6) and $-(\tilde{k}^{(2)}_{nTM}a)^2$ times (A1.7) results in:

$$-\left(\frac{p}{\tilde{k}_{nTM}^{(2)}a}\right)^2\sum_m[\tilde{C}_{TE_m}^{(1)}J_p(\tilde{k}_{mTE}^{(1)}a)]^2+\sum_m\frac{(\tilde{k}_{mTM}^{(1)})^2}{(\tilde{k}_{nTM}^{(2)})^2-(\tilde{k}_{mTM}^{(1)})^2}[\tilde{C}_{TM_m}^{(1)}J_p'(\tilde{k}_{mTM}^{(1)}a)]^2$$
$$=-\frac{1}{2\pi(\tilde{k}_{nTM}^{(2)}a)}\frac{J_p'(\tilde{k}_{nTM}^{(2)}a)}{J_p(\tilde{k}_{nTM}^{(2)}a)} \tag{A1.8}$$

From the relation given in (A1.3.2),

$$\sum_m\frac{(\tilde{k}_{mTE}^{(1)})^2}{(\tilde{k}_{mTE}^{(1)})^2-(\tilde{k}_{nTE}^{(2)})^2}[\tilde{C}_{TE_m}^{(1)}J_p(\tilde{k}_{mTE}^{(1)}a)]^2$$
$$=\frac{1}{2\pi(\tilde{k}_{nTE}^{(2)}a)}\frac{J_p(\tilde{k}_{nTE}^{(2)}a)}{J_p'(\tilde{k}_{nTE}^{(2)}a)} \tag{A1.9}$$

The expressions given in (A1.1)-(A1.4) can be used also for the waveguide transition of two sector waveguides.

Let the outer radius of both of sector waveguides be ‘b’ and the angular width be Θ. Assume the inner radius of the first sector waveguide ‘a’ (a<b) and the inner radius of the second sector waveguide ‘c’ (c<b). Substituting the field expansion functions described in (2.63) and (2.69) into (A1.4), the surface integrals will be simple integrals that can be calculated analytically. Considering that both sectors satisfy the boundary conditions specified in (2.65) and (2.71), the coefficients a_{mn}, b_{mn}, c_{mn} can be written as:

$$a_{mn}=\nu\frac{\Theta}{2}C_{TE_m}^{(1)}C_{TM_n}^{(2)}F_\mu^{(TM)}(k_{nTM}^{(2)}a)F_\mu^{(TE)}(k_{mTE}^{(1)}a)$$
$$b_{mn}=(1+\delta_{\mu0})\frac{\Theta}{2}\frac{k_{nTE}^{(2)}a(k_{mTE}^{(1)})^2}{(k_{nTE}^{(2)})^2-(k_{mTE}^{(1)})^2}C_{TE_m}^{(1)}C_{TE_n}^{(2)}F_\mu^{(TE)'}(k_{nTE}^{(2)}a)F_\mu^{(TE)}(k_{mTE}^{(1)}a) \tag{A1.10}$$
$$c_{mn}=(1+\delta_{\mu0})\frac{\Theta}{2}\frac{k_{mTM}^{(1)}a(k_{nTM}^{(2)})^2}{(k_{nTM}^{(2)})^2-(k_{mTM}^{(1)})^2}C_{TM_m}^{(1)}C_{TM_n}^{(2)}F_\mu^{(TM)}(k_{nTM}^{(2)}a)F_\mu^{(TM)'}(k_{mTM}^{(1)}a)$$

where $\delta_{\mu0}$ is the Kronecker delta.

Since the sine and cosine functions are orthogonal functions, the function indices can be written as μ_n=μ_m=μ.

The expression given in (A1.3.1) can be written after some manipulations as:

$$\begin{aligned}
&\nu^2\sum_m (C^{(1)}_{TE_m} F^{(TE)}_\mu (k^{(1)}_{mTE}a))^2 + (k^{(2)}_{nTM}a)^4 \sum_m \frac{(k^{(1)}_{mTM}a)^2}{[(k^{(1)}_{mTM}a)^2-(k^{(2)}_{nTM}a)^2]^2}[C^{(1)}_{TM_m} F^{(TM)'}_\mu (k^{(1)}_{mTM}a)]^2 \\
&= \frac{1}{\Theta}[(k^{(2)}_{nTM}b)^2(\frac{F^{(TM)'}_\mu (k^{(2)}_{nTM}b)}{F^{(TM)}_\mu (k^{(2)}_{nTM}a)})^2 - (k^{(2)}_{nTM})^2(1-(\frac{\nu}{k^{(2)}_{nTM}a})^2) \\
&-(k^{(2)}_{nTM}a)^2(\frac{F^{(TM)'}_\mu (k^{(2)}_{nTM}a)}{F^{(TM)}_\mu (k^{(2)}_{nTM}a)})^2 - 2(k^{(2)}_{nTM}a)\frac{F^{(TM)'}_\mu (k^{(2)}_{nTM}a)}{F^{(TM)}_\mu (k^{(2)}_{nTM}a)}]
\end{aligned} \tag{A1.11}$$

The equality given in (A1.3.4) can be written in the same way as:

$$\begin{aligned}
&\sum_m \frac{(k^{(1)}_{mTM}a)^4}{[(k^{(2)}_{nTM})^2-(k^{(1)}_{mTM})^2]^2}[C^{(1)}_{TM_m} F^{(TM)'}_\mu (k^{(1)}_{mTM}a)]^2 \\
&= \frac{1}{\Theta}[(\frac{b}{a})^2(\frac{F^{(TM)'}_\mu (k^{(2)}_{nTM}b)}{F^{(TM)}_\mu (k^{(2)}_{nTM}a)})^2 - (1-(\frac{\nu}{k^{(2)}_{nTM}a})^2) - (\frac{F^{(TM)'}_\mu (k^{(2)}_{nTM}a)}{F^{(TM)}_\mu (k^{(2)}_{nTM}a)})^2]
\end{aligned} \tag{A1.12}$$

The linear combination of (A1.11) and (A1.12) results in:

$$\begin{aligned}
&-\nu^2\sum_m \frac{[C^{(1)}_{TE_m} F^{(TE)}_\mu (k^{(1)}_{mTE}a)]^2}{(k^{(2)}_{nTM}a)^2} + \sum_m \frac{(k^{(1)}_{mTM})^2}{(k^{(1)}_{mTM})^2-(k^{(2)}_{nTM})^2}[C^{(1)}_{TM_m} F^{(TM)'}_\mu (k^{(1)}_{mTM}a)] \\
&= \frac{2}{\Theta}\frac{1}{(k^{(2)}_{nTM}a)}(\frac{F^{(TM)'}_\mu (k^{(2)}_{nTM}a)}{F^{(TM)}_\mu (k^{(2)}_{nTM}a)})
\end{aligned} \tag{A1.13}$$

and the relation given in (A1.3.2) leads to,

$$\sum_m \frac{(k_{mTE}^{(1)})^2}{(k_{mTE}^{(1)})^2 - (k_{nTE}^{(2)})^2} (C_{TE_m}^{(1)} F_\mu^{(TE)}(k_{mTE}^{(1)} a))^2$$
$$= -\frac{2}{(1+\delta_{\mu 0})\Theta} \frac{1}{(k_{nTE}^{(2)} a)} \frac{F_\mu^{(TE)}(k_{nTE}^{(2)} b)}{F_\mu^{(TE)\prime}(k_{nTE}^{(2)} a)} \tag{A1.14}$$

A2 Closed-Form Expressions for Magnetic and Electric Fields

The closed-form expressions for the infinite summations over the radial index to simplify the magnetic and electric field components can be found by the same way given in Appendix A1. Similarly, the cross section of two waveguides will be used to determine the closed-form expressions.

The transition between two hollow circular waveguides with radius ‘a’ and ‘b’, where a<b will be examined.

Substituting the coefficients given in the equations (A1.5) into equation (A1.1.1), the following two relations can be obtained:

$$\sum_m \frac{jp}{(\tilde{k}_{nTM}^{(2)} a)^2} (\tilde{C}_{TE_m}^{(1)})^2 J_p(\tilde{k}_{mTE}^{(1)} a) \frac{jp}{r/a} J_p(\tilde{k}_{mTE}^{(1)} r)$$
$$+ \sum_m \frac{\tilde{k}_{mTM}^{(1)} a}{(\tilde{k}_{mTM}^{(1)} a)^2 - (\tilde{k}_{nTM}^{(2)} a)^2} (\tilde{C}_{TM_m}^{(1)})^2 J_p{}'(\tilde{k}_{mTM}^{(1)} a) \tilde{k}_{mTM}^{(1)} a J_p{}'(\tilde{k}_{mTM}^{(1)} r)$$
$$= -\frac{1}{2\pi} \frac{1}{\tilde{k}_{nTM}^{(2)} a} \frac{J_p'(\tilde{k}_{nTM}^{(2)} r)}{J_p(\tilde{k}_{nTM}^{(2)} a)}$$

(A2.1)

$$\sum_m \frac{jp}{(\tilde{k}_{nTM}^{(2)} a)^2} (\tilde{C}_{TE_m}^{(1)})^2 J_p(\tilde{k}_{mTE}^{(1)} a) \tilde{k}_{mTE}^{(1)} a J_p{}'(\tilde{k}_{mTE}^{(1)} r)$$
$$- \sum_m \frac{\tilde{k}_{mTM}^{(1)} a}{(\tilde{k}_{mTM}^{(1)} a)^2 - (\tilde{k}_{nTM}^{(2)} a)^2} (\tilde{C}_{TM_m}^{(1)})^2 J_p{}'(\tilde{k}_{mTM}^{(1)} a) \frac{jp}{r/a} J_p(\tilde{k}_{mTM}^{(1)} r)$$
$$= \frac{1}{2\pi} \frac{1}{(\tilde{k}_{nTM}^{(2)} a)^2} \frac{jp}{r/a} \frac{J_p(\tilde{k}_{nTM}^{(2)} r)}{J_p(\tilde{k}_{nTM}^{(2)} a)}$$

and the relation given in (A1.1.3) leads to;

$$\sum_m \frac{(\tilde{k}^{(1)}_{mTM}a)^2}{(\tilde{k}^{(1)}_{mTM}a)^2-(\tilde{k}^{(2)}_{nTM}a)^2}(\tilde{C}^{(1)}_{TM_m})^2 J_p{}'(\tilde{k}^{(1)}_{mTM}a)\tilde{k}^{(1)}_{mTM}aJ_p(\tilde{k}^{(1)}_{mTM}r)$$
$$=-\frac{1}{2\pi}\frac{J_p(\tilde{k}^{(2)}_{nTM}r)}{J_p(\tilde{k}^{(2)}_{nTM}a)} \qquad \text{(A2.2)}$$

These two equations can be used to determine TM waves of the hollow circular waveguide (the equations (2.116) and (2.117)).

By the same way, the following two identities can be found and they can be used to express TE waves of the hollow circular waveguide (the equations (2.114) and (2.115)) by taking into account the relation given in (A1.1.2).

$$\sum_m \frac{(\tilde{k}^{(1)}_{mTE})^2}{(\tilde{k}^{(1)}_{mTE})^2-(\tilde{k}^{(2)}_{nTE})^2}(\tilde{C}^{(1)}_{TE_m})^2 J_p(\tilde{k}^{(1)}_{mTE}a)J_p(\tilde{k}^{(1)}_{mTE}r)$$
$$=-\frac{1}{2\pi}\frac{1}{\tilde{k}^{(2)}_{nTE}a}\frac{J_p(\tilde{k}^{(2)}_{nTE}r)}{J'_p(\tilde{k}^{(2)}_{nTE}a)}$$

$$\text{(A2.3)}$$

$$\sum_m \frac{(\tilde{k}^{(1)}_{mTE})^2}{(\tilde{k}^{(1)}_{mTE})^2-(\tilde{k}^{(2)}_{nTE})^2}(\tilde{C}^{(1)}_{TE_m})^2 J_p(\tilde{k}^{(1)}_{mTE}a)\tilde{k}^{(1)}_{mTE}aJ'_p(\tilde{k}^{(1)}_{mTE}r)$$
$$=\frac{1}{2\pi}\frac{J'_p(\tilde{k}^{(2)}_{nTE}r)}{J'_p(\tilde{k}^{(2)}_{nTE}a)}$$

Now, the transition between two sector waveguides will be examined. Similarly, substituting the coefficients given in (A1.10) into the equation (A1.1.1) results in:

$$
\begin{aligned}
&\sum_m \frac{\nu}{(k_{nTM}^{(2)}a)^2}(C_{TE_m}^{(1)})^2 F_\mu^{(TE)}(k_{mTE}^{(1)}a)\frac{-\nu}{r/a}F_\mu^{(TE)}(k_{mTE}^{(1)}r) \\
&+\sum_m \frac{k_{mTM}^{(1)}a}{(k_{mTM}^{(1)}a)^2-(k_{nTM}^{(2)}a)^2}(C_{TM_m}^{(1)})^2 F_\mu^{(TM)'}(k_{mTM}^{(1)}a)k_{mTM}^{(1)}aF_\mu^{(TM)'}(k_{mTM}^{(1)}r) \\
&=\frac{2}{\Theta}\frac{1}{k_{nTM}^{(2)}a}\frac{F_\mu^{(TM)'}(k_{nTM}^{(2)}r)}{F_\mu^{(TM)}(k_{nTM}^{(2)}a)} \qquad for \quad \mu\geq 1
\end{aligned}
\tag{A2.4}
$$

$$
\begin{aligned}
&\sum_m \frac{\nu}{(k_{nTM}^{(2)}a)^2}(C_{TE_m}^{(1)})^2 F_\mu^{(TE)}(k_{mTE}^{(1)}a)k_{mTE}^{(1)}aF_\mu^{(TE)'}(k_{mTE}^{(1)}r) \\
&-\sum_m \frac{k_{mTM}^{(1)}a}{(k_{mTM}^{(1)}a)^2-(k_{nTM}^{(2)}a)^2}(C_{TM_m}^{(1)})^2 F_\mu^{(TM)'}(k_{mTM}^{(1)}a)\frac{\nu}{r/a}k_{mTM}^{(1)}aF_\mu^{(TM)}(k_{mTM}^{(1)}r) \\
&=-\frac{2}{\Theta}\frac{1}{(k_{nTM}^{(2)}a)^2}\frac{\nu}{r/a}\frac{F_\mu^{(TM)}(k_{nTM}^{(2)}r)}{F_\mu^{(TM)}(k_{nTM}^{(2)}a)} \qquad for \quad \mu\geq 1
\end{aligned}
$$

Taking into account the equation (A1.1.3), it can be reached that:

$$
\begin{aligned}
&\sum_m \frac{(k_{mTM}^{(1)}a)^2}{(k_{mTM}^{(1)}a)^2-(k_{nTM}^{(2)}a)^2}(C_{TM_m}^{(1)})^2 F_\mu^{(TM)'}(k_{mTM}^{(1)}a)\frac{\nu}{r/a}k_{mTM}^{(1)}aF_\mu^{(TM)}(k_{mTM}^{(1)}r) \\
&=-\frac{2}{\Theta}\frac{F_\mu^{(TM)}(k_{nTM}^{(2)}r)}{F_\mu^{(TM)}(k_{nTM}^{(2)}a)} \qquad for \quad \mu\geq 1
\end{aligned}
\tag{A2.5}
$$

Last two equations can be used to determine TM waves for the sector waveguide (the equations (2.121) and (2.122))

The following two identities can be found and they can be used to express TE waves of the sector waveguide (the equations (2.119) and (2.120)) by taking into account the relation given in (A1.1.2).

$$\sum_m \frac{(k_{mTE}^{(1)})^2}{(k_{mTE}^{(1)})^2-(k_{nTE}^{(2)})^2}(C_{TE_m}^{(1)})^2 F_\mu^{(TE)}(k_{mTE}^{(1)}a)F_\mu^{(TE)}(k_{mTE}^{(1)}r)$$
$$=-\frac{2-\delta_{\mu 0}}{\Theta}\frac{1}{k_{nTE}^{(2)}a}\frac{F_\mu^{(TE)}(k_{nTE}^{(2)}r)}{F_\mu^{(TE)\prime}(k_{nTE}^{(2)}a)}$$

(A2.6)

$$\sum_m \frac{(k_{mTE}^{(1)})^2}{(k_{mTE}^{(1)})^2-(k_{nTE}^{(2)})^2}(C_{TE_m}^{(1)})^2 F_\mu^{(TE)}(k_{mTE}^{(1)}a)k_{mTE}^{(1)}aF_\mu^{(TE)\prime}(k_{mTE}^{(1)}r)$$
$$=-\frac{2-\delta_{\mu 0}}{\Theta}\frac{F_\mu^{(TE)\prime}(k_{nTE}^{(2)}r)}{F_\mu^{(TE)\prime}(k_{nTE}^{(2)}a)}$$

APPENDIX B

DESCRIPTION OF GRAPHICAL USER INTERFACE

In this section, a guideline of the graphical user interface will be introduced. The screen given in Figure B.1 appears when the command ‘tezimGUI’ is written on the command line of MATLAB.

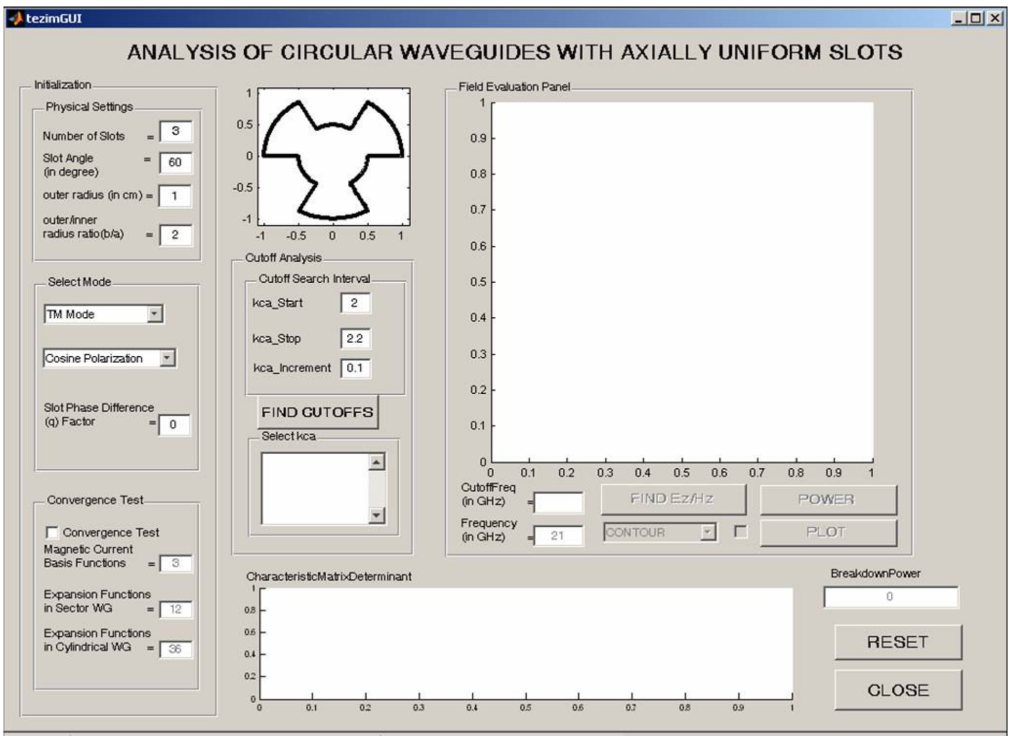

Figure B.1 GUI starting view

At the left hand side, the initialization section has to be set before starting to the analysis. This section is divided to three sub categories. In the first part, the geometrical settings of the waveguide structure should be done. These are:

Number of Slots : it can be 2 or more. Initially it is set to 3.

Slot Angle (in degree) : Initially it is set to 60 degree. It can be changed in the allowed range related to the number of slots.

Outer radius (in cm) : Initially it is set to 1 cm. It should be chosen according to the desired frequency range.

Outer/inner radius ratio (b/a) : Initially it is set to 2. So, the inner radius ‘a’ is 0.5 cm.

When the geometrical settings are changed, the waveguide structure view will be automatically displayed at the small figure window at the right side.

In the second part of the initialization section is ‘Select Mode’ part. Here, the modal preferences should be set. It is possible to select with the aid of a pull down menu, the mode type, TM or TE (it is initially set to TM mode) and the polarization type, sine or cosine polarization (it is initially set to cosine polarization). The slot phase difference (q) factor defines different class of modes and it can be set between 0 and N-1 (N is the number of slots). The q factor is initially set to 0.

The convergence test part is the third part of initialization section. Initially this part is inactive. When the convergence test check box is chosen, the number of surface magnetic current basis functions, the number of field expansion functions in sector waveguide and the number of field expansion functions in hollow circular waveguide edit boxes are activated and can be set to different values.

After the initialization, it is now the time to set the search interval for cutoff wavenumber(s) (kca_Start and kca_Stop) and the sampling rate (kca_Increment). The sampling rate is initially set to 0.1, but sometimes when the zero crossings and asymptotes are so close to each other; it is required to adjust the increment value to smaller values like 0.01 or 0.001.

The push-button ‘Find Cutoffs’ starts the first stage of the analysis. If any cutoff could not be found a warning is displayed. In this case, the interval has to be changed or if it is expected to have at least one, the increment value for sampling has to be lowered. If there is any zero crossing in the search interval, they are listed in the ‘Select kca’ list box and the corresponding determinant curve is displayed in the figure window named as ‘CharacteristicMatrixDeterminant’ at the bottom of GUI window. Using this determinant graph, it is easy to recognize which values of kca are concerned to an asymptote and which one is a real zero crossing.

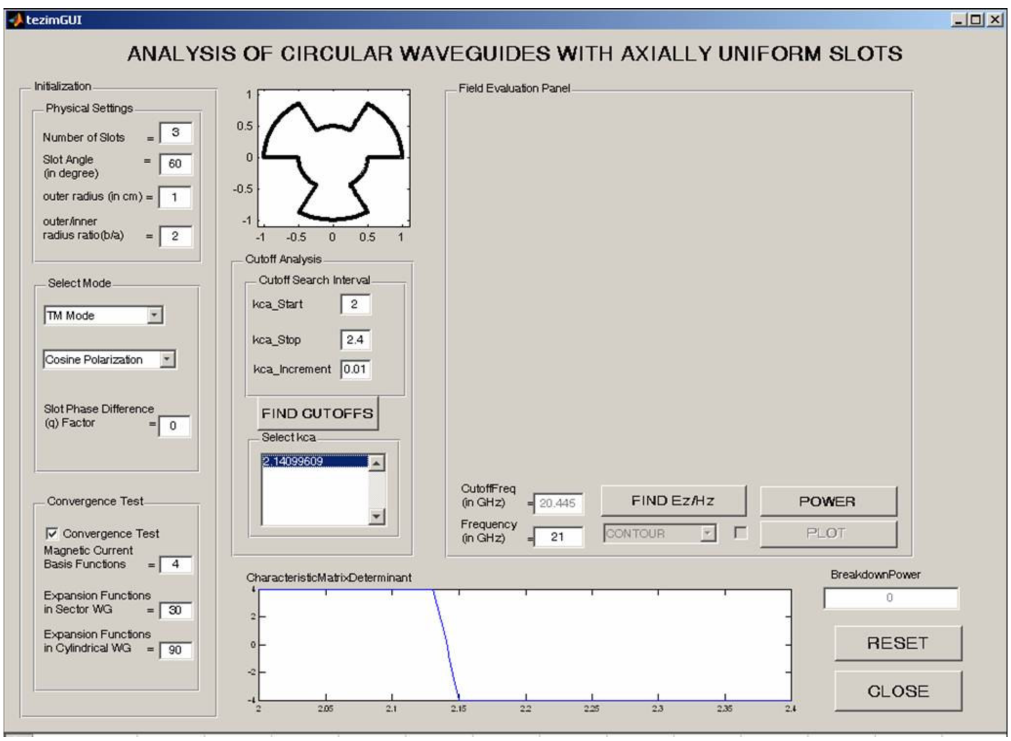

Figure B.2 GUI view at the end of cutoff analysis

When at least one cutoff wavenumber kca is found in the specified interval, the field evaluation panel at the right hand side will be activated. The related cutoff frequency for selected cutoff wavenumber is displayed automatically in GHz. Here, the operation frequency has to be set for field and power analysis.

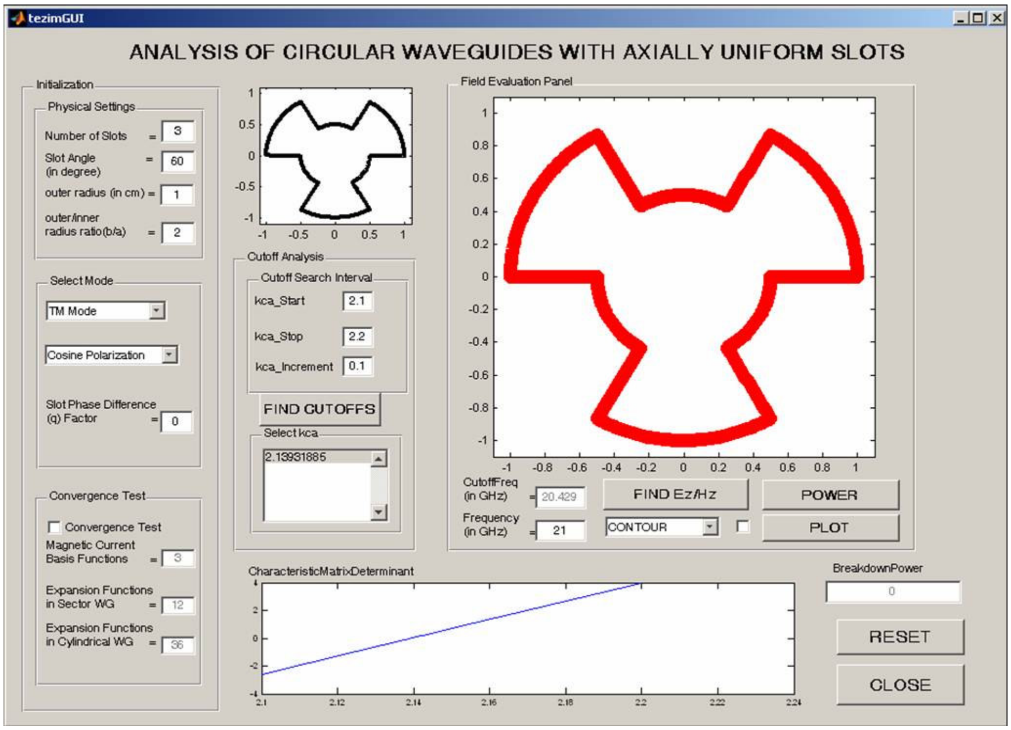

Figure B.3 GUI view at the end of field evaluation.

The push-button 'Find Ez/Hz' starts the field analysis for the selected cutoff wavenumber ($k_c a$). When the calculations for field evaluation is terminated the figure window and plot button of the field evaluation panel are activated as given in figure B.3.

Contour and surf plot options are available. When the plot button is pushed the field lines is displayed as given in Figure B.4.

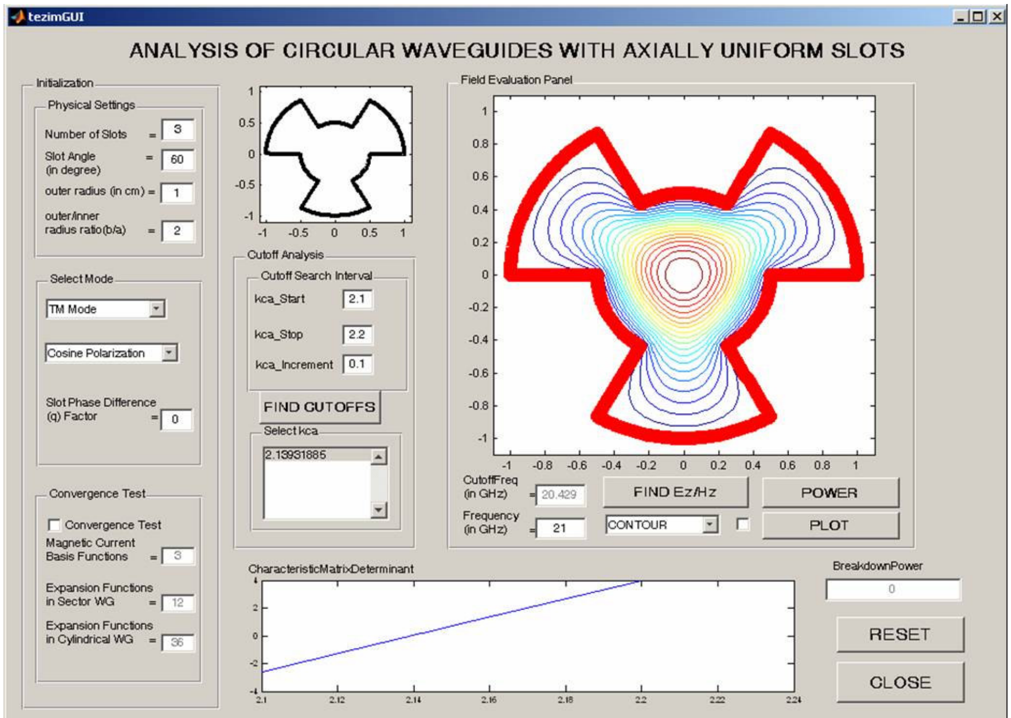

Figure B.4 GUI view at the end of plot process.

The power calculation over the waveguide structure can be also done for the related cutoff wavenumber and specified operation frequency. The distribution of power vector can be displayed by 'plot' button with the same way of plotting the field distributions. The amount of breakdown power for selected frequency and dimensions can be seen on the 'Breakdown Power' box at the right side of GUI screen.

The version of MATLAB used in this analysis is Version 7.0.1.24704 (R14) Service Pack 1, September13, 2004. A program bug is encountered for the surf plots of the fields. A reset button is added to overcome this bug for the application in this version. When the version 7.2.0.232 (R2006a), January 27, 2006 is used, no problem is encountered.